THE HONG KONG
POLYTECHNIC UNIVERSITY
香港理工大學
Pao Yue-kong Library
包玉剛圖書館

Copyright Undertaking

This thesis is protected by copyright, with all rights reserved.

By reading and using the thesis, the reader understands and agrees to the following terms:

1. The reader will abide by the rules and legal ordinances governing copyright regarding the use of the thesis.
2. The reader will use the thesis for the purpose of research or private study only and not for distribution or further reproduction or any other purpose.
3. The reader agrees to indemnify and hold the University harmless from and against any loss, damage, cost, liability or expenses arising from copyright infringement or unauthorized usage.

IMPORTANT

If you have reasons to believe that any materials in this thesis are deemed not suitable to be distributed in this form, or a copyright owner having difficulty with the material being included in our database, please contact lbsys@polyu.edu.hk providing details. The Library will look into your claim and consider taking remedial action upon receipt of the written requests.

Pao Yue-kong Library, The Hong Kong Polytechnic University, Hung Hom, Kowloon, Hong Kong

http://www.lib.polyu.edu.hk

LARGE-SCALE OPTIMIZATION FOR SHIPPING OPERATIONS MANAGEMENT

YIWEI WU

PhD

The Hong Kong Polytechnic University

2024

The Hong Kong Polytechnic University

Department of Logistics and Maritime Studies

Large-scale optimization for shipping operations management

Yiwei WU

A thesis submitted in partial fulfillment of the
requirements for the degree of
Doctor of Philosophy

January 2024

CERTIFICATE OF ORIGINALITY

I hereby declare that this thesis is my own work and that, to the best of my knowledge and belief, it reproduces no material previously published or written, nor material that has been accepted for the award of any other degree or diploma, except where due acknowledgment has been made in the text.

_____(Signed)

Yiwei WU (Name of student)

Abstract

Shipping plays an important role in the global economy and international trade. It is not only the core logistics link connecting markets around the world, but also the cornerstone of driving global economic growth, ensuring the efficient allocation of resources, and promoting the comprehensive development of society. In this context, large-scale optimization in the field of shipping operations management is particularly important. Such optimization is not only crucial for improving transportation efficiency and reducing costs, but also directly affects important indicators such as customer satisfaction and service quality maintenance. Through large-scale optimization, such as precise scheduling, fleet deployment, and cargo management, shipping can maintain competitive advantages in a fiercely competitive market environment, while also promoting the sustainable development and environmental protection. In general, shipping is not only a key component of the global economy, but its internal large-scale optimization is also an important driving force for the advancement of the industry. This thesis investigates three important issues in large-scale optimization for shipping operations management, where the first one relates to the decarbonization of shipping, the second one relates to fleet repositioning for uncertain demand, and the third one relates to government ship scheduling with the consideration of health impacts.

The first study introduces a joint optimization problem of speed optimization, voyage planning, and fleet deployment considering the impacts of displacement and sailing speed on fuel consumption. The problem is highly motivated by the global warming. To limit carbon dioxide emissions released by the shipping industry, the Energy Efficiency Operational Index (EEOI), a carbon intensity indicator, is widely adopted to assess each ship's energy efficiency and guide the shipping operations management. Specifically, this study formulates a nonlinear mixed-integer programming (MIP) model which minimizes both the weekly cost and the average EEOI value of all deployed ships. To solve this nonlinear MIP model, a tailored exact algorithm is designed. The numerical results show that the instances with at most seven ship routes can be solved by the proposed algorithm within four minutes. The second study investigates a fleet deployment problem involving demand fulfillment, cargo allocation, fleet repositioning, and ship chartering with the consideration of multi-period periods, heterogeneous ships, and uncertain shipping demand, which is motivated by the huge uncertainty in the shipping market brought by the COVID-19 pandemic. To address this problem, this study uses multistage stochastic programming to formulate a linear MIP model and develops a Benders-based branch-

and-cut algorithm. Numerical results indicate that compared to two-stage stochastic programming, multistage stochastic programming can help to obtain better solutions. Particularly, 90% of the benefit of the multistage model is due to better demand fulfillment as well as cargo allocation decisions, while 10% of the benefit is due to improved fleet deployment decisions. The first two studies focus on commercial ships, whereas the last study shifts its attention to government ships. This shift is attributed to the current stringent regulations on air emissions from ships, highlighting the need for the government to lead by example through meticulous scheduling of its government ships. Specifically, the third study focuses on a routing, scheduling, and speed optimization problem of government ships that account for the health effects of air pollutant emissions under different weather conditions. To this end, this study proposes a trip-based formulation and a set-covering formulation for the problem, and designs a branch-and-price-and-cut algorithm to effectively solve the problem. Efficiency of the proposed algorithm for computational instances is verified.

Key words: Large-scale optimization; shipping operations management; exact algorithm design.

Acknowledgements

Firstly, I would like to extend my sincere thanks to my supervisor, Prof. Shuaian (Hans) Wang, for his invaluable help and guidance throughout my PhD study. His patience and willingness to help when I encountered challenges were greatly appreciated.

Secondly, my heartfelt appreciation goes to Prof. Lu Zhen from Shanghai University for his guidance and support during my research. I am also grateful to Prof. Chung Piaw Teo from the National University of Singapore as well as Prof. René de Koster and Dr. Angelos Tsoukalas from Erasmus University for their support when I was a visiting PhD student.

I would also like to express my gratitude to the Department of Logistics and Maritime Studies at The Hong Kong Polytechnic University for its comprehensive support.

Lastly, I am deeply grateful to my parents for always backing my decisions. Their constant encouragement was crucial in the completion of my thesis.

Table of Contents

List of Figures

List of Tables

List of Abbreviations

- Branch-and-Bound (B&B)
- Branch-and-Price-and-Cut (BPC)
- Benders-Based Branch-and-Cut (BBC)
- Carbon Dioxide (CO_2)
- Carbon Intensity Indicator (CII)
- Column Generation (CG)
- Dual Primal Subproblem (DPS)
- Elementary Shortest Path Problems with Resource Constraints (ESPPRC)
- Energy Efficiency Operational Index (EEOI)
- Fleet Deployment Problem (FDP)
- Fleet Repositioning Problem (FRP)
- Intergovernmental Panel on Climate Change (IPCC)
- International Maritime Organization (IMO)
- Linear Programming (LP)
- Linear Relaxation of the Master Problem (LMP)
- Linear Relaxation of the Restricted Master Problem (RLMP)
- Liquefied Natural Gas (LNG)
- Master Problems (MPs)
- Mixed-Integer Linear Programming (MILP)
- Mixed-Integer Programming (MIP)
- Multi-Trip VRP with Time Windows (MTVRPTW)
- Nitrogen Oxides (NO_X)
- Origin-Destination (O-D)
- Primal Subproblem (PS)
- Restricted Master Problem (RMP)
- Sulfur Oxides (SO_X)
- United Nations (UN)
- United Nations Conference on Trade and Development (UNCTAD)
- Upper Bound Tightening (UBT)
- Vehicle Routing Problem (VRP)
- Very Low Sulfur Fuel Oil (VLSFO)

Chapter 1: Introduction

Maritime shipping plays an important role in the transportation of goods and global trade. This is particularly evident in the over 80% of international trade volumes handled by the global shipping network (UNCTAD, 2022). These networks, through interconnected shipping routes and ports spread across the world, form a vast and complex system. The ports are not merely physical ports of call; they are also the key carriers for the efficient operation of the global supply chain network. Thus, maritime transport serves not only as a bridge connecting nations but also as the cornerstone of the global economy.

Shipping operations management is a multifaceted and extremely complex field, requiring in-depth analysis and comprehensive consideration of a wide range of influencing factors. These factors include fleet deployment, speed optimization, demand fulfillment, cargo allocation, etc. In real-life scenarios, the complexity of shipping operations management is further increased because different decision-making factors are intertwined with each other and influence each other. Therefore, large-scale optimization for shipping operations management becomes crucial, which is necessary to ensure that the maritime industry can operate efficiently.

In addition to traditional shipping operations management factors, recent years have necessitated the integration of several emerging elements. This includes the implementation of green shipping practices, the uncertainty of the ever-changing shipping market, and the health impact of shipping activities. The incorporation of these new factors poses higher requirements and challenges to shipping operations management. Hence, this thesis explores large-scale optimization for shipping operations management from three types of problems related to (i) decarbonizing shipping, (ii) fleet repositioning for uncertain demand and (iii) government ship scheduling with the consideration of health impacts.

1.1 DECARBONIZING SHIPPING

To slow the increase in the global temperature, the United Nations (UN)'s Intergovernmental Panel on Climate Change (IPCC) emphasizes the need to halve worldwide emissions by 2030. This action is crucial to limit the Earth's warming to no

more than 1.5°C within this century (IPCC, 2018). As revealed during the United Nations Climate Change Conference of the Parties, it is projected that in 2022, carbon dioxide (CO_2) emissions from fossil fuels rise by 1%, reaching an unprecedented level of 37.5 billion tonnes (NatureNews, 2022). If this trend continues, it is conceivable that within a mere nine years, sufficient CO_2 could be emitted to elevate the global temperature by 1.5°C above pre-industrial levels, which may lead to serious consequences for Earth (Tollefson, 2022). For example, coral reefs would decline by 70% to 90% with a global temperature rise of 1.5°C (IPCC, 2018). Hence, more efforts for decarbonization are needed.

1.2 FLEET REPOSITIONING FOR UNCERTAIN DEMAND

The uncertainty in the shipping market is primarily driven by seasonal demand fluctuations and unforeseen events that cause global economic trends to fluctuate. Moreover, according to United Nations Conference on Trade and Development (UNCTAD) projections, an asymmetric recovery, logistical bottlenecks, and soaring costs have increased uncertainty (UNCTAD, 2022). As a result, the demand pattern may undergo significant changes over the long period. For instance, the abrupt emergence of COVID-19 led to an 8.4% decrease in container throughput at the Port of Shanghai during the initial four months of 2020, necessitating adjustments in the shipping network (CWTN, 2021). To adapt to these changes, ship fleets often need to be repositioned through the addition, removal, or modification of shipping routes. Hence, fleet repositioning is a critical step in adjusting shipping networks to changes in market demands and operating conditions.

1.3 GOVERNMENT SHIP SCHEDULING WITH THE CONSIDERATION OF HEALTH IMPACTS

Faced with the current stringent regulations on air emissions from ships, the government should lead by example by strictly scheduling government ships. Government ships carry out a large number of trips for routine tasks, such as patrol of territorial water areas, maintenance works, and training. These trips are planned solely based on the requirement of the tasks (e.g., two trips each week) without considering the health impacts of the air emissions from ships. However, with the large volume of ship traffic and the current stringent regulations on air emissions from ships, it is challenging to further reduce the absolute amounts of air pollutants from government ships. Fortunately, environmental science demonstrates that the damage to the health

of the population caused by unit amount of air pollutant varies significantly with the weather conditions. This creates an opportunity for multi-disciplinary research on the management of the location and time of air pollutant emissions from ships to minimize the sum of the fuel cost of the trips and the health damage of the air pollutants from the trips.

1.4 THESIS OUTLINE

The structure of the remainder of this thesis is outlined as follows. Chapter 2 explores a sustainable liner shipping framework, focusing on fleet deployment, voyage planning, and speed optimization through a nonlinear MIP mode. Chapter 3 explores a multi-period, heterogeneous fleet deployment challenge within an uncertain shipping network, which contains aspects like fleet repositioning, ship chartering, demand fulfillment, and cargo allocation. Chapter 4 explores a routing, scheduling, and speed optimization problem for government ships that account for the health effects of air pollutant emissions at different weather conditions. Chapter 5 concludes the thesis and discusses future research directions.

Chapter 2: Nonlinear programming for fleet deployment, voyage planning and speed optimization in sustainable liner shipping[1]

2.1 INTRODUCTION

Climate change is arguably one of the greatest challenges of our time. Although shipping is regarded as an environmentally efficient mode of transportation, it generates tremendous air emissions that have harmful effects on the global environment. CO_2 accounts for the vast majority of greenhouse gas emissions from the transportation sector (USEPA, 2022). Moreover, United Kingdom broker Simpson Spence Young estimated that CO_2 emissions from global shipping in 2021 increased 4.9% from 2020 and surpassed 2019 levels (Young, 2022). Unless serious actions are taken soon, CO_2 emissions from global shipping may increase by between 50% and 250% by 2050 (IMO, 2014), which undoubtedly contributes to global warming.

Maritime decarbonization is particularly necessary to achieve the long-term goal of the Paris Agreement adopted at the Paris climate conference in 2015 (UN, 2015), that is, to limit the increase in the average global temperature to well below 2 °C, preferably to 1.5 °C, above pre-industrial levels. For this reason, many emission limits and regulations are promulgated to reduce CO_2 emissions and stop global warming. For example, the International Maritime Organization (IMO), which is the United Nations specialized agency for international shipping, has set strategies to reduce carbon emissions per unit of transport work by at least 40% by 2030 and reduce the total annual greenhouse gas emissions from international shipping by at least 50% by 2050, with 2008 as a baseline (IMO, 2018). Despite the intensifying regulatory environment, international shipping released 833 million tons of CO_2 in 2021, an increase of 4.9% from 2020 (Lloyd's, 2022). Hence, it is urgent for liner companies to

[1] Wu, Y., Huang, Y., Wang, H., Zhen, L., 2023. Nonlinear programming for fleet deployment, voyage planning and speed optimization in sustainable liner shipping. *Electronic Research Archive* 31(1): 147–168.

consider how to reduce carbon emissions when scheduling shipping activities to meet international requirements.

The carbon emissions per unit of transport work can be referred to as the carbon intensity, and one of the carbon intensity indicators is the Energy Efficiency Operational Index (EEOI), which was introduced by the IMO in 2009 and enforced in 2011 to measure the energy efficiency level of each operating ship (IMO, 2009). The EEOI value of a ship over a year reflects the energy efficiency of the ship and may help liner companies to schedule ship fleets when considering the maritime decarbonization target. The EEOI value of a ship can be calculated by dividing annual carbon emissions of the ship (g) by actual ton-miles carried by the ship (the amount of transported cargo times total travel distance) in the year (IMO, 2011). Therefore, the EEOI value of a ship is directly influenced by the type of used fuel, cargo load and total distance travelled. The lower the EEOI value is, the better the energy efficiency performance. From an operational perspective, several operation decisions, such as voyage planning and speed optimization, which further influences fleet deployment, can be jointly optimized to reduce the EEOI because these decisions directly affect fuel consumption. Moreover, displacement (tons), i.e., the total weight of the ship itself, cargo, ballast water and bunker, also influences fuel consumption (Meng et al., 2016). Hence, seeking the optimal fleet deployment, voyage planning and speed to achieve shipping operations management optimization is an efficient way to reduce EEOI, achieve energy savings and reduce emissions.

This chapter is motivated by the abovementioned real-world challenge in green shipping, and it may contribute to shipping operations management by proposing a nonlinear mixed-integer programming (MIP) model and a tailored exact algorithm. Two assumptions are considered in this study: 1) Ships are homogenous on each route in terms of the cost structure, which is consistent with the assumptions considered in Zhen et al. (2019b); 2) ships' dwell time at all ports of call on a ship route is given, which is in line with the assumptions considered in Zhen et al. (2019a). This chapter provides liner companies with scientific methods to optimize fleet deployment, voyage planning and speed to reduce both the total weekly cost and the average EEOI value of all deployed ships on all routes with the consideration of the influences of sailing speed, displacement and voyage option on fuel consumption. 11 sets of numerical experiments with different route compositions are first conducted to evaluate the

performance of the proposed algorithm. Moreover, sensitivity analyses with crucial parameters, including the weighting factor, unit price of fuel, Suez Canal toll fee per ship, weekly fixed operating cost and cargo load in each leg, are carried out to show the influence of these aspects on the results to look for managerial insights.

2.1.1 Literature review

The core part of this chapter is related to the widely-studied fleet deployment problem. Readers interested in overviews of the above problem can refer to Meng et al. (2014), Wang and Meng (2017) and Christiansen et al. (2020). This chapter focuses on an integrated optimization problem of fleet deployment, voyage planning and speed optimization to minimize both the total weekly cost and the average EEOI value of all deployed ships on all routes. Thus, this section reviews the streams of related literature from the following two perspectives: the fleet deployment problem and studies related to EEOI.

The first research stream is concerned with the fleet deployment problem. As an important concern for liner companies, the fleet deployment problem determines the number of ships to be deployed on various ship routes to maximize the total profit or to minimize the total cost. Lai et al. (2022) formulated a two-stage model for a fleet deployment problem with shipping revenue management under demand uncertainty whose randomness is represented by probability-free uncertain sets. They also developed a column-and-constraint generation based exact algorithm to solve the model. In recent years, sustainable development is the main development direction of the shipping industry (Zisi et al., 2021). One of the most important green shipping factors in the fleet deployment problem is reducing emissions from ships, such as CO_2, sulfur oxides (SO_X) and nitrogen oxides (NO_X). Zhu et al. (2018) investigated the influence of a maritime emissions trading system on fleet deployment and mitigation of CO_2 emissions. They proposed a stochastic integer programming model to determine fleet deployment and CO_2 emissions with different CO_2 prices. Considering sulfur emission control areas, Wang et al. (2021) studied an integrated problem of schedule design, fleet deployment, sailing optimization and path selection, and they proposed a nesting algorithmic framework to solve the problem. Pasha et al. (2021) designed a decomposition-based heuristic algorithm to solve an integrated problem of service frequency determination, fleet deployment, speed optimization and ship schedule design considering emissions released by ships with the aim of maximizing

the total turnaround profit. Zhao et al. (2021b) formulated a two-stage stochastic linear model for a fleet renewal problem considering three sulfur reduction technologies and uncertain markets. With the consideration of sulfur emission limits, Chen et al. (2022) built an ellipsoidal uncertainty set to describe demand uncertainties and developed a robust optimization model for an alliance fleet deployment problem with slot exchange. Moreover, Zhao et al. (2021a) investigated how to reduce SO_X and NO_X emissions in shipping economically by determining the optimal technology choice.

The second topic considered in the related works is EEOI. Operational data, such as speed and deadweight, are usually used to analyze EEOI. Existing papers on EEOI mainly focus on two aspects, namely, estimation of EEOI values and scheduling based on EEOI values. In terms of the estimation of EEOI values, Acomi and Acomi (2014) used commercial software to estimate the value of EEOI before a voyage, and they compared estimated values and true values according to speeds, days on anchor and waiting days. In terms of scheduling based on EEOI values, Hou et al. (2019) formulated a sailing speed optimization model with consideration of uncertain ice loads to minimize the EEOI value of each ship in ice areas. Sun et al. (2019) developed a dynamic optimization model for sailing speeds of ships to improve fuel efficiency as well as reduce EEOI. They used a neural network to predict fuel consumption rate and ship speed, and they applied a genetic algorithm to optimize engine revolution and seek the minimum EEOI value. Considering the uncertainty in ice loads as well as water velocity, Ichsan et al. (2019) studied a decided route on the sea tollway of Indonesia and optimized the rate of EEOI of ships deployed on the route. With the aim of minimizing EEOI values of seven types of specialized ships, Prill et al. (2020) assumed that the EEOI of each ship is related to the deadweight of the ship, the type and amount of consumed fuel and the voyage distance travelled by the ship, and they proposed a new method of determining the EEOI of each ship by optimizing sailing speeds of ships and the realization time of each exploitation task. Hou et al. (2021) developed a ship speed optimization model which brought a 15% reduction in EEOI in the computational experiment.

In summary, the prevailing trend in the fleet deployment problem is studying how to reduce emissions from the shipping industry because of the increasing public concern about environmental protection. However, few works focus on an integrated optimization problem of fleet deployment, voyage planning and speed optimization to

minimize both the total weekly cost and the average EEOI value of all deployed ships on all routes. Therefore, this chapter studies an integrated optimization problem of fleet deployment, voyage planning and speed optimization with consideration of the influences of sailing speed, displacement and voyage option on fuel consumption. Moreover, some other frequently ignored operating limits, such as Suez Canal toll fee, are considered in this chapter. This chapter proposes a nonlinear MIP model to minimize two objectives, i.e., the total weekly cost and the average EEOI value of all deployed ships on all routes, by determining the optimal fleet deployment, voyage planning and speed.

2.1.2 Contributions

Contributions of this chapter are summarized from the following three aspects. First, a nonlinear MIP model is proposed for this problem with the aim of minimizing both the total weekly cost and the average EEOI value of all deployed ships on all routes by determining the optimal sailing speed during each leg, the voyage option between the Suez Canal route and Cape of Good Hope route and the number of ships deployed on each ship route. Second, to deal with the challenge of solving a nonlinear MIP model, a tailored exact algorithm is proposed by considering specific characteristics of our problem. Efficiency of the proposed algorithm for computational instances of different sizes is verified. Third, sensitivity analyses with crucial parameters, including the weighting factor, unit price of fuel, Suez Canal toll fee per ship, weekly fixed operating cost and cargo load in each leg, are carried out to show the influences of these factors on the results to obtain managerial insights. For example, with the larger weight on the minimization of the total weekly cost, fewer ships are needed, which means that each deployed ship needs to sail at a higher speed and releases more CO_2 (i.e., higher EEOI value).

The remainder of this chapter is organized as follows. Section 2.2 elaborates on the problem background and proposes a nonlinear MIP model for the integrated problem. A tailored exact algorithm is designed in Section 2.3. Section 2.4 reports the computational experiments, including basic experiments to evaluate the efficiency of the proposed algorithm and sensitivity analyses to seek managerial insights. Chapter summaries are outlined in Section 2.5.

2.2 PROBLEM DESCRIPTION AND MODEL FORMULATION

This chapter is oriented toward an integrated optimization problem of fleet deployment, voyage planning and speed optimization with consideration of the influences of sailing speed, displacement and voyage option on fuel consumption. This section first elaborates on the detailed background of the problem in Section 2.2.1, explains the objective function of the problem in Section 2.2.2 and presents the mathematical model in Section 2.2.3.

2.2.1 Problem background

We consider a liner company operating on a network containing a set R of container ship routes (services). The liner company has already determined the optimal service plan including fleet deployment, sailing speed and voyage selection. However, in the context of the Carbon Intensity Indicator (CII) introduced by the IMO, especially considering EEOI, the liner company may need to reoptimize their service plan including fleet deployment, sailing speed and voyage options such as the Cape of Good Hope route or the Suez Canal route (Zhou et al., 2021) shown in Figure 2-1.

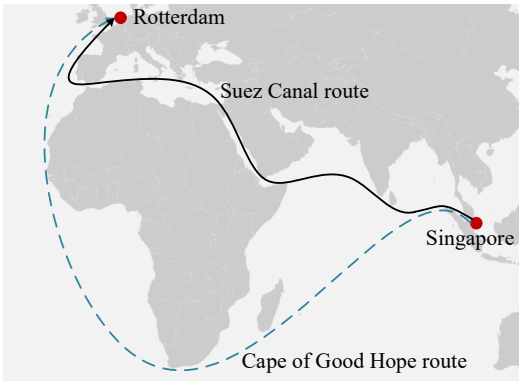

Figure 2-1 Comparison of two voyage options: Suez Canal route and Cape of Good Hope route.

Some ship routes, e.g., r ($r \in R$), operated by the liner company may contain the voyage between Asian ports and European ports. This chapter assumes that the liner company originally selects the Suez Canal route for these voyages because sailing through the Suez Canal saves a lot of time. In this case, let I_r and I_r' represent the set of legs that do not cross Asian and European ports on ship route r and the set of legs across Asian and European ports on ship route r, respectively. For example, Table 2-1 summarizes the sets of I_r and I_r' of route r whose port rotation is Qingdao-Shanghai-Ningbo-Yantian-Rotterdam-Hamburg-Antwerp-Singapore-Qingdao. This chapter

then lets γ_{ri} denote a binary variable which equals 1 if and only if the voyage option of leg i, $i \in I'_r$, on ship route r selects the Suez Canal voyage and equals 0 if selecting the Cape of Good Hope voyage. In addition, sailing speeds of deployed ships during each leg should be between $\underline{v}$ and $\overline{v}$, where $\underline{v}$ and $\overline{v}$ represent the minimum and maximum speeds of ships on ship routes, respectively. Let V represent a set of all possible sailing speeds indexed by v, and $V = \{\underline{v}, \underline{v} + 0.1, \dots, \overline{v} - 0.1, \overline{v}\}$.

Table 2-1 Summary of sets I_r and I'_r.

Sets	Legs		
I_r	Qingdao → Shanghai	Shanghai → Ningbo	Ningbo → Yantian
	Rotterdam → Hamburg	Hamburg → Antwerp	Singapore → Qingdao
I'_r	Yantian → Rotterdam	Antwerp → Singapore	

In terms of fleet deployment and speed optimization, EEOI values of all deployed ships on all ship routes should be regarded as an important consideration because when stricter CO_2 emission reduction regulations issued by international organizations take effect, liner companies must find ways to reduce their deployed ships' EEOI values. The incorporation of EEOI may result in higher costs for liner companies in practice. However, companies certainly aim to minimize their total cost while complying with EEOI regulations. Therefore, this study considers the influences of sailing speed, displacement and voyage option on fuel consumption. Bi-objective programming has been widely applied before when minimizing carbon emissions and maximizing profit of liner companies, such as in Zhao et al. (2019). From the perspective of the liner company, this chapter develops a bi-objective model to balance the total weekly cost, including the weekly fixed operating cost, weekly Suez Canal toll fee and weekly fuel cost, and the average EEOI value of all deployed ships on all ship routes by determining fleet deployment, voyage planning and sailing speed of all deployed ships. The above strategic-level problem involves many intertwined decisions, so a scientific decision-making methodology is needed for this problem.

2.2.2 Objective function

This problem is formulated as a bi-objective programming model. These two objective functions are the total weekly cost and the average EEOI value of all deployed ships on all routes. In the following paragraphs, we first explain separately

how to formulate these two objective functions and then introduce how to deal with the bi-objective programming.

The first objective function focuses on the total weekly cost, which contains three parts: the weekly fixed operating cost, weekly Suez Canal toll fee and weekly fuel cost. Specifically, the first part is the weekly fixed operating cost of deployed ships. Because a fleet of homogeneous ships is deployed on each route to maintain a weekly service frequency, the total fixed operating cost for all deployed ships on all routes during one week can be calculated as $\sum_{r\in R} o\beta_r$, where o and β_r denote the weekly operating cost for deploying one ship on ship routes and the number of ships deployed on route r, respectively. Next is the weekly Suez Canal toll fee faced by the liner company. Let q_r denote the Suez Canal toll fee of each ship deployed on route r (USD/ship). Hence, we can calculate the weekly Suez Canal toll fee by $\sum_{r\in R}\sum_{i\in I'_r} q_r\gamma_{ri}$.

The last part of the total weekly cost is the fuel cost, which depends on fuel consumption. Each ship contains a main engine, which provides propulsion power for the ship, and an auxiliary engine, which provides power for uses other than propulsion. Specifically, in terms of fuel consumption of the main engine, most of the existing fuel consumption models in the literature (Wang and Meng, 2012b; Zhao et al., 2020; Zhen et al., 2019a) agree that a ship's unit fuel consumption significantly depends on its sailing speed and calculated the unit fuel consumption function by $\dot{c}v^{\ddot{c}}$ to conduct liner shipping network analyses, where v is sailing speed (knots), and $\dot{c}$ and $\ddot{c}$ are positive coefficients. However, in addition to sailing speed, several other factors also influence fuel consumption. The first one is displacement (tons), i.e., the total weight of the ship itself, cargo, ballast water and bunker. Meng et al. (2016) investigated the relationship between the fuel consumption rate of a container ship and several factors, including sailing speed, displacement and weather/sea conditions. However, it is extremely difficult to record the precise weather/sea conditions because the effects of waves, wind and currents are interwoven in practice. Hence, the influence of weather/sea conditions on fuel consumption is not considered in this study. Also, this chapter formulates the unit fuel consumption function as $c_1 v^{c_2} d^{c_3}$ (tons/hour), which is given by Meng et al. (2016), where c_1, c_2 and c_3 are positive coefficients, and v and d represent the actual sailing speed (knots) and displacement (tons) of the ship during one leg, respectively. Finally, in terms of fuel consumption of the auxiliary engine, we

assume the auxiliary engine of a ship deployed on ship route r consumes an amount e_r of fuel per day. In summary, the total amount of fuel consumed by a ship's main engine on ship route r, denoted by ε_r, can be calculated by $\varepsilon_r = \sum_{i\in I_r}\sum_{v\in V} c_1 v^{c_2}\alpha_{riv} {d_{ri}}^{c_3}\frac{l_{ri}}{v} + \sum_{i\in I'_r}\sum_{v\in V} c_1 v^{c_2}\alpha_{riv} {d_{ri}}^{c_3}\frac{l_{ri}\gamma_{ri}+l'_{ri}(1-\gamma_{ri})}{v}$, where α_{riv}, d_{ri}, l_{ri} and l'_{ri} represent, respectively, a binary variable which equals 1 if and only if the speed of the ship sailing during leg i on route r is v and 0 otherwise, actual displacement (tons) of the ship during leg i on ship route r, length (n mile) of the ith leg if $i \in I_r$ or length of the ith leg taking the Suez Canal route if $i \in I'_r$ on ship route r and length (n mile) of the ith ($i \in I'_r$) leg taking the Cape of Good Hope route on ship route r. Weekly fuel consumption of auxiliary engines of all deployed ships on route r is $7e_r\beta_r$ because the total time for a ship completing travel along route r including dwell time and sailing time is $7\beta_r$ days to maintain a weekly container shipping service frequency. In summary, the total weekly fuel cost of all deployed ships on all routes is $\sum_{r\in R}(a_1\varepsilon_r + 7a_2e_r\beta_r)$, where a_1 and a_2 are the unit prices of fuels consumed by the main and auxiliary engines, respectively (USD/ton). Therefore, the total weekly cost can be calculated by $\sum_{r\in R}[o\beta_r + \sum_{i\in I'_r} q_r\gamma_{ri} + a_1\varepsilon_r + 7a_2e_r\beta_r]$.

The second objective is the average EEOI value of all deployed ships on all routes. According to the IMO (2011), the EEOI of a ship is described by the ratio of the total amount of CO_2 emissions released by the ship over a year to the product of the ship's cargo transported and total distance over a year, and it is related to fuel consumption, sailing speed, load tonnage and mileage of voyage. The calculation formula of EEOI is Eq (2-1), which is given by the IMO (2011).

$$\text{EEOI} = \frac{\text{total carbon emissions of the ship during ballast and laden voyages (g)}}{\text{amount of cargo transported} \times \text{total distance laden}}. \qquad (2\text{-}1)$$

Here, notice that the EEOI of a ship is also equal to the ratio of the total amount of CO_2 emissions released by the ship over a week to the product of the ship's cargo transported and total distance over a week because of the weekly service frequency. In addition, we assume that the ships owned by the liner company generate g tons of CO_2 when burning one ton of fuel, and let m_{ri} denote the volume of cargo load in the ship during leg i, $i \in I_r \cup I'_r$. Also, since we calculate the amount of CO_2 emissions in tons, but the amount of CO_2 emissions in the EEOI calculation formula is in grams, we need to multiply the amount of CO_2 emissions by 10^6 when calculating the EEOI value of

each operating ship. Therefore, the average EEOI value of all ships deployed on all routes is $\sum_{r\in R}\frac{10^6(\varepsilon_r+7e_r\beta_r)g}{\sum_{i\in I_r}m_{ri}l_{ri}+\sum_{i\in I'_r}m_{ri}[l_{ri}\gamma_{ri}+l'_{ri}(1-\gamma_{ri})]}/\sum_{r\in R}\beta_r$.

Since this chapter aims to minimize both of the above objectives, i.e., the total weekly cost and the average EEOI value of all deployed ships on all routes, this study applies a typical way to solve the problem, which is the weighted sum method. We use λ as a weighting factor for the bi-objective programming which reveals the relative importance between the above two objective functions. Hence, the objective function of this problem is formulated as $\lambda\left[\sum_{r\in R}(o\beta_r+\sum_{i\in I'_r}q_r\gamma_{ri}+a_1\varepsilon_r+7a_2e_r\beta_r)\right]+(1-\lambda)(\sum_{r\in R}\frac{10^6(\varepsilon_r+7e_r\beta_r)g}{\sum_{i\in I_r}m_{ri}l_{ri}+\sum_{i\in I'_r}m_{ri}[l_{ri}\gamma_{ri}+l'_{ri}(1-\gamma_{ri})]}/\sum_{r\in R}\beta_r)$.

2.2.3 Model formulation

Based on the above analysis of the objective function, this chapter formulates a nonlinear MIP model in this section. Before formulating the mathematical model for this problem, we list the notations used in this paper as follows.

Indices and sets:

R: set of all ship routes, $r \in R$.

I_r: set of all legs that do not cross Asian and European ports on ship route r, $i \in I_r$.

I'_r: set of all legs across Asian and European ports on ship route r, $i \in I'_r$.

V: set of all possible sailing speeds, $v \in V$, $V = \{\underline{v}, \underline{v}+0.1, \dots, \overline{v}-0.1, \overline{v}\}$, where $\underline{v}$ and $\overline{v}$ represent the minimum and maximum speeds of ships on ship routes, respectively.

Z_+: set of all non-negative integers.

Parameters:

a_1, a_2: unit prices of fuels consumed by the main and auxiliary engines, respectively (USD/ton).

c_1, c_2, c_3: coefficients to calculate the unit fuel consumption for travelling per hour, which mainly depends on sailing speed and displacement (tons/hour).

d_{ri}: actual displacement of the ship during leg i on ship route r (tons).

e_r: amount of fuel consumed by the auxiliary engine of a ship deployed on ship route r per day (tons/day).

g: amount of CO_2 released by a ship when burning one ton of fuel (tons).

l_{ri}: length of the ith leg if $i \in I_r$ or length of the ith leg taking the Suez Canal route if $i \in I'_r$ on ship route r (n mile).

l'_{ri}: length of the ith ($i \in I'_r$) leg taking the Cape of Good Hope route on ship route r (n mile).

m_{ri}: cargo load in leg i, $i \in I_r \cup I'_r$, on ship route r (tons).

o: weekly operating cost of one ship deployed on ship routes (USD).

q_r: Suez Canal toll fee for a ship deployed on route r (USD/ship).

s_r: maximum number of ships that can be deployed on ship route r.

t_r: total duration a ship dwells at all ports of call on ship route r (hours).

λ: weighting factor for the bi-objective programming.

Variables:

α_{riv}: binary, equals 1 if and only if the speed of the ship sailing during leg i on ship route r is v; 0 otherwise.

γ_{ri}: binary, equals 1 if and only if the voyage option of leg i, $i \in I'_r$, on ship route r selects Suez Canal route; 0 if Cape of Good Hope route.

β_r: integer, number of ships deployed on ship route r.

ε_r: continuous, weekly fuel consumption of the main engine of all deployed ships on ship route r (tons).

Mathematical model

Based on the above definitions of parameters and variables, a nonlinear MIP model is formulated as follows.

[**M2-1**] $\text{Min } \lambda\left[\sum_{r\in R}(o\beta_r + \sum_{i\in I'_r} q_r\gamma_{ri} + a_1\varepsilon_r + 7a_2 e_r\beta_r)\right]$

$$+(1-\lambda)\left(\sum_{r\in R}\frac{10^6(\varepsilon_r+7e_r\beta_r)g}{\sum_{i\in I_r} m_{ri}l_{ri}+\sum_{i\in I'_r} m_{ri}[l_{ri}\gamma_{ri}+l'_{ri}(1-\gamma_{ri})]}\Big/\sum_{r\in R}\beta_r\right) \qquad (2\text{-}2)$$

subject to

$$1 \le \beta_r \le s_r \qquad \forall\, r \in R \qquad (2\text{-}3)$$

$$\sum_{v\in V}\left(\sum_{i\in I_r}\frac{l_{ri}}{v}\alpha_{riv}+\sum_{i\in I_r'}\frac{l_{ri}\gamma_{ri}+l_{ri}'(1-\gamma_{ri})}{v}\alpha_{riv}\right)+t_r=168\beta_r \quad \forall\, r \in R \qquad (2\text{-}4)$$

$$\varepsilon_r=\sum_{i\in I_r}\sum_{v\in V}c_1 v^{c_2}\alpha_{riv}{d_{ri}}^{c_3}\frac{l_{ri}}{v}+\sum_{i\in I_r'}\sum_{v\in V}c_1 v^{c_2}\alpha_{riv}{d_{ri}}^{c_3}\frac{l_{ri}\gamma_{ri}+l_{ri}'(1-\gamma_{ri})}{v}$$

$$\forall\, r \in R \qquad (2\text{-}5)$$

$$\sum_{v\in V}\alpha_{riv}=1 \qquad \forall r \in R, i \in I_r \cup I_r' \qquad (2\text{-}6)$$

$$\alpha_{riv} \in \{0,1\} \qquad \forall r \in R, i \in I_r \cup I_r', v \in V \qquad (2\text{-}7)$$

$$\beta_r \in Z_+ \qquad \forall r \in R \qquad (2\text{-}8)$$

$$\gamma_{ri} \in \{0,1\} \qquad \forall r \in R, i \in I_r \cup I_r' \qquad (2\text{-}9)$$

$$\varepsilon_r \ge 0 \qquad \forall r \in R. \qquad (2\text{-}10)$$

Objective (2-2) minimizes the weighted sum of two objectives considered in this chapter. Constraints (2-3) guarantee that at least one ship and at most s_r ships should be deployed on each route. Constraints (2-4) ensure that the total number of hours for a ship completing its travel on a route is the number of ships deployed on the route times 168, because all services follow the weekly arrival pattern, and one week has 168 hours. Constraints (2-5) calculate the weekly fuel consumption of the main engine of all deployed ships on ship route r. Constraints (2-6) ensure that sailing speeds of deployed ships during each leg on all ship routes satisfy the feasible speed range of ships. Constraints (2-7)–(2-10) state the ranges of the defined decision variables.

2.3 ALGORITHM DESIGN

It is challenging to solve the nonlinear model [M2-1], which contains multiple nonlinear parts, including objective function (2-2) and constraints (2-4) and (2-5). By reviewing several algorithms and their features in some existing fleet deployment studies, we find that specially tailored solution methods are usually designed for their models because these fleet deployment studies contain specific characteristics. For example, Zhen et al. (2019b) proposed a tailored dynamic linearization algorithm to solve a mixed-integer second-order cone programming model. In addition, considering

specific characteristics of our problem, we find that nonlinear parts in model [M2-1] can be replaced by enumerating the possible values, and the model after the above transformation can be solved directly and effectively by Gurobi. Since the number of possible values of the nonlinear parts in model [M2-1] is small, this chapter designs an efficient exact algorithm based on the enumeration method to solve the model [M2-1]. Due to the efficiency and accuracy of the proposed algorithm, the proposed algorithm can quickly find the optimal solution of the model in a very short time.

Before introducing our algorithm, one transformation of constraint (2-4) is first introduced. Since sailing speed is discretized, the feasibility of constraint (2-4), which contains the equality symbol, might be affected. Hence, constraint (2-4) is replaced with constraint (2-11). Here, notice that the equality symbol in constraint (2-4) is replaced with the less than or equal to symbol in constraint (2-11).

$$\sum_{v\in V}\left(\sum_{i\in I_r}\frac{l_{ri}}{v}\alpha_{riv}+\sum_{i\in I_r'}\frac{l_{ri}\gamma_{ri}+l_{ri}'(1-\gamma_{ri})}{v}\alpha_{riv}\right)+t_r\le 168\beta_r \quad \forall r\in R. \tag{2-11}$$

As a result, the final version of model [M2-1] becomes the following:

[**M2-2**] objective (2-2)

subject to constraints (2-3), (2-5)–(2-11).

Finally, we design the following exact algorithm, whose framework is introduced in Algorithm 2-1 to solve the model [M2-2]. The main difficulty in solving the model [M2-2] is the nonlinear part in objective (2-2). Two key techniques are applied to this nonlinear part. Specifically, the first one focuses on $\sum_{r\in R}\beta_r$ in the denominator. According to constraint (2-11), the number of ships deployed on route r, denoted by $\beta_r^{\min}$, is at least $\beta_r^{\min}=\left\lceil\left(\sum_{i\in I_r}\frac{l_{ri}}{\overline{v}}+\sum_{i\in I_r'}\frac{\min(l_{ri},l_{ri}')}{\overline{v}}+t_r\right)/168\right\rceil$ (recall that $\overline{v}$ represents the maximum speed of ships on ship routes). Because constraints (2-3) guarantee that at most s_r ships could be deployed on route r, the value of $\sum_{r\in R}\beta_r$ ranges from $\sum_{r\in R}\beta_r^{\min}$ to $\sum_{r\in R}s_r$, which means we can directly enumerate the number of ships deployed on all ship routes. The other one is $\sum_{i\in I_r'}m_{ri}[l_{ri}\gamma_{ri}+l_{ri}'(1-\gamma_{ri})]$. In most cases, not all routes need to be reoptimized in terms of voyage option because these routes do not contain voyages across Asia and Europe. Even if all routes need to be reoptimized in terms of voyage option, the total number of voyage options on a single route is $|I_r'|$, which means there are $2^{|I_r'|}$ permutations of the values

of γ_{ri} ($\forall r \in R, i \in I_r'$) for route r. Moreover, the value of $|I_r'|$ is either 0 or 2 because in real life, a liner route is either for a certain continent, or it only crosses Asian and European ports twice. Hence, the number of permutations is significantly small, and we can directly enumerate all permutations.

Algorithm 2-1. Framework of the proposed exact algorithm for solving model [M2-2]

$x \leftarrow \sum_{r \in R} \beta_r^{\min}$ // x records the number of ships deployed on all ship routes
$\mathrm{OBJ}^* \leftarrow \infty$ //OBJ^* records the incumbent objective function value of model [M2-2]
$(x, \gamma_{ri}, \forall r \in R, i \in I_r')^* \leftarrow$null //$(x, \gamma_{ri}, \forall r \in R, i \in I_r')^*$ records the incumbent values of corresponding variables in [M2-2]
While $x \leq \sum_{r \in R} s_r$ **do**
  Add constraint $\sum_{r \in R} \beta_r = x$ to model [M2-2]
  Obtain $2^{|I_1'|} \times 2^{|I_2'|} \times \cdots \times 2^{|I_{|R|}'|}$ permutations of $(\underbrace{\gamma_{1,1}, \gamma_{1,|I_1'|}}_{\text{route 1}}, \underbrace{\gamma_{2,1}, \gamma_{2,|I_2'|}}_{\text{route 2}}, \cdots, \underbrace{\gamma_{|R|,1}, \gamma_{|R|,|I_{|R|}'|}}_{\text{route } |R|})$
  $n \leftarrow 1$ //n is a counting number
  While $n \leq 2^{|I_1'|} \times 2^{|I_2'|} \times \cdots \times 2^{|I_{|R|}'|}$ **do**
    Solve the updated model by Gurobi with given values (γ_{ri}, $\forall r \in R, i \in I_r'$) of the n^{th} permutation
    If model is feasible **then**
      If $\mathrm{OBJ} < \mathrm{OBJ}^*$ **then** // OBJ records the current objective function value obtained by Gurobi
        $(x, \gamma_{ri}, \forall r \in R, i \in I_r')^* \leftarrow (x, \gamma_{ri}, \forall r \in R, i \in I_r')$
        $\mathrm{OBJ}^* \leftarrow \mathrm{OBJ}$
      End if
    End if
    $n \leftarrow n + 1$
  End while
  Delete constraint $\sum_{r \in R} \beta_r = x$ from model [M2-2]
  $x \leftarrow x + 1$
End while
Solve model [M2-2] by Gurobi with given $(x, \gamma_{ri}, \forall r \in R, i \in I_r')^*$
Return the objective value and values of the variables

2.4 COMPUTATIONAL EXPERIMENTS

In order to evaluate the efficiency of the proposed algorithm, this chapter performs a large number of computational experiments on a laptop (4 CPU cores, 1.6 GHz, Memory 8 GB). The mathematical models and algorithms proposed in this chapter are implemented in Gurobi 9.0.1 (Anaconda, Python). This section first summarizes the setting of our parameters in Section 2.4.1, validates the proposed algorithm in Section 2.4.2 and describes sensitivity analyses to seek managerial insights in Section 2.4.3.

2.4.1 Experimental setting

Sailing distance data, including l_{ri} and l'_{ri}, used in this study were obtained from the standard instances of LINER-LIB (Brouer et al., 2014). The value of the weekly fixed operating cost, i.e., o, is set to 180,000 USD, which is in line with the setting used in previous studies (Alharbi et al., 2015; Zhen et al., 2019a). In real life, main and auxiliary engines of a ship may use the same type of fuel, such as liquefied natural gas (LNG). Therefore, this chapter assumes that main and auxiliary engines use the same type of fuel when calculating fuel costs of the main and auxiliary engines for the sake of simplicity in the computational experiments. Therefore, unit prices of fuels (i.e., a_1 and a_2) are set to 544.5 USD/ton because the average price of very low sulfur fuel oil (VLSFO) in global 20 ports in 2021 is 544.5 USD/ton (S&B, 2022). For the sake of simplicity, a ship can only adjust its speeds by at least one knot in this chapter. The minimum and maximum values of sailing speed (i.e., $\underline{v}$ and $\overline{v}$) are set to 8 and 22 knots, respectively, which are also consistent with the settings used in related works (Wang et al., 2015; Zhen et al., 2020). The values of c_1, c_2 and c_3 are set to 0.00022, 2.5506 and 0.2072, respectively, which are consistent with the settings in related studies (Wang et al., 2015; Meng et al., 2016). The value of the total duration, i.e., t_r, that a ship dwells at all ports of call on ship route r is randomly selected from $[24 \times (|I_r| + |I'_r|), 48 \times (|I_r| + |I'_r|)]$. The value of s_r (i.e., the maximum number of ships that can be deployed on ship route r) depends on the length of one cycle time, and it is set to 4 for regional ship routes or 10 for intercontinental shipping routes. The amount of CO_2 released by a ship when burning one ton of VLSFO, i.e., g, is set to 3.15 tons, which is in line with the realistic data from Lloyd's (2021). Some other parameters are generated by sampling from some normal distributions. Specifically, values of Suez Canal toll fee (i.e., q_r) of a ship on all routes are uniformly distributed over (400,000, 700,000) (USD/ship), which is in line with actual Suez Canal toll fees (HKTDC, 2020). The average value of daily fuel consumption for the auxiliary engines (e_r) on all routes is set to 3 tons per day (normal distribution with standard deviation 0.5). The average value of cargo load (m_{ri}) on all legs is set to 180,000 tons (normal distribution with standard deviation 3000), and the value of actual displacement (d_{ri}) on all legs is set to $m_{ri} + 20{,}000$ tons.

2.4.2 Performance of the algorithm

This chapter used the proposed exact algorithm to solve the model [M2-2] and conducted 11 sets of numerical experiments with different route compositions, which are summarized in Table 2-2. We first fix $\lambda = 0.5$ and record computational results, including objective function value (OBJ_T), CPU running time (Time) and selected voyage option (Voyage option) in Table 2-3. Since the difference between the two objective function values in our model is very large, we normalize these two objective functions by dividing them by their respective maximum values. To obtain the maximum values, we set λ (i.e., the weighting factor for the bi-objective programming) to 0 and solve all computational experiments of the model [M2-2] to get the maximum objective function value $OBJ_1 = 15148529.7881$. Similarly, we set λ to 1 and solve all computational experiments of the model [M2-2] to get the maximum objective function value $OBJ_2 = 0.3384$.

Table 2-2 Summary of seven routes.

Route ID	Port rotation (city)
1	Kaohsiung→Tokyo→Nagoya→Kaohsiung
2	General Santos City→Manila→Singapore→General Santos City
3	Hong Kong→Xiamen→Kaohsiung→Manila→Hong Kong
4	Kaohsiung→Keelung→Shanghai→Tanjung Pelepas→Jakarta→Kaohsiung
5	Laem Chabang→Colombo→Rotterdam→Hamburg→Singapore→Laem Chabang
6	Qingdao→Shanghai→Hong Kong→Singapore→Rotterdam→Singapore→ Qingdao
7	Kaohsiung→Hong Kong→Singapore→Rotterdam→Singapore→Xiamen→ Kaohsiung

From Table 2-3, we can see that the computing time increases with more routes, which is intuitive because more routes will bring more decision variables and constraints. Since the computing time of six routes is quick enough, case 10 is used for the following numerical experiments. The Suez Canal route is chosen in all experiments. This is due to the fact that the Suez Canal route is more popular on trips because it saves more sailing time. Our algorithm has good performance because it can solve the numerical experiment with seven ship routes and 32 legs within four minutes, which means our algorithm can be applied well to real problems and quickly provides optimal solutions for liner companies.

Table 2-3 Computational results of the basic analysis.

Case ID	Route ID	OBJ_T	Time (s)	Voyage option
1	1, 5	0.53	1.20	Suez Canal
2	2, 6	0.61	1.51	Suez Canal
3	3, 5, 6	0.52	13.34	Suez Canal
4	4, 5, 6	0.56	14.38	Suez Canal
5	2, 4, 5, 6	0.69	16.76	Suez Canal
6	3, 4, 5, 6	0.70	18.54	Suez Canal
7	1, 3, 4, 5, 6	0.79	20.79	Suez Canal
8	2, 3, 4, 5, 6	0.84	24.40	Suez Canal
9	1, 2, 3, 5, 6	0.85	25.40	Suez Canal
10	1, 2, 3, 4, 5, 6	0.91	30.03	Suez Canal
11	1, 2, 3, 4, 5, 6, 7	0.94	222.25	Suez Canal

2.4.3 Sensitivity analyses

The impact of λ on the bi-objective programming is first described in this section. The value of λ ranges from 0 to 1. Table 2-4 shows the normalized objective function value of model [M2-2] (OBJ_T), the total weekly cost value (OBJ_1), the average EEOI value of all deployed ships on all routes (OBJ_2), the total number of deployed ships ($\sum_{r\in R}\beta_r$), the selected voyage option (Voyage option), and the computing time (Time). It is obvious that OBJ_1 decreases with increasing λ, which is reasonable because a larger λ indicates a larger weight on OBJ_1. However, OBJ_2 stays the same at the beginning, then goes down and finally goes up. In addition, the total number of deployed ships decreases as the value of λ increases. Finally, the change of the value of λ does not affect the voyage option, and the change of the value of λ has no obvious effect on the solution time. Therefore, with increasing λ (i.e., larger weight on the minimization of the total weekly cost), fewer ships are needed, which means that each deployed ship sails at a higher speed and releases more CO_2 (i.e., higher EEOI value). However, since the average EEOI value of all deployed ships on all routes is relatively small, the increase in the λ value in the early stage has no proportional effect on the second objective function value, i.e., OBJ_2.

We next studied the impact of unit price of fuel on the operation decisions. According to S&B (2022), the lowest and highest prices of VLSFO in global 20 ports from January 01, 2020, to July 14, 2022, are 211.25 USD/ton, and 1120.50 USD/ton, respectively. Hence, we set the value of a from 200 to 1,200 USD/ton to investigate its influence. Relevant results, including OBJ_T, OBJ_1, OBJ_2, $\sum_{r\in R}\beta_r$ and Voyage option, are presented in Table 2-5. In order to make the result more intuitive, we also gi-

Table 2-4 Impact of the weighting factor λ on the bi-objective programming.

λ	OBJ_T	OBJ_1 (USD)	OBJ_2 (g/ton/n mile)	$\sum_{r\in R}\beta_r$	Voyage option	Time (s)
0.0	0.9460	11349298.0951	0.3592	36	Suez Canal route	32.85
0.1	0.9514	11349298.0951	0.3592	36	Suez Canal route	31.37
0.2	0.9568	11349298.0951	0.3592	36	Suez Canal route	31.39
0.3	0.9622	11349298.0951	0.3592	36	Suez Canal route	33.15
0.4	0.9676	11349298.0951	0.3592	36	Suez Canal route	32.88
0.5	0.9572	11156852.8702	0.3536	35	Suez Canal route	32.13
0.6	0.9491	10967201.7128	0.3505	34	Suez Canal route	32.25
0.7	0.9434	10789871.1308	0.3517	33	Suez Canal route	31.02
0.8	0.9352	10619882.8389	0.3542	32	Suez Canal route	30.75
0.9	0.9311	10500058.7455	0.3737	31	Suez Canal route	31.25
1.0	0.9201	10442771.8214	0.3796	30	Suez Canal route	28.62

Notes: (1) "OBJ_T," "OBJ_1," "OBJ_2" and "$\sum_{r\in R}\beta_r$" represent the normalized OBJ value of model [M2-2], total weekly cost value, average EEOI value of all deployed ships on all routes and the total number of deployed ships, respectively. (2) "Voyage option" represents the voyage selection of deployed ships across Asian and European ports, i.e., Suez Canal route or Cape of Good Hope route. (3) "Time" represents CPU running time (s).

ve Figure 2-2, whose abscissa is the fuel price, and the primary and secondary ordinate axes are OBJ_1 and OBJ_2, respectively. When the unit price of fuel increases, both OBJ_T and OBJ_1 increase because the weekly fuel cost increases, but OBJ_2 is not influenced by fuel price. In addition, changes in the fuel price do not affect fleet deployment and voyage option decisions. The above observations are reasonable because changes in the unit price of fuel do not cause changes in fleet deployment strategies and sailing speeds, resulting in no changes in CO_2 emissions and no changes in the value of the second objective function. However, the continuous increase in the unit price of fuel leads to an increase in the weekly fuel consumption cost, which eventually leads to an increase in the value of the first objective function.

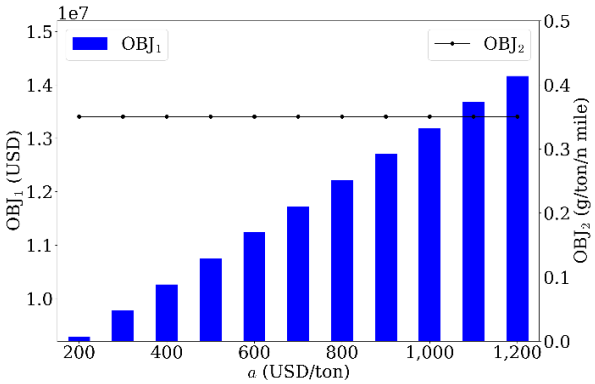

Figure 2-2 Comparison of objective values under different values of a.

Table 2-5 Impact of unit price of fuel on the operation decisions.

a (USD/ton)	$\mathrm{OBJ_T}$	$\mathrm{OBJ_1}$ (USD)	$\mathrm{OBJ_2}$ (g/ton/n mile)	$\sum_{r\in R}\beta_r$	Voyage option
200.00	0.8602	9,285,432.4798	0.3505	34	Suez Canal route
300.00	0.8860	9,773,609.3254	0.3505	34	Suez Canal route
400.00	0.9118	10,261,786.1709	0.3505	34	Suez Canal route
500.00	0.9376	10,749,963.0165	0.3505	34	Suez Canal route
600.00	0.9634	11,238,139.8621	0.3505	34	Suez Canal route
700.00	0.9892	11,726,316.7077	0.3505	34	Suez Canal route
800.00	1.0150	12,214,493.5533	0.3505	34	Suez Canal route
900.00	1.0408	12,702,670.3988	0.3505	34	Suez Canal route
1000.00	1.0666	13,190,847.2444	0.3505	34	Suez Canal route
1100.00	1.0924	13,679,024.0900	0.3505	34	Suez Canal route
1200.00	1.1183	14,167,200.9356	0.3505	34	Suez Canal route

Notes: (1) "$\mathrm{OBJ_T}$," "$\mathrm{OBJ_1}$," "$\mathrm{OBJ_2}$," and "$\sum_{r\in R}\beta_r$" represent the normalized OBJ value of model [M2-2], total weekly cost value, average EEOI value of all deployed ships on all routes and the total number of deployed ships, respectively. (2) "Voyage option" represents the voyage selection of deployed ships across Asian and European ports, i.e., Suez Canal route or Cape of Good Hope route.

Next, we discuss the impact of Suez Canal toll fee per ship on the operation decisions. According to HKTDC (2020), Suez Canal toll fees for a ship range from 400,000 to 700,000 USD. Hence, we set the Suez Canal toll fee for a ship from 350,000 to 750,000 USD/ship to investigate its influence. Relevant results, including $\mathrm{OBJ_T}$, $\mathrm{OBJ_1}$, $\mathrm{OBJ_2}$, $\sum_{r\in R}\beta_r$ and Voyage option, are given in Table 2-6. In order to make the result more intuitive, we also give Figure 2-3, whose abscissa is the Suez Canal toll fee per ship, and the primary and secondary ordinate axes are $\mathrm{OBJ_1}$ and $\mathrm{OBJ_2}$, respectively. When the Suez Canal toll fee per ship increases, both $\mathrm{OBJ_T}$ and $\mathrm{OBJ_1}$ increase, but $\mathrm{OBJ_2}$ does not change with increasing q_r. In addition, changes in the Suez Canal toll fee per ship do not affect fleet deployment and voyage option decisions, which further makes the EEOI of each ship unchanged, as the ship's CO_2 emissions and mileage do not change. The above observations are reasonable because the weekly Suez Canal toll fee is small compared to the weekly fuel consumption and operating costs of deployed ships. Therefore, the increase in the Suez Canal toll fee per ship does not lead to changes in fleet deployment, sailing speeds and voyage planning.

Table 2-6 Impact of Suez Canal toll fee per ship on the operation decisions.

q_r (USD/ship)	$\mathrm{OBJ_T}$	$\mathrm{OBJ_1}$ (USD)	$\mathrm{OBJ_2}$ (g/ton/n mile)	$\sum_{r\in R}\beta_r$	Voyage option
350,000.00	0.8775	10,042,966.9490	0.3289	34	Suez Canal route
400,000.00	0.8881	10,242,966.9490	0.3289	34	Suez Canal route
450,000.00	0.8986	10,442,966.9490	0.3289	34	Suez Canal route
500,000.00	0.9092	10,642,966.9490	0.3289	34	Suez Canal route
550,000.00	0.9198	10,842,966.9490	0.3289	34	Suez Canal route
600,000.00	0.9304	11,042,966.9490	0.3289	34	Suez Canal route
650,000.00	0.9409	11,242,966.9490	0.3289	34	Suez Canal route
700,000.00	0.9515	11,442,966.9490	0.3289	34	Suez Canal route
750,000.00	0.9621	11,642,966.9490	0.3289	34	Suez Canal route

Notes: (1) "$\mathrm{OBJ_T}$," "$\mathrm{OBJ_1}$," "$\mathrm{OBJ_2}$," and "$\sum_{r\in R}\beta_r$" represent the normalized OBJ value of model [M2-2], total weekly cost value, average EEOI value of all deployed ships on all routes and the total number of deployed ships, respectively. (2) "Voyage option" represents the voyage selection of deployed ships across Asian and European ports, i.e., Suez Canal route or Cape of Good Hope route.

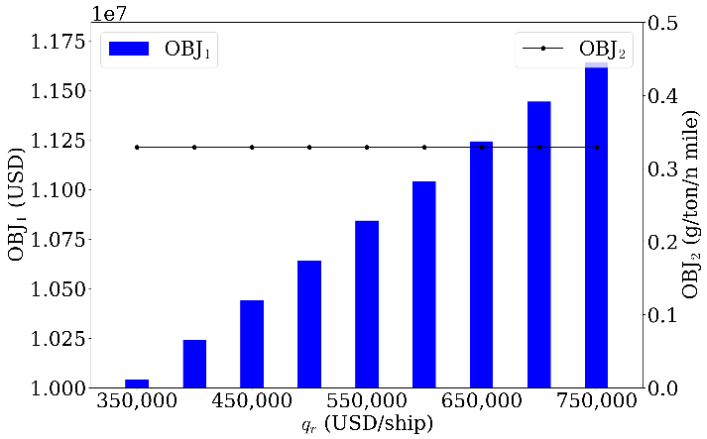

Figure 2-3 Comparison of objective values under different values of q_r.

In the basic experiment, the value of the weekly fixed operating cost (o) is set to 180,000 USD. However, weekly operating costs may double several times due to outbreaks and other reasons. To analyze the impact of weekly fixed operating cost on the operation decisions, we set the value of o from 150,000 USD to 390,000 USD. Relevant results, including $\mathrm{OBJ_T}$, $\mathrm{OBJ_1}$, $\mathrm{OBJ_2}$ $\sum_{r\in R}\beta_r$ and Voyage option are given in Table 2-7. In order to make the result more intuitive, we also give Figure 2-4, whose abscissa is the weekly operating cost, and the primary and secondary ordinate axes are $\mathrm{OBJ_1}$ and $\mathrm{OBJ_2}$, respectively. When the weekly operating cost increases, all of $\mathrm{OBJ_T}$, $\mathrm{OBJ_1}$ and $\mathrm{OBJ_2}$ increase, but $\mathrm{OBJ_2}$ remains unchanged in the three intervals [150,000, 240,000], [270,000, 300,000] and [330,000, 390,000]. In addition, changes in the

weekly fixed operating cost directly influence fleet deployment but do not affect voyage option decision. The above observations are reasonable because the weekly fixed operating cost accounts for a large proportion of the total weekly cost. The continuous increase in the weekly fixed operating cost causes liner companies to reduce the number of deployed ships, which causes ships to sail at higher speeds to maintain the weekly arrival pattern. Moreover, high speeds of deployed ships cause more CO_2 emissions.

Table 2-7 Impact of weekly fixed operating cost on the operation decisions of ship fleets.

o (USD)	OBJ_T	OBJ_1 (USD)	OBJ_2 (g/ton/n mile)	$\sum_{r\in R}\beta_r$	Voyage option
150,000.00	0.8952	9,947,201.7128	0.3505	34	Suez Canal route
180,000.00	0.9491	10,967,201.7128	0.3505	34	Suez Canal route
210,000.00	1.0030	11,987,201.7128	0.3505	34	Suez Canal route
240,000.00	1.0569	13,007,201.7128	0.3505	34	Suez Canal route
270,000.00	1.0980	13,759,871.1308	0.3517	33	Suez Canal route
300,000.00	1.1503	14,749,871.1308	0.3517	33	Suez Canal route
330,000.00	1.1884	15,419,882.8389	0.3542	32	Suez Canal route
360,000.00	1.2392	16,379,882.8389	0.3542	32	Suez Canal route
390,000.00	1.2899	17,339,882.8389	0.3542	32	Suez Canal route

Notes: (1) "OBJ_T," "OBJ_1," "OBJ_2" and "$\sum_{r\in R}\beta_r$" represent the normalized OBJ value of model [M2-2], total weekly cost value, average EEOI value of all deployed ships on all routes and the total number of deployed ships, respectively. (2) "Voyage option" represents the voyage selection of deployed ships across Asian and European ports, i.e., Suez Canal route or Cape of Good Hope route.

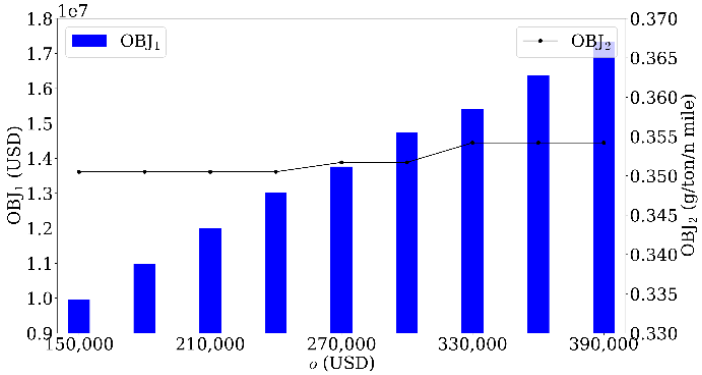

Figure 2-4 Comparison of objective values under different values of o.

Finally, we investigate the impact of cargo load on the operation decisions. In the basic experiment, the average value of cargo load (m_{ri}) is set to 180,000 tons (normal distribution with standard deviation 3,000). Hence, we set the average value of cargo load in each leg from 80,000 to 240,000 (normal distribution with standard

deviation 3,000) to investigate its influence. Relevant results, including $\mathrm{OBJ_T}$, $\mathrm{OBJ_1}$, $\mathrm{OBJ_2}$, $\sum_{r\in R}\beta_r$ and Voyage option, are given in Table 2-8. In order to make the result more intuitive, we also give Figure 2-5, whose abscissa is the cargo load in each leg, and the primary and secondary ordinate axes are $\mathrm{OBJ_1}$ and $\mathrm{OBJ_2}$, respectively. When the cargo load in each leg increases, $\mathrm{OBJ_T}$ and $\mathrm{OBJ_1}$ increase, but $\mathrm{OBJ_2}$ and the number of deployed ships decrease. However, voyage option decision is not influenced by changes in the cargo load. The above observations are reasonable because, with the increase in the cargo load, the product of the ship's cargo transported and the total distance over a week becomes larger. Although the ship sails at a higher speed due to the fewer deployed ships, the increase in the product of the ship's cargo transported and total distance over a week has a more significant impact on the expected EEOI value of all deployed ships than the increase in sailing speeds. Therefore, the average EEOI value of all deployed ships increases significantly with the increase in cargo load.

Table 2-8 Impact of cargo load in each voyage on the operation decisions.

m_{ri} (ton)	$\mathrm{OBJ_T}$	$\mathrm{OBJ_1}$ (USD)	$\mathrm{OBJ_2}$ (g/ton/n mile)	$\sum_{r\in R}\beta_r$	Voyage option
80,000.00	1.3500	10,919,422.4394	0.7334	35	Suez Canal route
100,000.00	1.2115	10,978,604.3255	0.5990	35	Suez Canal route
120,000.00	1.1185	11,030,417.9005	0.5082	35	Suez Canal route
140,000.00	1.0375	10,887,008.8904	0.4385	34	Suez Canal route
160,000.00	0.9879	10,928,874.5838	0.3892	34	Suez Canal route
180,000.00	0.9491	10,967,201.7128	0.3505	34	Suez Canal route
200,000.00	0.9180	11,002,602.1327	0.3192	34	Suez Canal route
220,000.00	0.8925	11,035,537.2494	0.2934	34	Suez Canal route
240,000.00	0.8713	11,066,364.2305	0.2717	34	Suez Canal route

Notes: (1) "$\mathrm{OBJ_T}$," "$\mathrm{OBJ_1}$," "$\mathrm{OBJ_2}$" and "$\sum_{r\in R}\beta_r$" represent the normalized OBJ value of model [M2-2], total weekly cost value, average EEOI value of all deployed ships on all routes and the total number of deployed ships, respectively. (2) "Voyage option" represents the voyage selection of deployed ships across Asian and European ports, i.e., Suez Canal route or Cape of Good Hope route.

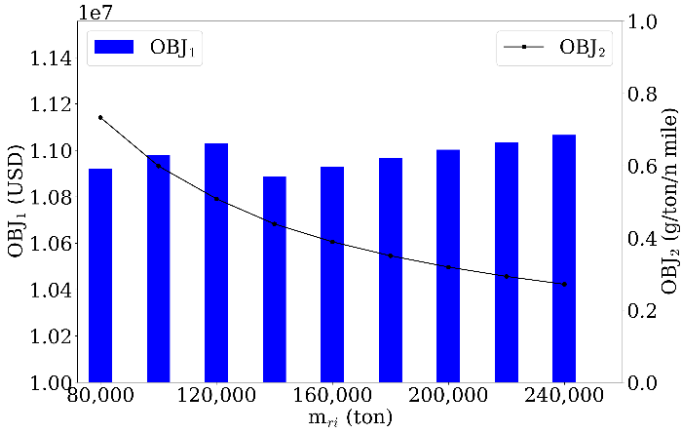

Figure 2-5 Comparison of objective values under different values of m_{ri}.

In summary, this chapter investigates the impact of λ on the bi-objective programming and the impacts of unit price of fuel, Suez Canal toll fee per ship, weekly fixed operating cost and cargo load on the operation decisions. Specifically, with increasing λ (larger weight on the minimization of the total weekly cost), fewer ships are needed, which means that each deployed ship sails at a higher speed and releases more CO_2 (i.e., higher EEOI value). In addition, the increase in the λ value in the early stage has no significant effect on the second objective function value. For the impact of unit price of fuel on the operation decisions, if changes in the unit price of fuel do not cause changes in fleet deployment strategies and sailing speeds, the amount of CO_2 emissions and the expected EEOI value of all deployed ships will stay the same. However, the continuous increase in the unit price of fuel leads to an increase in the weekly fuel consumption cost, which eventually leads to an increase in the total weekly cost. For the impact of Suez Canal toll fee per ship on the operation decisions, since the weekly Suez Canal toll fee is less than the weekly fuel consumption and operating costs of deployed ships, the increase in the Suez Canal toll fee per ship does not lead to changes in fleet deployment, sailing speeds and voyage options. However, for the impact of the weekly fixed operating cost on the operation decisions, since the weekly fixed operating cost accounts for a large proportion of the total weekly cost, the continuous increase in the weekly fixed operating cost causes liner companies to reduce the number of deployed ships and causes ships to sail at higher speeds. Finally, for the impact of cargo load on the operation decisions, with the increase in the cargo load, the increase in the product of the ship's cargo transported and total distance over a week has a more significant impact on the expected EEOI value of all deployed ships

than the increase in sailing speeds. Therefore, the average EEOI value of all deployed ships increases significantly with the increase in cargo load.

2.5 SUMMARY

The existing literature lacks research on the integrated optimization problem of fleet deployment, voyage planning and speed optimization with consideration of the influences of sailing speed, displacement and voyage option on fuel consumption. To fill this research gap, this chapter formulates a nonlinear MIP model capturing all these elements and designs a tailored exact algorithm for the model.

Chapter 3: How to operate ship fleets under uncertainty[2]

This chapter focuses on one of the most important practical issues that liner companies face: how to address a liner's multi-period heterogeneous fleet deployment problem in an uncertain shipping network considering fleet repositioning, ship chartering, demand fulfillment, and cargo allocation. A multistage stochastic programming model is developed for this critical problem.

3.1 INTRODUCTION

The shipping industry plays a vital role in international trade and the global economy (Fransoo and Lee, 2013; Roy et al., 2020). Supported by the recent global economic recovery, approximately 11 billion tons of goods are transported by ship in 2021 (UNCTAD, 2022). In particular, global containerized trade, which declines by 1.3% in 2020 and rebounds in 2021, reaches 165 million 20-foot equivalent units (TEUs) in 2021 (UNCTAD, 2022), which implies that the shipping industry is currently thriving. However, fluctuations in world trade and unexpected incidents including pandemics bring great uncertainty to the shipping market. Hence, for liner companies, how to operate ship fleets under uncertainty is particularly important.

For a liner company, operating ship fleets involves many intertwined decisions, such as the number of heterogeneous ships (categorized by their load capacities) deployed on each route, which is related to the specific sailing sequence of these ships on each route and to the shipping demands. Managers in the liner company also need to determine whether to charter in or out ships when there is a deficit or a surplus in some ship types, how to reposition ship fleets between different ship routes, and whether to fulfill the transportation demand in the current shipment period or postpone it to next period. Operating ship fleets under uncertainty is already an intractable problem (Christiansen et al., 2013); the above-intertwined decisions further complicate the problem.

[2] Wu, Y., Wang, S., Zhen, L., Laporte, G., Tan, Z., Wang, K., 2023. How to operate ship fleets under uncertainty. *Production and Operations Management* 32(10): 3043–3061.

Uncertainty in the shipping market mainly stems from the changing trends in the world economy caused by seasonal demand changes and unexpected incidents. Moreover, UNCTAD projections point out that an asymmetric recovery, logistical bottlenecks, and soaring costs have further heightened uncertainty (UNCTAD, 2022). Hence, the demand structure may change greatly over a long period of time. For example, affected by the abrupt outbreak of COVID-19, container throughput at the Port of Shanghai from January to April 2020 fell by 8.4% year on year (CWTN, 2021), which inevitably caused changes in the shipping network.

Liner companies, therefore, have to adjust their ship fleets every few months to remain competitive, in response to uncertainty in shipping demands. The uncertain future may contain plenty of possible scenarios; intertwined decisions of demand fulfillment and allocation need to be made for every possible scenario in each time period of the planning horizon. A core long-term decision is how to deploy a heterogeneous ship fleet in a shipping network with uncertain demand. When optimizing the operation plan of ship fleets, liner companies need careful evaluation and decision supports from scientific methodologies, e.g., multistage decision models, to comprehensively plan the deployment of ship fleets and their repositioning operations to the deployed routes under uncertainty to compete in the growing market. However, throughout the shipping liner industry, the planning of networks, including the construction of routes and fleet movements, is still primarily performed manually, and the fleet repositioning cost is rarely factored into liner shipping models (Wang, 2013). Hence, this chapter proposes a multistage fleet operation optimization model, which involves the first-stage decisions of determining the number of ships of different types deployed on each route, the number of ships of different types chartered in and out, and the ship type selected for each round trip on each route; and the decisions in the following stages of determining the numbers of accepted, delayed, and shipped containers for all origin-destination (O-D) pairs in each time period (one time period corresponds to one stage). The objective of this decision model is to maximize the expected total net profit earned by the liner company during the planning horizon, which consists of five terms: the expected operational revenue, the ship repositioning cost, the operating costs of all deployed ships, the rental cost of charter-in ships, and the total revenue of charter-out ships.

This chapter is motivated by the above-mentioned real-world challenge and contributes to the shipping operations management-related literature by proposing an optimization model and a Benders-based branch-and-cut (BBC) algorithm with several acceleration strategies. This chapter provides liner companies with scientific methods to integrate fleet repositioning, ship chartering, demand fulfillment, and cargo allocation into fleet deployment optimization to balance the cost-profit trade-off. More specifically, a mixed-integer linear programming (MILP) model is proposed for a liner's multi-period heterogeneous fleet deployment problem (FDP) in an uncertain shipping network considering fleet repositioning, ship chartering, demand fulfillment, and cargo allocation. This problem is NP-hard, and in this chapter, we aim to propose an exact and efficient algorithm to solve it on a practical scale.

While leveraging real-world shipping routes, computational experiments in different problem scales are conducted to evaluate the model and the performance of the proposed BBC algorithm. The impacts of the acceleration strategies are then investigated. Moreover, the impacts of uncertainty on the shipping operations management are investigated, showing that multistage stochastic programming can lead to higher profit than using two-stage stochastic programming or deterministic programming. An intensive analysis of why multistage stochastic programming can lead to better solutions is also conducted. Lastly, three practical questions regarding the driver analysis of liner company profitability, the benefit analysis of adaptive fleet sizes, and the influence of pandemic diseases on liner shipping are discussed. Managerial insights are obtained to guide the operations of ship fleets under uncertainty for liner companies according to the computational experiments. We believe that the emergence of the novel models and algorithms, especially the quantitative decision methodology, offers liner companies an opportunity to improve their decision efficiency in an uncertain maritime transportation market.

The remainder of this chapter is organized as follows. Related works are reviewed and discussed in Section 3.2. Section 3.3 elaborates on the problem background. Section 3.4 proposes a multistage stochastic programming model for operating heterogeneous ship fleets under uncertainty. A BBC algorithm with two acceleration strategies is developed in Section 3.5. Section 3.6 reports the computational experiments. Summaries are then outlined in Section 3.7.

3.2 LITERATURE REVIEW

This chapter focuses on the FDP and subsequently designs an exact algorithm to solve it. Thus, this section reviews the streams of related literature from the following two perspectives: the FDP, and the design of exact algorithms for maritime-related problems. Readers interested in overviews of the above two streams of problems can refer to Christiansen et al. (2013), Meng et al. (2014), Lee and Song (2017), and Christiansen et al. (2020).

The first research stream is related to the FDP. As an essential planning problem in liner companies, the FDP assigns available fleets to predetermined voyages to maximize the total profit or to minimize the total expense. When assigning fleets to predetermined services, several aspects need to be considered. One of the most important aspects is ship chartering. Wang and Meng (2012a) proposed an MILP model for an FDP that allows a liner company to deploy its own and charter-in ships. Another important aspect is different types of fleets in a shipping network, which is a heterogeneous FDP. Wang et al. (2013) studied a heterogeneous FDP with the aim of minimizing the total cost while maintaining a service level under container demand uncertainty. Ng (2014) proposed a distribution-free integer programming model to optimally determine the number and type of fleets deployed on ship routes to minimize the total cost while ensuring that the capacity of fleets meets the shipment demand. Tierney et al. (2015) noted that the fleet repositioning problem (FRP) has received little attention in the literature related to the FDP and studied the FRP with the consideration of cargo flows. Xia et al. (2015) jointly planned the fleet deployment, speed optimization and cargo allocation to maximize the total profit of a liner company. Ng (2017) developed an MILP model for an FDP with the aim of minimizing the total cost containing the operating cost and the cost of charter-in ships minus the revenue of charter-out ships. Wetzel and Tierney (2020) integrated the FRP into the FDP to optimally determine fleet deployment and how to move ships to their routes. It should be noted that most of the literature on the FDP (e.g., Tierney et al., 2015; Kepaptsoglou et al., 2015; Zhen et al., 2019a) is based on homogeneous ships as this approximation simplifies the model and the analysis.

However, this chapter considers heterogeneous ships and allows different types of ships to be deployed on the same route, which makes our problem more realistic because liner companies often operate different types of ships and deploy ships

according to transport needs. Thus, Table 3-1 mainly reviews papers that consider heterogeneous ships. In addition, the majority of the reviewed works only consider deterministic issues. Even though a few papers consider uncertainty, they mainly use two-stage stochastic programming to deal with it. However, two-stage stochastic programming assumes that all information about uncertainty is realized after decisions on the first-stage problem are made, which may be outside some complex and realistic environments. In our problem, managers in liner companies usually only know the exact transport demand for one time period and probability distributions of demand for time periods immediately beyond decision time instead of knowing exact transport demands for all future time periods. Hence, to address the sequential realization of uncertainties, we use multistage stochastic programming in which uncertainty for a given stage is realized only after decisions of the previous stage are made. With regard to decision variables, the majority of reviewed works optimize cargo allocation, and a few consider other realistic issues, e.g., fleet repositioning and ship chartering. Hence, this chapter studies an integrated problem of fleet deployment, fleet repositioning, ship chartering, and demand fulfilment and allocation that allow container delay. Finally, few works offer exact algorithms for the proposed problem, but this study does. Besides, although some papers did not emphasize algorithmic design, they offered mathematical formulations such as novel MILP models by Wang and Meng (2012a), Ng (2014), and Ng (2017), as well as approximate solution approaches such as sample average approximation (SAA) by Wang et al. (2013).

The second topic considered in the related works is the design of exact algorithms for maritime problems. Many existing papers on maritime shipping, e.g., Brouer et al. (2014), Tierney et al. (2015), Xia et al. (2015), and Wetzel and Tierney (2020), use heuristics to solve the problems. However, this chapter develops an exact algorithm, so this section compares some algorithmic features of several representative works that design exact algorithms for maritime-related problems. Table 3-2 summarizes the comparison of exact algorithms proposed in the literature for maritime-related problems. Vis and Roodbergen (2009) studied a container terminal scheduling problem of container storage and retrieval and proposed a combination of the assignments in a bipartite network for parts and dynamic programming for the connections between these parts. Specifically, they used dynamic programming to determine the shortest tour and then designed a tailored algorithm to determine the

sequence of storage and retrieval requests. Engineer et al. (2012) developed a branch-price-and-cut algorithm for a maritime inventory-routing problem.

Table 3-1 Comparison with representative works on FDPs.

Paper	Fleet	Model	Num. of stages	Decisions (besides deployment)				Methodology
				Fleet repositioning	*Ship chartering*	*Cargo allocation*	***Others***	
Wang and Meng (2012a)	Hetero	Deter	N/A	√	√	√	Slot-purchasing, empty container repositioning	MILP
Wang et al. (2013)	Hetero	Stoch	Two		√	√	N/A	SAA
Ng (2014)	Hetero	Stoch	Two		√		N/A	MILP
Tierney et al. (2015)	Homo	Deter	N/A	√		√	Speed, empty equipment repositioning	Heuristic
Xia et al. (2015)	Hetero	Deter	N/A			√	Speed	Heuristic
Akyüz and Lee (2016)	Hetero	Deter	N/A			√	Speed, empty container repositioning	Exact
Ng (2017)	Hetero	Deter	N/A		√		N/A	MILP
Zhen et al. (2019a)	Homo	Stoch	Two			√	Speed, berth, yard allocation	Exact
Wetzel and Tierney (2020)	Hetero	Deter	N/A	√	√	√	Speed	Heuristic
This paper	Hetero	Stoch	Multi	√	√	√	Container delay	Exact

Notes: (1) "Homo" and "Hetero" denote homogeneous and heterogeneous fleet deployment, respectively. (2) "Deter" and "Stoch" denote deterministic model and stochastic model considering uncertainty, respectively. (3) "MILP" and "SAA" denote mixed-integer linear programming model and sample average approximation, respectively.

Dynamic programming is widely used to solve the mixed-integer pricing problem, and some acceleration strategies, including preprocessing, boundary constraints, and cuts (port capacity cuts, vessel capacity cuts, and timing cuts) are embedded in the algorithm. Akyüz and Lee (2016) embedded a column generation algorithm within the branch-and-bound algorithm to solve a simultaneous fleet deployment and container routing problem. They also applied a label-correcting algorithm to deal with the shortest path problem in the column generation subproblems. Xu and Lee (2018) developed an exact branch-and-bound algorithm for a continuous berth allocation problem. They obtained a new lower bound which they incorporated within a new heuristic adopting a best-fit strategy and new dominance

rules for pruning nodes to enhance the performance of the algorithm. Karsten et al. (2018) developed an exact algorithm based on Benders decomposition and column generation for a simultaneous optimization problem of ship sailing speed and container routing. They also incorporated warm start, valid inequalities, and callbacks within the algorithm. Wang et al. (2019) designed a branch-and-cut algorithm based on Benders decomposition for a single intercontinental service design problem. They added subtour elimination constraints, linear approximation, and valid cuts (symmetry cut, mixed integer knapsack cut, and Pareto-optimal Benders cuts) to the algorithm. Zhen et al. (2019a) designed a dynamic linearization algorithm for an integrated problem of fleet deployment and demand fulfillment. Wang and Meng (2020) used two decomposition methods (stage decomposition and scenario decomposition) to solve a mixed-integer programming model of a semi-liner shipping service design problem. Primal-dual acceleration and multiple-cut acceleration techniques were applied to enhance the performance of the algorithm. Lee et al. (2021) used a constraint generation approach with several pruning techniques for a two-stage robust optimization model in a liner service procurement problem with service schedules. In summary, the exact algorithm design in these papers is often based on two different methodologies to take advantage of their relative merits and supplemented by some acceleration techniques to improve the convergence of the algorithm.

In summary, the prevailing trend in the FDP is to consider heterogeneous ships, and the majority of existing studies on the heterogeneous FDP have not considered uncertain issues. To the best of our knowledge, this chapter is the only one that formulated the problem as a multistage stochastic programming model. Besides, this chapter integrates some operational decisions which are usually ignored in the existing literature, e.g., fleet repositioning, ship chartering, demand fulfillment, cargo allocation, and cargo delay, into the FDP because fleet repositioning and ship chartering problems belong to medium- to long-term decisions, which have a direct impact on liner companies' operations. Moreover, an exact algorithm based on Benders decomposition and branch-and-cut algorithms is developed to solve the proposed FDP. Two types of acceleration strategies, including approximate upper bound tightening inequalities and Pareto-optimal cuts, are applied to improve the performance of the proposed algorithm.

Table 3-2 Comparison on exact algorithms for solving maritime related problems.

Paper	Basic methodologies		Other tactics
	Primal	Secondary	
Vis and Roodbergen (2009)	DP	Tailored algorithm	N/A
Engineer et al. (2012)	BPC	DP	Preprocessing, boundary constraints, cuts
Akyüz and Lee (2016)	Branch-and-bound	CG	Label-correcting algorithm
Xu and Lee (2018)	Branch-and-bound	Best-fit heuristic	New lower bound, new dominance rules
Karsten et al. (2018)	BD	CG	Warm start, valid inequalities, callbacks
Wang et al. (2019)	BD	Branch-and-cut	Subtour elimination cut, linear approximation cut, and valid cuts
Zhen et al. (2019a)	Dynamic linearization	N/A	N/A
Wang and Meng (2020)	Stage decomposition	Scenario decomposition	Primal-dual, multiple-cut acceleration
Lee et al. (2021)	Constraint generation	N/A	Pruning techniques
This paper	BD	Branch-and-cut	Inequalities, Pareto-optimal cuts

Note: DP: dynamic programming, BPC: Branch-price-and-cut, BD: Benders decomposition, CG: Column generation.

3.3 PROBLEM BACKGROUND

This chapter is oriented toward liner operations management under uncertainty. From an academic perspective, a rigorous and complete title of the core problem in this chapter could be stated as a liner's multi-period heterogeneous FDP in an uncertain shipping network considering fleet repositioning, ship chartering, demand fulfillment, and cargo allocation. Before presenting a mathematical formulation for the problem, the following sections elaborate on the detailed features from five standpoints: (1) the shipping network with uncertainty, (2) the model's multistage feature for considering multi-period planning and multistage decision, (3) the heterogeneous fleet with different ship types, (4) the liner's fleet repositioning decision, and (5) the ship chartering when there is a deficit or a surplus in some ship types.

3.3.1 Shipping network with uncertainty

As one of the most common modes in container transport services, weekly service for a ship route means that the headway between two adjacent ships serving the same ship route is seven days. Suppose a liner company operates a set R of ship routes (services) that visit ports on a weekly shipping schedule to transport containers.

Figure 3-1 depicts an illustrative shipping network with three routes denoted by $R = \{1, 2, 3\}$. Each ship route has fixed port rotations, and the itinerary of each route forms a loop. To maintain a weekly service frequency, a fleet of ships instead of a single ship is generally deployed on each route in the service network. For example, it takes a ship three weeks to finish a round trip of ship route 2 in Figure 3-1 (a round trip is an itinerary of a ship route that forms a loop in practice), implying that a fleet of three ships is required to be deployed on route 2 to maintain a weekly service frequency. Then, denoting the number of ships deployed on route r by n_r, it is easy to understand that the total time for a ship completing the travel along a round trip of the route is $7n_r$ days. One fact that needs to be emphasized is that container ships visit ports of call weekly. In this case, the minimum decision-making time unit for liner companies is one week. Here, notice that the "weekly schedule for ships" is not an assumption but a practice. However, travel times are not affected by the weekly service frequency, so travel times required for each voyage leg do not need to be more than a week, and we only need to know in which week the ships visit the port. Secondly, the "time period" considered in this chapter is actually used to indicate the decision-making time points. That is, liner companies make decisions at the beginning of time period 0, 1, amongst others, but do not make decisions at other time points. Therefore, this chapter does allow the model to incorporate a voyage leg if its travel time is shorter than a week.

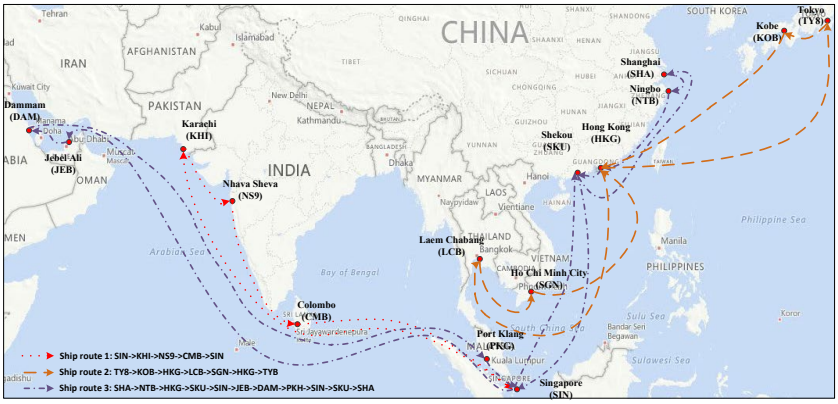

Figure 3-1 Example of a shipping network with three routes.

The liner company that operates the above shipping network earns revenue by transporting containers between each O-D pair indexed by (o, d), and the set of all O-D pairs is denoted by D. For each O-D pair, the liner company decides the number of containers to accept, which determines the corresponding revenue. In a period, liner company may accept more containers than it can transport as, e.g., it anticipates low

demand in subsequent periods. As a result, some container shipments are delayed and the company incurs a penalty cost.

Over a long planning horizon, container shipment demand constantly fluctuates instead of staying the same across different periods. For example, affected by the abrupt outbreak of COVID-19, the demand for face masks surged. Hence, considering a shipping network under container shipment demand uncertainty brings our problem closer to reality. In order to deal with this uncertainty, stochastic programming is utilized for the formulation of the problem. As is usual in stochastic programming formulations (Dong et al., 2015), uncertainty is represented by a finite set of scenarios, and each of which is composed of collective random outcomes for the demand of containers.

3.3.2 Multi-period planning and multistage decision

As a strategic decision, multi-period heterogeneous fleet deployment is often determined for a long planning horizon. Therefore, the external and internal environment inevitably changes under uncertainty, and managers in liner companies tend to divide the planning horizon into shorter time periods to depict the uncertainty at different periods. Whereas the decisions between adjacent time periods are also correlated, some postponed transport demands in one time period need to be fulfilled in the future time period. An example with two ship routes is shown in Figure 3-2. In order to maintain the weekly arrival pattern, three ships and two ships are deployed on ship routes 1 and 2, respectively. After the transport demand for one time period is realized, the liner company needs to determine the number of accepted containers to maximize the profit earned. However, some accepted containers may be postponed because of the capacity constraints, resulting in the corresponding penalty cost. This chapter allows containers to be delayed for multiple periods until the end of the planning horizon, which means that these delayed containers need to be shipped in or before the last time period of the planning period. Hence, how to determine the numbers of accepted, shipped, and delayed containers in each period to maximize the total profit is considered in this chapter.

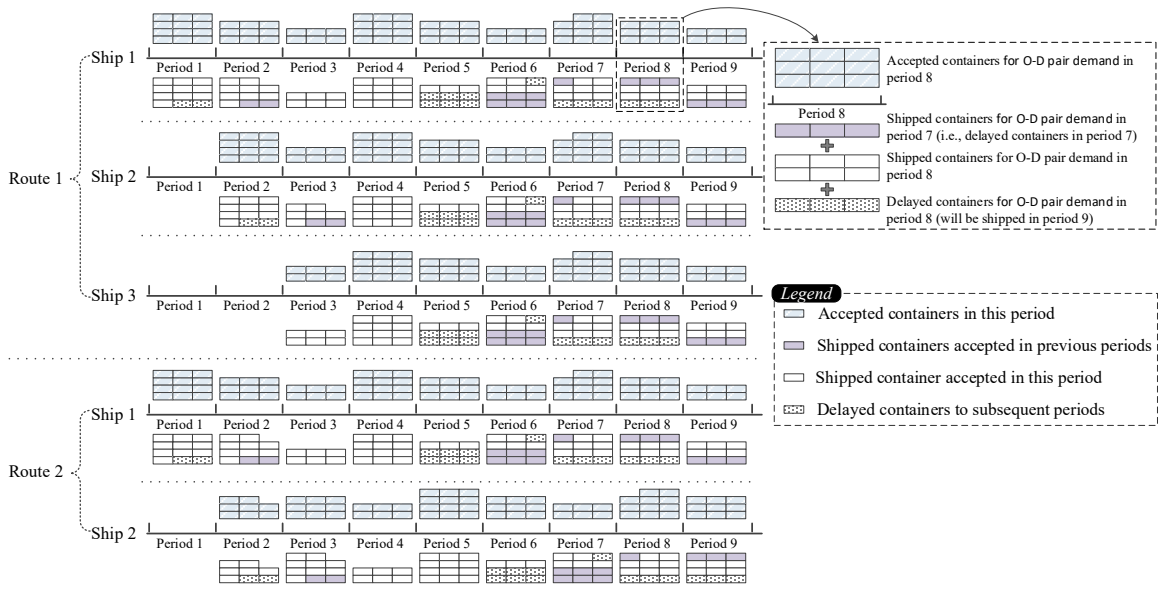

Figure 3-2 Multi-period container cargo fulfillment and allocation planning for one O-D pair.

Two-stage stochastic programming based on discrete probability distributions is widely adopted to tackle uncertain shipment demands. However, multistage stochastic programming may be more suitable to reflect the uncertain environment in this problem. The main difference between two-stage and multistage programming is demonstrated in Figure 3-3. Two-stage stochastic programming assumes that all information about uncertainty is realized after decisions of the first-stage problem have been made, which is not in line with our problem. In our problem, managers in liner companies usually only know the exact transport demand for one time period and probability distributions of demand in the time periods immediately following the moment of their decision instead of knowing the exact transport demand for all future time periods. Hence, we use multistage stochastic programming in which uncertainty for a given stage is realized only after the decision of the previous stage has been made.

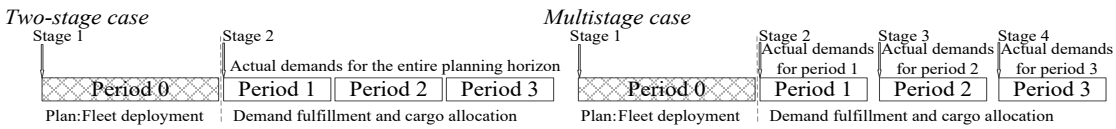

Figure 3-3 Difference between two-stage and multistage cases.

The specific difference between two-stage and multistage problems and the method of constructing scenarios for them are elaborated in Section 3.4.1. More explanations about Figure 3-3 are described below. Here, notice that stage 1 corresponds to period 0, and each of periods 1, 2,⋯ corresponds to one week. But stage

1 (i.e., period 0) is regarded as a few weeks before stage 2 (i.e., period 1) because liner companies usually design shipping services and advertise them for booking several months in advance (Maersk, 2022). Hence, fleet deployment decisions (including available ships of different types on all ship routes in the network, the sailing sequence of these deployed ships, and the numbers of charter-in and charter-out ships when there is a deficit or a surplus in some ship types) are determined only in the first stage (which is also period 0). At the end of period 0, all deployed ships including repositioned ships should be in place. In the following stages (i.e., from period 1), when the container shipment demands become realized, the model determines the numbers of accepted, delayed and shipped containers for each O-D pair in each time period under each scenario.

3.3.3 Heterogeneous ship fleets

A liner company usually owns heterogeneous ship fleets and therefore deploys different types of ships on each ship route (service). Hence, not restricting the deployment of the same type of ships on a ship route makes our problem more realistic. Moreover, many previous papers (e.g., Tierney et al., 2015; Kepaptsoglou et al., 2015; Zhen et al., 2019a) related to fleet deployment assume that deployed ships are homogenous on each route in terms of the capacity and cost structure, whereas this assumption does not always hold in practice because ships do not have the same capacity or cost (Wang, 2015). Besides, deploying heterogeneous ship fleets and homogenous ship fleets on a certain route can affect the transport capacity of the route. This effect and the container shipment demand uncertainty on a temporal dimension aggravate the gap between transport capacity and shipment demand. Hence, heterogeneous ship fleets are considered in this chapter, which is also in line with the setting in some existing papers (Wang, 2015).

This chapter classifies ship fleets into different ship types. We consider a set K of available ship types indexed by k and categorized by their load capacities and costs. We use the example from Figure 3-1 to discuss the ship types. Suppose the liner company owns several ships and deploys two 4000-TEU ships, three 8000-TEU ships, and four 4000-TEU ships on ship routes 1, 2, and 3, respectively, and one 4000-TEU ship owned by other shipping liners is idle at the Port of Singapore; hence, the set of all available types is $K = \{\text{type } 1 = 4000\text{- TEU ship}, \text{type } 2 = 8000\text{- TEU ship}\}$. Moreover, since the liner company normally operates a fleet of heterogeneous ships

on a given route, the specific sailing sequence of these ships is also important. The sailing sequence of heterogeneous ships on the route directly affects the transport capacity of each round trip of the route, which further restricts the transport demand fulfillment and the allocation of containers and influences the revenue of the company.

3.3.4 Fleet repositioning

The shipping industry operates in a competitive and dynamic environment where liner companies may adjust their shipping networks several times a year. By adjusting services in their networks, these liner companies may adapt to container shipment demand changes caused by seasonal variations, the COVID-19 pandemic, or other economic trends. To this end, liner companies generally add, remove or modify services from their networks, which inevitably requires reassignments of ships between different services of the company, namely, the FRP.

If a ship that used to serve a specific route is rescheduled to serve another route, then a repositioning cost caused by fuel consumption and lost revenue is needed. Repositioning a single ship can cost hundreds of thousands of US dollars (Tierney et al., 2015). Figure 3-4 shows an example of fleet repositioning. In Figure 3-4, the ship repositions from a phase-out service (dotted black line) to a phase-in service (dashed orange line). The repositioning path is represented by a solid green line. The figure shows that the phase-out happens in the Port of Singapore (SIN). After the phase-out, the ship sails to the Port of Ho Chi Minh City (SGN) and phases into the goal service, which results in a high repositioning cost. Although repositioning ships is an expensive activity due to potential losses in revenue and high fuel costs, rational fleet repositioning enables the networks to adapt to the global economy and remain competitive. Hence, optimizing how to reposition ships is of particular interest to the liner shipping industry.

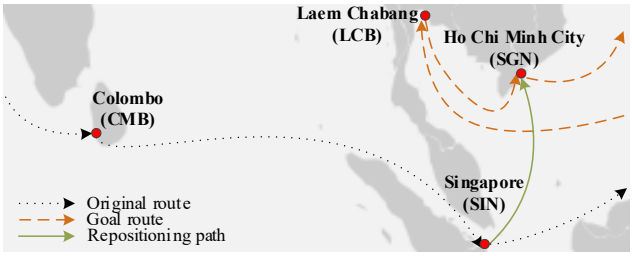

Figure 3-4 Fleet repositioning from an original route to a goal route.

3.3.5 Ship chartering

With regard to maritime cargo transport, ship chartering is one of the most commonly used methods. In order to take part in the seaborne trade, liner companies have to make significant investments in ships. However, not all liner companies have enough ships to meet the adjustment need of their shipping networks because the investment capital of container ships is extremely large. For this reason, liner companies may prefer to charter ships from other shipping liners rather than purchase new ships to cope with the increased container volume. Besides, when there is a surplus in some ship types, liner companies wish to charter out idle ships to other companies. It is, therefore, necessary to consider the FRP that allows ship chartering.

To explain the heterogeneous FRP with chartering more clearly, we use the example in Section 3.3.3 to characterize the repositioning of ships. Let H represent the set of all ship groups owned by the liner company and other shipping liners. Here, notice that ships in the same group are of the same ship type. And let H_1 and H_2 represent the subsets of ship groups owned by the liner company and other shipping liners, respectively. Hence, H_1 has three groups, i.e., $H_1 = \{h_1, h_2, h_3\}$, which are the 4000-TEU ships on route 1, 8000-TEU ships on route 2, and 4000-TEU ships on route 3; H_2 has only one group, i.e., $H_2 = \{h_4\}$, which is the 4000-TEU ship idle at the Port of Singapore. Let f_{hr} denote the repositioning cost for a ship in group h to route r. Obviously, a reasonable fleet repositioning plan can greatly reduce the rescheduling cost.

3.3.6 Summary of the problem

Before formulating the mathematical model for this problem, we make the following assumption. Both the number of containers to be transported and the number of ships to sail on a service to achieve a weekly frequency are defined in weekly terms, which follows industry practice (most liner services have a weekly frequency) and related studies (Xia et al., 2015).

In sum, the shipping network operated by a global liner company should be designed in response to the global economic trends and changes in cargo volumes. Liner companies, therefore, have to regularly adjust their service networks to remain competitive, thereby requiring liner companies reoperate ship fleets during the planning horizon. To deal with these complex and intertwined decisions, this chapter

investigates a liner's multi-period heterogeneous FDP in an uncertain shipping network considering fleet repositioning, ship chartering, demand fulfillment, and cargo allocation, which involves the first-stage decisions of determining the number of ships from each group deployed on all ship routes, the number of ships of different types deployed on each route, the number of ships of different types chartered in and out, and the ship type selected for each round trip on all routes, and the decisions in the following stages of determining the numbers of accepted, delayed, and shipped containers for all O-D pairs in each time period. The objective of the problem is to maximize the expected total net profit earned by the liner company during the planning horizon, which consists of five terms: the expected operational revenue, the operating cost of all deployed ships, the ship repositioning cost, the rental cost of charter-in ships, and the total revenue of charter-out ships. Sections 3.4 and 3.5 elaborate on the mathematical model for the problem and an exact algorithm for solving it, respectively.

3.4 MODEL FORMULATION

This section presents a multistage stochastic MILP model for the problem. Nonanticipativity constraints, which are a very important part of a multistage stochastic programming model, are first elaborated before formulating the model.

3.4.1 Multistage stochastic programming with nonanticipativity constraints

As explained in Section 3.3.2, two-stage stochastic programming assumes that all information about uncertainty in the whole planning horizon (multiple time periods) is realized after the decisions of the first-stage problem have been made, whereas multistage stochastic programming considers that uncertainty for a given time period (stage) is only realized after decisions of the previous time period (stage) have been made. It should be noted that stage 1 corresponds to period 0, in which fleet deployment is determined; the decisions in the planning horizon from period 1 to the last period are about operational-level plans for transport demand fulfillment and allocation.

As an intuitive representation of the branching process induced by the gradual observation of the stochastic progress, a scenario tree is usually used to construct scenarios in multistage problems. The left part of Figure 3-5 depicts an example with four periods and 10 scenarios to illustrate the scenario tree. One artificial root node, i.e., node 0, is in period 0, in which fleet deployment is determined. Three nodes (i.e.,

nodes 1–3) are in period 1. In period 2, four different realizations of uncertain demands, represented by nodes 4–7, become known. The above branching process goes on till the last period, i.e., period 3, where the outcome related to each leaf node in the last period in a unique path from the root to a leaf corresponds to a scenario, which results in a total of 10 scenarios. Hence, it is obvious that a scenario in a multistage stochastic programming model is a path from the root node to a leaf node. For multistage problems, nonanticipativity constraints must be added to ensure that the decisions in a certain period depend only on the data revealed up to that period but not on the information which will be realized in the future (Adulyasak et al., 2015). In other words, the decisions in a period of two different scenarios should be identical if the two scenarios share the same parent node in the scenario tree during the period. Here, let $\boldsymbol{y}_{t,s}$ represent decision variables that need be decided in period t under scenario s. For the example of the left part of Figure 3-5, the nonanticipativity constraints for periods 1–3 are summarized in the right part of Figure 3-5.

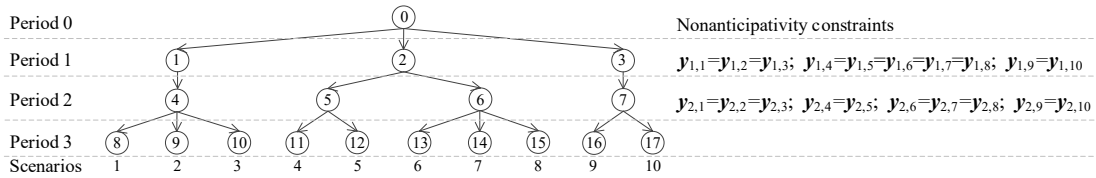

Figure 3-5 Illustration of a scenario tree and nonanticipativity constraints for multistage programming.

3.4.2 Mathematical model

A multistage stochastic programming model is formulated for this problem.

Sets and Indices:

R: set of ship routes in the shipping network, $r \in R$.

K: set of available ship types, $k \in K$.

R_k: subset of routes on which ships of type k can be deployed, $R_k \subset R$.

K_r: subset of ship types that can be deployed on route r, $K_r \subset K$.

H: set of all ship groups owned by the liner company and other shipping liners, $h \in H$; ships in the same group are of the same ship type.

H_1: subset of ship groups owned by the liner company, $H_1 \subset H$.

H_2: subset of ship groups owned by other shipping liners, $H_2 \subset H$.

D: set of all O-D pairs of ports that are traversed by all routes in the shipping network, $(o, d) \in D$.

T: set of time periods of the planning horizon starting from period 1, $t \in T$.

E_r: set of round trips that are operated on route r during the planning horizon, $e \in E_r$.

I_r: set of voyage legs of route r, $i \in I_r$.

S: set of scenarios, $s \in S$.

Z_+: set of non-negative integers.

Parameters:

n_r: number of ships deployed on ship route $r \in R$, which equals the number of periods to traverse the ship route by a deployed ship.

v_k: number of containers that can be carried by a ship of type k, which is the capacity of ships of type k.

$f_{h,r}$: repositioning cost for a ship in group $h \in H$ to route $r \in R$.

u_h: number of ships in group $h \in H$.

y_h: ship type of ships in group $h \in H$.

$c_{k,r}$: operating cost of completing the voyages during the planning horizon by a ship of type k deployed on route r.

g_k: rental cost of chartering in a ship of type k from other shipping liners.

m_k: revenue of chartering out a ship of type k to other shipping liners, $m_k < g_k$.

$q^s_{o,d,t}$: newly generated container shipment demand (number of containers) in period t at port o to be transported to port d under scenario s.

$l_{o,d}$: revenue generated by each accepted container for a specific O-D pair (o, d).

$p_{o,d}$: penalty cost per period incurred by each delayed container for a specific O-D pair (o, d).

$j_{r,e}$: index (i.e., sequence position in $\{1, \dots, n_r\}$) of the ship that operates the e^{th} round trip of route r.

$a_{r,e,i,o,d,t}$: binary, if O-D pair $(o,d) \in D$ demands to be shipped in period $t \in T$ at origin port o will be carried by a ship on voyage leg $i \in I_r$ by e^{th} round trip on route r, it equals 1; otherwise it equals 0.

w^s: probability of scenario s.

b_t^s: index of node in the scenario tree at period t related to scenario s.

Decision variables:

$\alpha_{h,r}$: integer, number of ships from group $h \in H$ deployed on route $r \in R$.

$\beta_{k,r}$: integer, number of ships of type $k \in K_r$ deployed on route $r \in R$.

$\pi_{k,r,j}$: binary, if a ship of type $k \in K_r$ is deployed on the j^{th} ($j \in \{1, \dots, n_r\}$) sequence position of route $r \in R$ (i.e., the j^{th} ship on route r belongs to type k), it equals 1; otherwise it equals 0.

$\theta_{o,d,t}^s$: continuous, number of accepted containers for the demand of O-D pair $(o,d) \in D$ accumulated in period $t \in T$ under scenario s.

$\varphi_{o,d,t}^s$: continuous, number of delayed containers for the demand of O-D pair $(o,d) \in D$ up to period $t \in T \cup \{0\}$ under scenario s, where by convention, $\varphi_{o,d,0}^s := 0$.

$\varepsilon_{o,d,t}^s$: continuous, number of shipped containers by deployed regular ships in the first stage for the demand of O-D pair (o,d) in period t (including both those accepted in period t and the delayed containers in previous periods) under scenario s.

$\tilde{\theta}_{o,d,t}^{b_t^s}$: continuous, variable $\theta_{o,d,t}^s$ related to node b_t^s.

$\tilde{\varphi}_{o,d,t}^{b_t^s}$: continuous, variable $\varphi_{o,d,t}^s$ related to node b_t^s.

$\tilde{\varepsilon}_{o,d,t}^{b_t^s}$: continuous, variable $\varepsilon_{o,d,t}^s$ related to node b_t^s.

Since this problem is a multistage problem, we need to make the decisions of stage t without knowing demands of future periods. Readers who are interested in more detailed description about multistage stochastic programming with recourse can refer to Birge and Louveaux (2011). According to the notation introduced, a multistage stochastic programming model is formulated as follows:

[M3-1]

$$Z_1 = \text{Max} \sum_{s\in S} w^s \sum_{(o,d)\in D} \sum_{t\in T} (l_{o,d}\theta^s_{o,d,t} - p_{o,d}\varphi^s_{o,d,t}) - \sum_{h\in H} \sum_{r\in R_{y_h}} f_{h,r}\alpha_{h,r} -$$

$$\sum_{k\in K} \sum_{r\in R_k} c_{k,r}\beta_{k,r} - \sum_{h\in H_2} \sum_{r\in R_{y_h}} g_{y_h}\alpha_{h,r} + \sum_{h\in H_1} m_{y_h}(u_h - \sum_{r\in R_{y_h}} \alpha_{h,r}) \quad (3\text{-}1)$$

subject to

$$\beta_{k,r} = \sum_{j\in\{1,\dots,n_r\}} \pi_{k,r,j} \qquad \forall k \in K, r \in R_k \qquad (3\text{-}2)$$

$$\sum_{k\in K_r} \pi_{k,r,j} = 1 \qquad \forall\, r \in R, j \in \{1,\dots,n_r\} \qquad (3\text{-}3)$$

$$\sum_{r\in R_{y_h}} \alpha_{h,r} \le u_h \qquad \forall\, h \in H \qquad (3\text{-}4)$$

$$\sum_{h\in H, y_h = k} \alpha_{h,r} = \beta_{k,r} \qquad \forall k \in K, r \in R_k \qquad (3\text{-}5)$$

$$\theta^s_{o,d,t} + \varphi^s_{o,d,t-1} = \varepsilon^s_{o,d,t} + \varphi^s_{o,d,t} \qquad \forall (o,d) \in D, s \in S, t \in T \qquad (3\text{-}6)$$

$$\sum_{(o,d)\in D} \sum_{t\in T} a_{r,e,i,o,d,t}\, \varepsilon^s_{o,d,t} \le \sum_{k\in K_r} v_k\, \pi_{k,r,j_{re}} \qquad \forall\, r \in R, e \in E_r, i \in I_r, s \in S \qquad (3\text{-}7)$$

$$\theta^s_{o,d,t} \le q^s_{o,d,t} \qquad \forall (o,d) \in D, s \in S,\ t \in T \qquad (3\text{-}8)$$

$$\varphi^s_{o,d,0} = 0 \qquad \forall (o,d) \in D, s \in S \qquad (3\text{-}9)$$

$$\varphi^s_{o,d,|T|} = 0 \qquad \forall (o,d) \in D, s \in S \qquad (3\text{-}10)$$

$$\theta^s_{o,d,t} = \tilde{\theta}^{b^s_t}_{o,d,t} \qquad \forall (o,d) \in D, s \in S,\ t \in T \qquad (3\text{-}11)$$

$$\varepsilon^s_{o,d,t} = \tilde{\varepsilon}^{b^s_t}_{o,d,t} \qquad \forall (o,d) \in D, s \in S,\ t \in T \qquad (3\text{-}12)$$

$$\varphi^s_{o,d,t} = \tilde{\varphi}^{b^s_t}_{o,d,t} \qquad \forall (o,d) \in D, s \in S, t \in T \cup \{0\} \qquad (3\text{-}13)$$

$$\alpha_{h,r} \in Z_+ \qquad \forall\, h \in H, r \in R_{y_h} \qquad (3\text{-}14)$$

$$\beta_{k,r} \in Z_+ \qquad \forall k \in K, r \in R_k \qquad (3\text{-}15)$$

$$\pi_{k,r,j} \in \{0,1\} \qquad \forall k \in K, r \in R_k, j \in \{1,\dots,n_r\} \qquad (3\text{-}16)$$

$$\theta^{s}_{o,d,t} \geq 0,\ \varepsilon^{s}_{o,d,t} \geq 0,\ \tilde{\theta}^{b^{s}_{t}}_{o,d,t} \geq 0,\ \tilde{\varepsilon}^{b^{s}_{t}}_{o,d,t} \geq 0 \qquad \forall (o,d) \in D, s \in S,\ t \in T \qquad (3\text{-}17)$$

$$\varphi^{s}_{o,d,t} \geq 0,\ \tilde{\varphi}^{b^{s}_{t}}_{o,d,t} \geq 0 \qquad \forall (o,d) \in D, s \in S, t \in T \cup \{0\}. \ (3\text{-}18)$$

Objective function (3-1) maximizes the expected net profit earned by the liner company during the planning horizon, which contains five terms. The first term is the expected operational revenue, which is measured by the total revenue obtained by accepting containers between O-D pairs minus the penalty cost of delay container delivery. The second term is the ship repositioning cost. The third term denotes the operating cost of all deployed ships during the planning horizon. The fourth and fifth terms are the rental cost of charter-in ships and the revenue of charter-out ships, respectively. Here, notice that $\sum_{h\in H_2}\sum_{r\in R_{y_h}} \alpha_{h,r}$ calculates the number of ships chartered (in) from other shipping liners, and $\sum_{h\in H_1}(u_h - \sum_{r\in R_{y_h}} \alpha_{h,r})$ is the number of ships chartered (out) to other shipping liners.

Several points need to be noted before explaining the constraints of this model. First, we allow one ship to complete multiple round trips during the planning horizon. Assume that the planning horizon contains three time periods, a ship is performing a route of Shanghai-Singapore-Shanghai from period 1, and the sailing time of each voyage leg is one time period, then the ship takes two time periods to finish a round trip of the route. Hence, the total net profit earned by this ship during three time periods contains the net profit of the ship during three voyage legs, i.e., Shanghai-Singapore, Singapore-Shanghai, and Shanghai-Singapore. Besides, constraints (3-7) guarantee the transport capacity of each deployed ship of each round trip because we only add the shipped demand of one round trip every time. Since we have a binary parameter $a_{r,e,i,o,d,t}$ which equals 1 if containers between O-D pair $(o,d) \in D$ to be shipped in period $t \in T$ at origin port o will be carried by a ship on voyage leg $i \in I_r$ by e^{th} round trip on route r and equals 0 otherwise, constraints (3-7) guarantee that for each route $r \in R$ in the shipping network, the number of shipped containers on voyage leg $i \in I_r$ of round trip $e \in E_r$ under scenario s cannot exceed the capacity of the j^{th}_{re} ship deployed on the route r. Second, it should be noted that the total cost of chartering in a ship contains two parts: the first part is the rental cost of the charter-in ship, which often depends only on the capacity of the ship chartered in, and is calculated in the fourth term of the objective; the other part is the repositioning cost of the charter-in ship, which

is related to the group to which the charter-in ship belongs and to the service it will be deployed on, and is calculated in the second term of the objective. Finally, since the objective function of this model is to maximize the total net profit earned by the liner company, only the revenue of chartering out ships is considered, i.e., the repositioning cost of charter-out ships is ignored as it is paid by the shipping liners to which the ships are chartered out, when dealing with the revenue of chartering out a ship.

Constraints (3-2) compute the number of ships of type k deployed on each route r. Constraints (3-3) guarantee that at each sequence position j of route r, the deployed ships must belong to only one type. Constraints (3-4) require that the total number of used ships on all routes from each ship group cannot exceed the total number of ships available in the group. Constraints (3-5) mean that the total number of used ships deployed on route r from all ship groups of type k equals the number of ships of type k deployed on route r. Constraints (3-6) are the balance equations for the numbers of accepted, delayed, and shipped containers, between each O-D pair (o, d) in each time period $t \in T$ under each scenario s. Constraints (3-7) guarantee that for each route $r \in R$ in the shipping network, the number of shipped containers on voyage leg $i \in I_r$ of round trip $e \in E_r$ cannot exceed the capacity of the j_{re}^{th} ship deployed on the route r under scenario s. More explanation about constraints (3-7) is described below. We need to emphasize the definition of round trip e. Since a round trip is a ship's itinerary of a ship route that forms a loop in practice, we use round trip e to represent the round trip operated from time period t, which means round trip 3 is the one completed by the ship starting from time period 3. In this case, the left-hand side of constraints (3-7) only adds the shipped demand in the period t concerning all O-D pairs carried by a ship on leg i by e^{th} round trip on route r under scenario s because of the existence of parameter $a_{r,e,i,o,d,t}$ (i.e., the total number of shipped containers carried by a ship on leg i by e^{th} round trip on route r under scenario s). Moreover, the right-hand side of constraints (3-7) is the capacity of the deployed ship corresponding to the particular round trip. Constraints (3-8) state that the number of accepted containers cannot exceed the demand under scenario s. Constraints (3-9) and (3-10) are the boundary conditions of $\varphi_{o,d,t}^{s}$ when t equals 0 and $|T|$, respectively. Specifically, constraints (3-9) mean that no containers are delayed before the start of the business for the O-D pair, and constraints (10) guarantee that all accepted containers should be shipped before the end of the planning horizon. Constraints (3-11)–(3-13) define nonanticipativity constraints of

multistage stochastic programming. Constraints (3-14)–(3-18) define the domains of decision variables.

Proposition 1. *The decision version of this problem is NP-complete*.

Proof. This chapter first initializes the decision version of a 0–1 Knapsack problem as follows. Given set $N = \{1, 2, \dots, n\}$, integers W, K, c_r, and w_r, for every $r \in N$, is there a subset S, $S \subseteq N$, such that $\sum_{r \in S} w_r \leq W$ and $\sum_{r \in S} c_r \geq K$. The above 0–1 Knapsack problem is one of the known NP-complete problems. This chapter then reduces the knapsack problem to our problem to show that the decision version of our problem is NP-complete. The decision version of our problem is in NP, which means given a set of operated ship routes and container flows, it can be decided in polynomial time whether the total profit generated is greater than a given constant K. This chapter now proves that the decision version of our problem is NP-hard. Our problem is initialized as a problem with a liner service network with $|R|$ ship routes, all of which connect ports a and b. Suppose the weekly demand from ports a to b is constant and denoted by D. The set T of planning periods has only one period and hence all container shipment demand must be fulfilled. Each route r, $r \in R$, has only two available ship types, a type of larger ship with capacity V_r^L and a type of smaller ship with capacity V_r^S (but the two ship types on different routes are different), $V_r^L > V_r^S$, and charter-out revenue and charter-in cost are both set to 0. Suppose further that the operating cost of the smaller ship and the larger ship on route r are 0 and Δ_r, respectively. Therefore, this problem is to identify on which route should larger-type ships be deployed sailing from a to b such that the total operating cost is minimized. Let x_r' be a binary variable that is equal to 1 if and only if the type of larger ship is deployed on ship route r. This optimization problem can be modelled as: $\min \sum_{r \in R} \Delta_r x_r'$ subject to $\sum_{r \in R} [V_r^L x_r' + (1 - x_r') V_r^S] \geq D$, $x_r' \in \{0, 1\}, \forall r \in R$. The decision version of the problem is, given a constant W, whether there exist binary values of $x_r', r \in R$ such that $\sum_{r \in R} \Delta_r x_r' \leq W$ and $\sum_{r \in R} [V_r^L x_r' + (1 - x_r') V_r^S] \geq D$. Given an instance of the knapsack problem, this chapter lets $R = S$, $\Delta_r = w_r$, $V_r^L - V_r^S = c_r$, $r \in R$, and $D = K + \sum_{r \in R} V_r^S$. It follows easily now that the decision version of our problem has a solution if and only if there is a feasible solution to the decision version of the 0–1 Knapsack problem. Therefore, the 0–1 Knapsack can be solved by solving our problem, implying the decision version of our problem is NP-complete. □

3.5 BENDERS-BASED BRANCH-AND-CUT (BBC) ALGORITHM

The NP-hardness of our problem means that it is highly unlikely that a polynomial-time algorithm can be designed for this problem. We need an efficient and exact algorithm to solve the problem of practical scale with realistic data. Due to a large number of decision variables and constraints in the problem, solving MILP model [M3-1] is difficult. Benders decomposition is a partitioning algorithm for large-scale MILP models and has been shown to be quite efficient in solving many stochastic programming problems (Rei et al., 2009; Adulyasak et al., 2015). However, the presence of integrality constraints in master problems (MPs) in the basic Benders decomposition algorithm makes solution time much longer. Hence, we now introduce a BBC algorithm to solve model [M3-1] which solves the linear programming (LP) relaxation of the MP at each iteration. Moreover, a tailored acceleration strategy and a standard acceleration technique from stochastic programming—Pareto-optimal cuts are applied to improve the convergence of the BBC algorithm.

We first introduce an overview of the BBC algorithm in Section 3.5.1, then explain implementation details of the Benders decomposition algorithm in Section 3.5.2, and finally describe acceleration strategies in Section 3.5.3.

3.5.1 Overview of solution approach

In brief, a BBC algorithm is a branch-and-bound algorithm in which Benders decomposition is used to compute upper bounds by solving linear relaxations of MPs (for maximization problems), and Benders cuts may be added to strengthen the linear relaxations of MPs. Specifically, in basic Benders decomposition algorithms, the presence of integrality constraints in the MP makes its solution time much longer than that of the dual subproblems. The computational complexity of the MP results in slow convergence of the Benders decomposition algorithms. To deal with this issue, Geoffrion et al. (1974) indicated that obtaining the optimal solution to the MP at each iteration is not necessary, which means that obtaining a near optimal solution efficiently may be beneficial. Nowadays, embedding Benders cuts within a branch-and-cut framework for solving the MP is one efficient way to deal with the above issue (Pearce and Forbes, 2018). An outline of our Benders-based branch-and-cut algorithm is summarized in Algorithm 3-1.

Algorithm 3-1. Benders-based branch-and-cut algorithm

1 Initialize the tree L: $L = \{\tilde{o}\}$ where $\tilde{o}$ is the original restricted master problem [M3-4] formulated in Section 3.5.2 without branching constraints.
OBJ* $\leftarrow -\infty$ // OBJ^* records the incumbent objective function value of [M3-4].
$(\boldsymbol{\alpha}, \boldsymbol{\beta}, \boldsymbol{\pi}, \Omega)^*$ $\leftarrow$null // $\boldsymbol{\alpha}$, $\boldsymbol{\beta}$, and $\boldsymbol{\pi}$ represent vectors of α_{hr} $(h \in H, r \in R_{y_h})$, β_{kr} $(k \in K, r \in R_k)$, and π_{krj} $(k \in K, r \in R_k, j \in \{1, \dots, n_r\})$, respectively; Ω is an extra variable defined in Section 3.5.2; $(\boldsymbol{\alpha}, \boldsymbol{\beta}, \boldsymbol{\pi}, \Omega)^*$ records the incumbent solution of corresponding decision variables in [M3-4].
2 **While** L is nonempty **do**
3 Select a node $o \in L$ according to the node selection rule elaborated in Section 3.5.3.
4 $L := L \backslash \{o\}$.
5 Solve the linear relaxation of o.
6 **If** LP is infeasible **then**
7 Prune the node.
8 **Else**
9 Obtain an optimal solution $(\boldsymbol{\alpha}, \boldsymbol{\beta}, \boldsymbol{\pi}, \Omega)$ and the optimal objective function value OBJ.
10 **If** OBJ $\leq$ OBJ* **then**
11 Prune the node.
12 **Else if** $\boldsymbol{\alpha}$, $\boldsymbol{\beta}$, and $\boldsymbol{\pi}$ are all integer **then**
13 Solve model [M3-3] formulated in Section 3.5.2 based on $(\boldsymbol{\alpha}, \boldsymbol{\beta}, \boldsymbol{\pi}, \Omega)$ and generate Benders cuts.
14 **If** no cuts are generated **then**
15 Update $OBJ^* = OBJ$ and $(\boldsymbol{\alpha}, \boldsymbol{\beta}, \boldsymbol{\pi}, \Omega)^* \leftarrow (\boldsymbol{\alpha}, \boldsymbol{\beta}, \boldsymbol{\pi}, \Omega)$.
16 Prune the node.
17 **Else**
18 Add the cuts to [M3-4] and go to line 5.
19 **End if**
20 **Else if** any element in $\boldsymbol{\alpha}$, $\boldsymbol{\beta}$, and $\boldsymbol{\pi}$ is fractional **then**
21 Branch according to the branching rule elaborated in Section 3.5.3, resulting in nodes o_1 and o_2, $L := L \cup \{o_1, o_2\}$.
22 **End if**
23 **End if**
24 **End while**
25 The algorithm terminate as the optimal solution is found

The central component of our solution approach is Benders decomposition elaborated in Section 3.5.2. It partitions the original problem into a master problem containing integer variables and a primal subproblem (PS) containing continuous variables, which are typically easier to solve than the original problem.

3.5.2 Benders decomposition

Benders decomposition partitions the original problem into a master problem containing integer variables and a subproblem containing continuous variables. By using LP duality, all variables belonging to the subproblem are projected out, and the MP contains the remaining variables and an artificial variable related to the objective function value of the subproblem. The values of the variables in the MP are first determined, and the subproblem is then solved given these fixed variables. After solving the linear subproblem, several new constraints, i.e., cuts, are added to the MP. To be specific, if the subproblem is feasible and bounded, an optimality cut is added

to the MP; otherwise, a feasibility cut is added. An upper bound can be obtained when the original problem finds a feasible solution, and a lower bound is obtained when the MP is solved to optimality for minimization problems. The process is repeated until an optimal solution is obtained.

The Benders decomposition algorithm has often been used to solve problems in the liner shipping industry (Chen et al., 2018). In our problem, it is obvious that first-stage decision variables are integer variables, while decision variables in the following stages belong to continuous variables. If the first-stage decisions are fixed, the resulting subproblem is a demand fulfillment and allocation problem. Let $\bar{\alpha}$, $\bar{\beta}$, and $\bar{\pi}$ denote the vectors of fixed $\alpha_{h,r}$, $\beta_{k,r}$, and $\pi_{k,r,j}$, respectively. The decision variables in the following stages are only dependent on $\bar{\pi}$, but independent of $\bar{\alpha}$ and $\bar{\beta}$. Hence, the expected operational net revenue function can be computed by solving the following PS:

$$[\text{M3-2}]\ Z_2 = \text{Max}\{\textstyle\sum_{s\in S} w^s \sum_{(o,d)\in D} \sum_{t\in T} (l_{o,d}\theta^s_{o,d,t} - p_{o,d}\varphi^s_{o,d,t})\} \tag{3-19}$$

subject to constraints (3-6), (3-8)–(3-13), (3-17)–(3-18),

$$\textstyle\sum_{(o,d)\in D} \sum_{t\in T} a_{r,e,i,o,d,t}\, \varepsilon^s_{o,d,t} \le \sum_{k\in K_r} v_k \bar{\pi}_{k,r,j_{r,e}} \ \forall\, r\in R, e\in E_r, i\in I_r, s\in S. \tag{3-20}$$

Due to the presence of the decision variables $\theta^s_{o,d,t}$, the above PS is always feasible because the number of accepted containers can be zero, which implies the numbers of delayed and shipped containers are also zero. Besides, since the parameters $l_{o,d}$ and $p_{o,d}$ are finite and because of constraints in model [M3-2], any feasible solution to the PS must be bounded. As a result, the dual of the PS is always feasible and bounded, which means only optimality cuts need to be added. Let $\omega = \{\omega_{o,d,t,s} | (o,d)\in D, t\in T, s\in S\}$, $\mu = \{\mu_{o,d,t,s} | (o,d)\in D, t\in T, s\in S\}$, $\eta = \{\eta_{o,d,s} | (o,d)\in D, s\in S\}$, $\zeta = \{\zeta_{o,d,s} | (o,d)\in D, s\in S\}$, $\rho^\theta = \{\rho^\theta_{o,d,t,s} | (o,d)\in D, t\in T, s\in S\}$, $\rho^\varphi = \{\rho^\varphi_{o,d,t,s} | (o,d)\in D, t\in T, s\in S\}$, $\rho^\varepsilon = \{\rho^\varepsilon_{o,d,t,s} | (o,d)\in D, t\in T\cup\{0\}, s\in S\}$, and $\sigma = \{\sigma_{r,e,i,s} | r\in R, e\in E_r, i\in I_r, s\in S\}$ be the dual variables related to constraints (3-6), (3-8)–(3-13), and (3-20), respectively. The dual of the PS is called the dual primal subproblem (DPS), and the polyhedron defined by the constraints of the DPS is denoted as P_Δ. Hence, the DPS can be formulated as follows:

$$[\text{M3-3}]\ Z_3 = \text{Min}\{\sum_{s\in S} w^s[\sum_{r\in R}\sum_{e\in E_r}\sum_{i\in I_r}\sum_{k\in K_r} v_k \bar{\pi}_{k,r,j_{r,e}}\sigma_{r,e,i,s} + \sum_{(o,d)\in D}\sum_{t\in T} q^s_{o,d,t}\mu_{o,d,t,s}]\} \quad (3\text{-}21)$$

$$\text{subject to } (\omega,\mu,\eta,\zeta,\rho^\theta,\rho^\varphi,\rho^\varepsilon,\sigma) \in P_\Delta. \quad (3\text{-}22)$$

We further introduce the set of extreme points of P_Δ as Φ_Δ. Besides, we define an extra variable Ω representing the expected total revenue. The previous multistage model can be reformulated as an MP.

$$[\text{M3-4}]\ Z_4 = \text{Max}\left\{\Omega - \sum_{h\in H}\sum_{r\in R_{y_h}} f_{h,r}\alpha_{h,r} - \sum_{k\in K}\sum_{r\in R_k} c_{k,r}\beta_{k,r} - \sum_{h\in H_2}\sum_{r\in R_{y_h}} g_{y_h}\alpha_{h,r} + \sum_{h\in H_1} m_{y_h}(u_h - \sum_{r\in R_{y_h}}\alpha_{h,r})\right\} \quad (3\text{-}23)$$

subject to constraints (3-2)–(3-5), (3-14)–(3-16),

$$\sum_{s\in S} w^s[\sum_{r\in R}\sum_{e\in E_r}\sum_{i\in I_r}\sum_{k\in K_r} v_k \pi_{k,r,j_{r,e}}\sigma_{r,e,i,s} + \sum_{(o,d)\in D}\sum_{t\in T} q^s_{o,d,t}\mu_{o,d,t,s}] \geq \Omega$$

$$\forall(\omega,\mu,\eta,\zeta,\rho^\theta,\rho^\varphi,\rho^\varepsilon,\sigma) \in \Phi_\Delta. \quad (3\text{-}24)$$

The Benders decomposition algorithm solves the master problem and the subproblem repeatedly. To be specific, the Benders decomposition algorithm first solves the MP to optimality, which leads to an upper bound for the original problem since this problem is a maximization problem. The DPS is then solved given the values of $\bar{\pi}_{k,r,j}$ from the optimal solution to the master problem. One or several new Benders cuts, i.e., constraints (3-24) (if any), are added to the master problem at each iteration. When decision variables $\boldsymbol{\alpha}$, $\boldsymbol{\beta}$, and $\boldsymbol{\pi}$ in model [M3-4] are all integers and no Benders cuts are generated, the objective function value of the model [M3-4] provides a lower bound for the original problem. When the upper and lower bounds of the original problem converge, the algorithm terminates.

3.5.3 Branching rule and node selection rule

The branching rule used in this chapter is a simple branching rule known as the maximum fractional branching. This rule selects the variable with the largest integer violation for branching. For simplicity, let I and x_i represent the index set of all fractional integer variables at a specific node in the branch-and-bound tree and the value of the decision variable of index i ($i \in I$), respectively. Hence, the index of the

variable with the largest integer violation can be obtained by $\underset{i \in I}{\operatorname{argmax}}\{\min(x_i - \lfloor x_i \rfloor, \lceil x_i \rceil - x_i)\}$. The node selection rule in this chapter is the best-bound-first node selection, which means that the node with the largest upper bound is always processed first.

3.5.4 Acceleration strategies

Ever since the Benders decomposition was introduced, numerous studies have been conducted to improve it. For example, Magnanti and Wong (1981) introduced a new method, i.e., strong or Pareto-optimal cuts, to accelerate the convergence of the Benders decomposition algorithm for MILP models. Cordeau et al. (2006) proposed valid inequalities to strengthen the LP relaxation of MILP models, thereby improving the performance of the Benders decomposition algorithm. Hence, this chapter discusses several acceleration strategies for the proposed BBC algorithm.

Since the quality of the upper bound in the initial stages is inferior, the optimality gap may be large in the initial stages of the algorithm, which results in the need of a large number of cuts. Hence, we can tighten the upper bound for the MP by using some initial cuts called upper bound tightening (UBT) inequalities. To obtain approximate UBT inequalities, we first develop a nominal second-stage problem. The following describes newly defined parameters and decision variables.

Newly defined parameters:

$\bar{q}_{o,d,t}$: expected number of newly generated container shipment demand in period t at port o to be transported to port d, $\bar{q}_{o,d,t} = \mathbb{E}_s[q^s_{o,d,t}]$.

Newly defined decision variables:

$\bar{\theta}_{o,d,t}$: continuous, the number of accepted containers for the demand of O-D pair $(o,d) \in D$ accumulated in period $t \in T$ with expected parameters.

$\bar{\varphi}_{o,d,t}$: continuous, the number of delayed containers for the demand of O-D pair $(o,d) \in D$ up to period $t \in T \cup \{0\}$ with expected parameters; by convention, $\bar{\varphi}_{o,d,0} := 0$.

$\bar{\varepsilon}_{o,d,t}$: continuous, the number of shipped containers for the demand of O-D pair $(o,d) \in D$ in period $t \in T$ with expected parameters.

The problem replacing the previous subproblem [M3-2] with the new second-stage problem, therefore, belongs to a two-stage deterministic problem. According to the notation introduced, the second-stage deterministic programming model is formulated as follows:

$$[\text{M3-5}]\ Z_5 = \text{Max}\{\sum_{(o,d)\in D}\sum_{t\in T}(l_{o,d}\bar{\theta}_{o,d,t} - p_{o,d}\bar{\varphi}_{o,d,t})\} \quad (3\text{-}25)$$

subject to

$$\bar{\theta}_{o,d,t} + \bar{\varphi}_{o,d,t-1} = \bar{\varepsilon}_{o,d,t} + \bar{\varphi}_{o,d,t} \qquad \forall (o,d) \in D, t \in T \quad (3\text{-}26)$$

$$\sum_{(o,d)\in D}\sum_{t\in T} a_{r,e,i,o,d,t}\,\bar{\varepsilon}_{o,d,t} \le \sum_{k\in K_r} v_k\,\bar{\pi}_{k,r,j_{r,e}} \quad \forall\, r \in R, e \in E_r, i \in I_r \quad (3\text{-}27)$$

$$\bar{\theta}_{o,d,t} \le \bar{q}_{o,d,t} \qquad \forall (o,d) \in D, t \in T \quad (3\text{-}28)$$

$$\bar{\varphi}_{o,d,0} = 0 \qquad \forall (o,d) \in D \quad (3\text{-}29)$$

$$\bar{\varphi}_{o,d,|T|} = 0 \qquad \forall (o,d) \in D \quad (3\text{-}30)$$

$$\bar{\theta}_{o,d,t}, \bar{\varepsilon}_{o,d,t} \ge 0 \qquad \forall (o,d) \in D, t \in T \quad (3\text{-}31)$$

$$\bar{\varphi}_{o,d,t} \ge 0 \qquad \forall (o,d) \in D, t \in T \cup \{0\}. \quad (3\text{-}32)$$

Objective function (3-25) maximizes the operational revenue earned by the liner company during the planning horizon in the second-stage deterministic problem. Constraints (3-26)–(3-32) update related constraints for the deterministic problem.

Similarly, the dual of the second-stage problem [M3-5] is always feasible and bounded, which means only optimality cuts need to be added. Let $\omega' = \{\omega'_{o,d,t} | (o,d) \in D, t \in T\}$, $\sigma' = \{\sigma'_{r,e,i} | r \in R, e \in E_r, i \in I_r\}$, $\mu' = \{\mu'_{o,d,t} | (o,d) \in D, t \in T\}$, $\eta' = \{\eta'_{o,d} | (o,d) \in D\}$, and $\zeta' = \{\zeta'_{o,d} | (o,d) \in D\}$ be the dual variables associated with constraints (3-26)–(3-30), respectively. We further denote the polyhedron defined by the constraints of the dual of the second-stage problem as P'_Δ. The dual subproblem for the second-stage problem [M3-5] can be formulated as follows:

$$[\text{M3-6}]\ Z_6 = \text{Min}\{\sum_{r\in R}\sum_{e\in E_r}\sum_{i\in I_r}\sum_{k\in K_r} v_k\bar{\pi}_{k,r,j_{re}}\sigma'_{r,e,i} + \sum_{(o,d)\in D}\sum_{t\in T}\bar{q}_{o,d,t}\mu'_{o,d,t}\} \quad (3\text{-}33)$$

subject to $(\omega', \sigma', \mu', \eta', \zeta') \in P'_{\Delta}$. (3-34)

We further introduce the set of extreme points of P'_{Δ} as Φ'_{Δ}. Hence, we can obtain the approximate UBT inequalities from the nominal second-stage problem of the original master problem:

$$\Theta[\sum_{r\in R}\sum_{e\in E_r}\sum_{i\in I_r}\sum_{k\in K_r} v_k \bar{\pi}_{k,r,j_{r,e}} \sigma'_{r,e,i} + \sum_{(o,d)\in D}\sum_{t\in T} \bar{q}_{o,d,t}\mu'_{o,d,t}] \geq \Omega$$

$$\forall(\omega', \sigma', \mu', \eta', \zeta') \in \Phi'_{\Delta}, \quad (3\text{-}35)$$

where Θ is a parameter for dynamic adjustment in the algorithm. At first, Θ is set to 1 to make the algorithm converge quickly. When inequalities (3-35) become tight, Θ is set to 1.01. Finally, inequalities (3-35) are removed to ensure the validity for the original master problem because inequalities (3-35) are derived from the nominal second-stage problem [M3-5] and may not hold for the original master problem. Here, notice that inequalities (3-35) are obtained as the approximate UBT inequalities from the nominal second-stage problem instead of Benders cuts for the original master problem.

Apart from the above introduced UBT inequalities, Pareto-optimal cuts are also applied to accelerate the BBC algorithm. Magnanti and Wong (1981) show that when the primal subproblem is a network flow optimization problem, such as transshipment on networks, degenerate solutions are usually obtained, which results in multiple optimal solutions for the dual problem. This phenomenon always leads to the generation of cuts of different strengths. Any of these cuts are obviously valid optimality cuts, but solving the model with all generated cuts may lead to much longer computational time. Magnanti and Wong (1981) further show that the selection of good cuts at each iteration is one of several important acceleration strategies for Benders decomposition. Hence, we use the method designed by Magnanti and Wong (1981) to identify strong (Pareto-optimal) cuts.

A Pareto-optimal cut is defined as a cut if it is not dominated by any other cut. We say that the cut generated from the dual solution $\omega_a, \mu_a, \eta_a, \zeta_a, \rho_a^{\theta}, \rho_a^{\varphi}, \rho_a^{\varepsilon}, \sigma_a$ dominates that from $\omega_b, \mu_b, \eta_b, \zeta_b, \rho_b^{\theta}, \rho_b^{\varphi}, \rho_b^{\varepsilon}, \sigma_b$ if and only if $\sum_{s\in S} w^s[\sum_{r\in R}\sum_{e\in E_r}\sum_{i\in I_r}\sum_{k\in K_r} v_k \pi_{k,r,j_{re}} \sigma^a_{r,e,i,s} + \sum_{(o,d)\in D}\sum_{t\in T_{od}} q^s_{o,d,t}\mu^a_{o,d,t,s}] \leq \sum_{s\in S} w^s[\sum_{r\in R}\sum_{e\in E_r}\sum_{i\in I_r}\sum_{k\in K_r} v_k \pi_{k,r,j_{r,e}} \sigma^b_{r,e,i,s} + \sum_{(o,d)\in D}\sum_{t\in T_{o,d}} q^s_{o,d,t}\mu^b_{o,d,t,s}]$ for

all $\pi \in \Phi$, where $\Phi = \{\pi_{k,r,j} | \begin{smallmatrix} \sum_{k\in K_r} \pi_{k,r,j}=1, \forall\, r\in R, j\in\{1,\dots,n_r\} \\ \pi_{k,r,j}\in\{0,1\}, \forall k\in K_r, r\in R, j\in\{1,\dots,n_r\} \end{smallmatrix}\}$, with a strict inequality for at least one point $\pi \in \Phi$. Hence, a cut generated from the dual solution $\omega_b, \mu_b, \eta_b, \zeta_b, \rho_b^\theta, \rho_b^\varphi, \rho_b^\varepsilon, \sigma_b$is a Pareto-optimal cut if there is no other dual solution $\omega_a, \mu_a, \eta_a, \zeta_a, \rho_a^\theta, \rho_a^\varphi, \rho_a^\varepsilon, \sigma_a$ whose generated cut dominates it. Let $ri(\Phi)$ denote the relative interior of Φ, and a point in $ri(\Phi)$ is called a core point. To generate a Pareto-optimal cut, any core point $\pi^0 \in ri(\Phi)$ can be used (Magnanti and Wong, 1981).

Although Magnanti and Wong (1981) prove that a Pareto-optimal cut can be generated from any core point π^0, $\pi^0 \in ri(\Phi) \subseteq \Phi$, Papadakos (2008) proves that π^0 does not have to be a core point or even a point of Φ. Since finding a Benders MP core point is difficult in most cases, we use a method similar to that of Papadakos (2008) and Bayram and Yaman (2018) to find approximate core points. We first let $\pi^0_{k,r,j} \leftarrow 1$ and update this point by the following formula:

$$\pi^0_{k,r,j} \leftarrow \frac{1}{2}\pi^0_{k,r,j} + \frac{1}{2}\bar{\pi}_{k,r,j} \qquad \forall\, k \in K, r \in R_k, j \in \{1,\dots,n_r\}. \quad (3\text{-}36)$$

To generate Pareto-optimal cuts more efficiently, we employ a method similar to that of Sherali and Lunday (2013) and Wang and Jacquillat (2020), which involves solving DPS only once by perturbing the right-hand-side of constraints (3-20) in PS as follows:

$$\sum_{(o,d)\in D} \sum_{t\in T} a_{r,e,i,o,d,t}\, \varepsilon^s_{o,d,t} \le \sum_{k\in K_r} v_k\, \bar{\pi}_{k,r,j_{re}} + \epsilon \sum_{k\in K_r} v_k\, \pi^0_{k,r,j_{re}}$$

$$\forall r \in R, e \in E_r, i \in I_r, s \in S, \quad (3\text{-}37)$$

where ϵ is a small perturbation coefficient and set to 10^{-6} which is consistent with the parameter setting used in previous works (e.g., Wang and Jacquillat, 2020).

3.6 COMPUTATIONAL EXPERIMENTS

To evaluate the proposed model and assess the efficiency of our algorithm, we perform extensive computational experiments on a laptop (Intel Core i7, 2.6 GHz; Memory, 16 G). In this chapter, the proposed mathematical models and algorithms are implemented using Visual Studio 2022 environment in C# programming language, and CPLEX 12.5.1 is used as the commercial solver.

3.6.1 Experimental setting

We first summarize the setting of our parameter values. Three ship routes depicted in Figure 3-6 are used to conduct computational experiments. Five types of ships are available in this chapter, and three parameters (v_k, g_k and m_k) and the daily operating cost of a ship related to ship types are summarized in Table 3-3, which are all the same as the setting in Ng and Lin (2018). The number of newly generated container shipment demand in period t at port o to be transported to port d under scenario s ($q^s_{o,d,t}$) is assumed to be uniformly distributed in [0, 5000] TEUs if the cargos of this O-D pair can be transported through the routes in Figure 3-6, which is consistent with the setting in Xia et al. (2015). The penalty cost for delayed containers per period ($p_{o,d}$) is set to 210 USD/TEU/week for all O-D pairs, which is in line with the setting used in Zhen et al. (2019b). The revenue for accepting a container ($l_{o,d}$) relates to the sailing distance and can be calculated by $500 + 0.2 \times \text{distance}$ (n mile) from the origin port to the destination port, which is in line with the setting in Wang et al. (2016). The operating cost of completing the voyages during the planning horizon by a ship of type k deployed on route r (c_{kr}) are set to the total sailing time periods (weeks) of a ship deployed on route r times 7 days/week times the daily operating cost of a ship. For the sake of simplicity, let X_1, X_2,…, and $X_{|T|}$ denote the sets of possible realizations of demands in periods 1, 2,…, and $|T|$, respectively. And let x_t, $x_t \in X_t$, denote the demand realization in period $t \in T$. The scenarios for each period are generated separately. Hence, the probability of the demand generalization $(x_1, x_2, \dots, x_{|T|}) \in X_1 \times \dots \times X_{|T|}$ is $\prod_{t \in T} \frac{1}{|X_t|}$. Finally, we need to emphasize that this study assumes that each time period corresponds to each stage; therefore, our decisions need to be updated every time period. In the future, the determination of the optimal duration of a stage can be further explored.

Table 3-3 The setting of four parameters related to ship types.

Parameters	Ship type k				
	1	2	3	4	5
v_k (TEU)	2,808	3,218	4,500	5,714	8,063
g_k (million USD)	2	2.6	3.5	4.7	6
m_k (million USD)	1.82	2.34	3.21	4.32	5.12
operating cost (thousand USD/day)	19.8	22.5	30.9	38.8	54.2

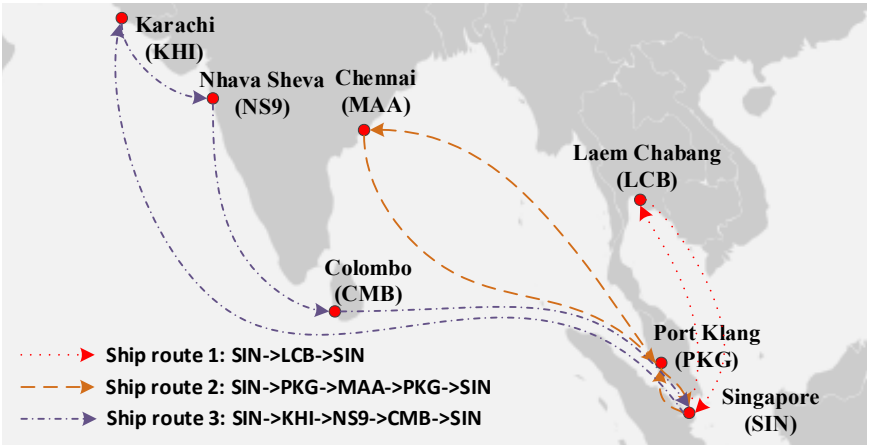

Figure 3-6 Three ship routes.

Nine ship groups are used in the computational experiments. The number of ships in each ship group and the ship type of each ship group are summarized in Table 3-4. Specifically, the first $|R|$ ship groups, owned by the liner company, are composed of ships on each ship route. Besides, 10 ships and 1 ship, owned by other shipping liners, are idle at the Port of Singapore (i.e., $h_{|R|+1}, \ldots, h_{|R|+5}$) and the Port of Hong Kong (i.e., $h_{|R|+6}$), respectively. The repositioning cost ($f_{h,r}$) for a ship belonging to group $h \in H$ to route r equals the repositioning time multiplied by the operating cost of a ship. The repositioning time of a ship in $h_1, \ldots, h_{|R|}$ to a ship route r, $r \in R$, is the sailing time between the phase-out and phase-in ports on these two ship routes plus a random number in [0, 3] days for cargo handling and plus three days for preparation, and the repositioning time from a ship in $h_{|R|+1}, \ldots, h_{|R|+6}$ to a ship route $r \in R$ is the sailing time between the phase-out and phase-in ports plus three days for preparation, which is consistent with the relevant setting used in Wang (2013).

Table 3-4 Summary of ship groups for the computational experiments.

Ship groups	On routes 1, 2, 3			At Port of Singapore					At Port of Hong Kong
	h_1	h_2	h_3	h_4	h_5	h_6	h_7	h_8	h_9
Number	1	2	3	2	2	2	2	2	1
Type	1	1	1	1	2	3	4	5	3

We conduct 10 sets of small instances (each with two or three routes, two, three, four, or six periods, and 36 to 343 scenarios), 10 sets of medium instances (each with two or three routes, three to nine periods, and 256 to 2,187 scenarios), and 10 sets of

large instances (each with five or 10 routes, four to seven periods, and 256 to 2,187 scenarios). The impact of the acceleration strategies proposed in Section 3.5.4 on the performance of the developed algorithms is also investigated. The impact of uncertainty on the operations management of liner companies is then investigated. Moreover, an intensive analysis of why multistage stochastic programming can lead to better solutions is also discussed. Three practical questions regarding the driver analysis of shipping company profitability, the benefit analyses of adaptive fleet sizes, and the influence of pandemic diseases on liner shipping are investigated to seek managerial insights into liner shipping.

3.6.2 Computational experiments

We apply three methods to solve the problem. The first method is solving model [M3-1] by CPLEX directly to provide optimal solutions. The second method is solving model [M3-4] by CPLEX's Benders decomposition framework (details are provided in Appendix A). The last method is solving model [M3-4] by applying the proposed BBC solution method. The numerical experiments are instances with various numbers of routes in a shipping network to be optimized, ports of call, time periods in the planning horizon, nodes generated from a parent node in the scenario tree for each period and the total number of scenarios, and different route compositions of the shipping network. The algorithms' performance is measured by the computing time and objective values between the results obtained by the three approaches. The solution time limit for each computational instance is six hours.

This section first reports small-scale computational experiments for the problem with the number of periods $|T| = 2$, 3, 4, and 6. The number of nodes generated from a parent node in the scenario tree for each period is the same and recorded as $|S_t|$, which leads to the total number of scenarios $|S| = |S_t|^{|T|}$. The total number of scenarios scales based on problem solving time. Table 3-5 records results of the comparison of the three methods for small-scale instances. As shown in Table 3-5, columns 2 to 5 on the left, i.e., Route ID, $|T|$, $|S_t|$, and $|S|$ represent the route composition of the service network, the number of time periods in the planning horizon, the number of new nodes generating from a parent node in the scenario tree, and the total number of scenarios, respectively. Values in columns P_1, P_2, and P_3 are the objective values obtained by CPLEX, CPLEX's Benders decomposition framework, and the proposed BBC method, respectively. It is obvious that all three

methods find the optimal solution in each of the 10 computational instances. CPU time of these three methods is also recorded and represented by T_1, T_2, and T_3, respectively. It can be clearly seen that although the proposed BBC algorithm is not the fastest method for small-scale instances, it is much faster than the CPLEX's Benders decomposition framework. Hence, the accuracy of the proposed BBC algorithm for small computational instances is verified.

Table 3-5 Comparison of the three methods for small-scale instances.

Case ID	Route ID	$\|T\|$	$\|S_t\|$	$\|S\|$	CPLEX		CPLEX's BD framework		BBC			
					P_1 (M$)	T_1 (s)	P_2 (M$)	T_2 (s)	P_3 (M$)	T_3 (s)	T_3/T_1 (%)	T_3/T_2 (%)
S1	1,2	2	6	36	32.26	0.30	32.26	2.09	32.26	0.50	166.67	23.92
S2	1,2	2	7	49	31.24	0.52	31.24	2.95	31.24	0.69	132.69	23.39
S3	1,2	2	8	64	31.14	0.72	31.14	3.93	31.14	0.62	86.11	15.78
S4	1,2	4	3	81	71.02	2.32	71.02	80.13	71.02	4.13	178.02	5.15
S5	1,2	4	4	256	68.81	14.22	68.81	499.09	68.81	11.84	83.26	2.37
S6	1,3	3	6	216	97.28	14.00	97.28	376.11	97.28	7.92	56.57	2.11
S7	1,3	3	7	343	96.83	31.05	96.83	706.29	96.83	8.26	26.60	1.17
S8	2,3	6	2	64	271.20	10.99	271.20	431.88	271.20	15.15	137.85	3.51
S9	1,2,3	6	2	64	428.88	18.76	428.88	1,399.35	428.88	34.68	184.86	2.48
S10	1,2,3	4	3	81	323.90	11.83	323.90	680.20	323.90	14.67	124.01	2.16
										Avg.	117.66	8.20

Notes: (1) The values in columns T_3/T_1 (%) and T_3/T_2 (%) are calculated by $T_3/T_1 \times 100$ and $T_3/T_2 \times 100$, respectively; (2) M$ denotes million dollars.

This section then conducts medium-scale computational experiments for the problem with $|T| = 3, 4, 5, 6, 7,$ and 9 periods. The total number of scenarios $|S|$ ranges from 256 to 2,187. Table 3-6 records results of the comparison of the three methods for large-scale instances. As shown in Table 3-6, columns 2 to 5 on the left, i.e., Route ID, $|T|$, $|S_t|$, and $|S|$, represent the route composition of the shipping network, the number of time periods in the planning horizon, the number of new nodes from a parent node in the scenario tree, and the total number of scenarios, respectively. Values in columns P_1, P_2, and P_3 are the objective values obtained by CPLEX, CPLEX's Benders decomposition framework, and the proposed BBC method, respectively. From Table 3-6, the difference in the solution performances of the three methods becomes larger. Specifically, CPLEX method and CPLEX's Benders decomposition framework cannot find any solution within six hours in $1/10 \times 100\% = 10\%$ and $6/10 \times 100\% = 60\%$ of the cases, respectively. However, the proposed BBC algorithm can obtain optimal solutions in all instances and can obtain optimal solutions in 1,215 seconds for case "M10" where the CPLEX method cannot find any solution within six hours. Among the instances that can be solved to optimality by CPLEX's Benders decomposition framework, the CPU time of the BBC

algorithm is, on average, 0.73% of that of CPLEX's Benders decomposition framework. Besides, the CPU time of the BBC method is, on average, 27.98% of that of CPLEX. Hence, the accuracy and efficiency of the proposed BBC algorithm for medium-scale computational instances are verified.

Table 3-6 Comparison of the three methods for medium-scale instances.

Case ID	Route ID	$\|T\|$	$\|S_t\|$	$\|S\|$	CPLEX	CPLEX's BD framework			BBC			
					P_1 (M$)	T_1 (s)	P_2 (M$)	T_2 (s)	P_3 (M$)	T_3 (s)	T_3/T_1 (%)	T_3/T_2 (%)
M1	1,3	3	8	512	95.77	81.2	95.77	1,698.52	95.77	13.94	17.17	0.82
M2	1,3	3	9	729	92.81	180.79	92.81	3,955.70	92.81	26.64	14.74	0.67
M3	1,2	4	5	625	69.36	82.27	69.36	6,587.40	69.36	48.87	59.40	0.74
M4	2,3	6	3	729	269.82	1,611.69	–	–	269.82	436.03	27.05	–
M5	1,2,3	4	4	256	323.72	150.23	323.72	12,336.77	323.72	83.46	55.55	0.68
M6	1,2,3	4	5	625	318.58	867.92	–	–	318.58	92.73	10.68	–
M7	1,2,3	6	3	729	427.42	3,136.55	–	–	427.42	511.87	16.32	–
M8	1,2,3	9	2	512	637.06	3,300.97	–	–	637.06	555.52	16.83	–
M9	1,2,3	5	4	1,024	350.90	4,122.53	–	–	350.90	1,404.70	34.07	–
M10	1,2,3	7	3	2,187	–	–	–	–	491.29	1,214.21	–	–
									Avg.		27.98	0.73

Notes: (1) The values in columns T_3/T_1 (%) and T_3/T_2 (%) are calculated by $T_3/T_1 \times 100$ and $T_3/T_2 \times 100$, respectively; (2) the en-dash means that no solution is found within six hours; (3) M$ denotes million dollars.

Finally, ten sets of large-scale computational experiments involving five and ten ship routes are conducted. As shown in Table 3-7, CPLEX method and CPLEX's Benders decomposition framework cannot find any solution within six hours in 60% and 100% of the cases, respectively. However, the proposed BBC algorithm can obtain optimal solutions in 90% of the cases, and the CPU time of the BBC method is, on average, 29.64% of that of CPLEX among the instances that can be solved to optimali-

Table 3-7 Comparison of the three methods for large-scale instances.

Case ID	Num of Routes	$\|T\|$	$\|S_t\|$	$\|S\|$	CPLEX	CPLEX's BD framework			BBC			
					P_1 (M$)	T_1 (s)	P_2 (M$)	T_2 (s)	P_3 (M$)	T_3 (s)	T_3/T_1 (%)	T_3/T_2 (%)
L1	5	4	4	256	912.26	1,011.53	–	–	912.26	627.32	62.02	–
L2	5	4	5	625	934.68	6,138.96	–	–	934.68	1,106.22	18.02	–
L3	5	5	4	1,024	–	–	–	–	1,182.27	1,481.75	–	–
L4	5	6	3	729	1,430.19	18,738.31	–	–	1,430.19	3,079.21	16.43	–
L5	5	7	3	2,187	–	–	–	–	1,730.46	12,898.50	–	–
L6	10	4	4	256	2,619.27	6366.55	–	–	2,619.27	1,407.62	22.11	–
L7	10	4	5	625	–	–	–	–	2,654.03	4,949.47	–	–
L8	10	5	4	1,024	–	–	–	–	3,268.52	10,380.10	–	–
L9	10	6	3	729	–	–	–	–	4,000.84	10,648.36	–	–
L10	10	7	3	2,187	–	–	–	–	–	–	–	–
									Avg.		29.64	–

Notes: (1) The values in columns T_3/T_1 (%) and T_3/T_2 (%) are calculated by $T_3/T_1 \times 100$ and $T_3/T_2 \times 100$, respectively; (2) the en-dash means that no solution is found within six hours; (3) M$ denotes million dollars.

ty by CPLEX method. Hence, the accuracy and efficiency of the proposed BBC algorithm for large-scale computational instances are verified.

This chapter also investigates the impact of acceleration strategies introduced in Section 3.5.4. Table 3-8 reports the performance of the BBC algorithm when the acceleration strategies, i.e., the UBT inequalities and Pareto-optimal cuts, are separately applied to the problem. The tests are performed in the above 30 small-, medium-, and large-scale instances. The results in Table 3-8 indicate that the UBT inequalities significantly reduce the solution time of the proposed algorithm by approximately 6.52%. The generation of Pareto-optimal cuts also results in an about 4.30% reduction in the solution time for the 30 instances.

Table 3-8 Impact of acceleration strategies.

Case ID	BBC		BBC+UBT inequalities		BBC+Pareto-optimal cuts	
	OBJ (M$)	T_1 (s)	T_2 (s)	T_2/T_1 (%)	T_3 (s)	T_3/T_1 (%)
S1	32.26	0.50	0.46	92.00	0.41	82.00
S2	31.24	0.69	0.63	91.30	0.57	82.61
S3	31.14	0.62	0.50	80.65	0.59	95.16
S4	71.02	4.13	3.97	96.13	4.06	98.31
S5	68.81	11.84	10.68	90.20	11.86	100.17
S6	97.28	7.92	7.61	96.09	8.24	104.04
S7	96.83	8.26	8.14	98.55	8.02	97.09
S8	271.20	15.15	14.14	93.33	14.75	97.36
S9	428.88	34.68	31.38	90.48	36.39	104.93
S10	323.90	14.67	13.05	88.96	12.23	83.37
M1	95.77	13.94	13.06	93.69	15.30	109.76
M2	92.81	26.64	24.50	91.97	24.00	90.09
M3	69.36	48.87	42.07	86.09	52.18	106.77
M4	269.82	436.03	372.49	85.43	462.11	105.98
M5	323.72	83.46	69.94	83.80	77.91	93.35
M6	318.58	92.73	79.05	85.25	77.52	83.60
M7	427.42	511.87	595.99	116.43	502.53	98.18
M8	637.06	555.52	600.20	108.04	604.54	108.82
M9	350.90	1,404.70	1,036.91	73.82	1242.71	88.47
M10	491.29	1,214.21	1,088.47	89.64	1081.29	89.05
L1	912.26	627.32	622.54	99.24	681.15	108.58
L2	934.68	1,106.22	1060.44	95.86	1109.02	100.25
L3	1,182.27	1,481.75	1517.08	102.38	1384.53	93.44
L4	1,430.19	3,079.21	3420.10	111.07	2520.04	81.84
L5	1,730.46	12,898.50	10920.79	84.67	13229.45	102.57
L6	2,619.27	1,407.62	1168.79	83.03	1271.58	90.34
L7	2,654.03	4,949.47	3748.60	75.74	4615.36	93.25
L8	3,268.52	10,380.10	10920.88	105.21	9469.13	91.22
L9	4,000.84	10,648.36	12990.66	122.00	10086.25	94.72
L10	–	–	~	~	~	~
			Avg.	93.48		95.70

Notes: (1) The values in columns T_2/T_1 (%), T_3/T_1 (%), and T_4/T_1 (%) are calculated by $T_2/T_1 \times 100$, $T_3/T_1 \times 100$, and $T_4/T_1 \times 100$, respectively; (2) the en-dash means that no solution is found within six hours; (3) the tilde means that a feasible solution is found within six hours; (4) M$ denotes million dollars.

The impact of uncertainty on the operations management of liner companies is then investigated. A deterministic programming model [M_{deter}], a two-stage stochastic programming model [M_{two}], and a perfect information model [$M_{perfect}$] are formulated in Appendix B and compared with the multistage stochastic programming

model [M3-1]. In [$\mathrm{M}_{\mathrm{deter}}$], the number of newly generated container shipment demand in each period for an O-D pair is set to the average value of demands in the multistage programming model over $s \in S$; in [$\mathrm{M}_{\mathrm{two}}$], under a specific scenario $s \in S$, values of demands of an O-D pair in each period are the same as the demand values of the O-D pair in each period in multistage stochastic programming model. The ship chartering and fleet deployment decisions obtained by [$\mathrm{M}_{\mathrm{deter}}$] and [$\mathrm{M}_{\mathrm{two}}$] will then be evaluated by making container acceptance, shipment, and delay decisions in each period in a myopic manner elaborated in Appendix A.2 to calculate the resulting expected profits, represented by Z_{deter} and Z_{two}, respectively. The optimal objective value of [M3-1] is denoted by Z_{multi}. As another benchmark, Appendix B presents a perfect information model whose average profit over all scenarios is represented by Z_{perfect}.

To compare the four models, Case ID "M8" in Table 3-6 is selected as the computational instance and ten random cases are conducted to investigate the impact of uncertainty on the operations management of liner companies. Relative results are recorded in Table 3-9. The six rightmost columns record the comparison of multistage stochastic model and deterministic programming model, the comparison of multistage stochastic model and two-stage stochastic model, and the comparison of multistage stochastic model and perfect information model, respectively. Obviously, when decision-makers have perfect information, they can obtain the maximum expected profit. Besides, the gap between the objective values of the multistage stochastic model and the perfect information model is quite small (the average value of $\frac{\mathrm{GAP}_3}{Z_{\mathrm{multi}}}$ is 0.55%). Note, however, that in reality, it is almost impossible to obtain perfect information. Comparing with the other two models, using multistage stochastic programming can lead to higher profit than using two-stage stochastic programming (the average value of $\frac{\mathrm{GAP}_2}{Z_{\mathrm{multi}}}$ is 6.78%) or deterministic programming (the average value of $\frac{\mathrm{GAP}_1}{Z_{\mathrm{multi}}}$ is 16.00%).

We then conduct an intensive analysis of why multistage stochastic programming can lead to better solutions. Detailed results of the 10 sets of experiments are recorded in Table 3-10. Columns 2–4 on the left (C_{deter}, C_{two}, and C_{multi}) record the total routing capacities on all ship routes by using deterministic programming, two-stage stochastic programming, and multistage stochastic programming, respectively. It can easily be seen that the routing capacity by using deterministic programming is too small

compared with the capacities of two-stage stochastic programming and multistage stochastic programming and thus unable to effectively deal with demand uncertainty. The routing capacity using deterministic programming is only $17{,}135/34{,}829 \times 100 \approx 49.20\%$ and $17{,}135/35{,}528 \times 100 \approx 48.23\%$ of the capacities of two-stage stochastic programming and multistage stochastic programming, respectively, and deterministic programming is thus unable to deal effectively with demand uncertainty. The total routing capacity using multistage stochastic programming is larger than that using two-stage stochastic programming in two cases and the same in the other eight cases (but the total routing capacities of each ship route by using multistage and two-stage stochastic programming may still differ), leading to more containers accepted (an average of 841,693 TEUs accepted in the multistage model vs. 823,769 TEUs in the two-stage model). The multistage model has an average of 35,114 TEUs of delayed containers, which is much smaller than the average of 180,529 TEUs using the two-stage model.

Table 3-9 Comparison of the multistage, deterministic, and two-stage programming models and the perfect information model.

Case ID	Z_{multi} (M$)	Z_{deter} (M$)	Z_{two} (M$)	Z_{perfect} (M$)	Value of stochastic solution		Multistage vs two-stage programming		Value of perfect information	
					Gap_1 (M$)	$\frac{\text{Gap}_1}{Z_{\text{multi}}}$ (%)	Gap_2 (M$)	$\frac{\text{Gap}_2}{Z_{\text{multi}}}$ (%)	Gap_3 (M$)	$\frac{\text{Gap}_3}{Z_{\text{multi}}}$ (%)
1	641.52	536.52	603.08	645.29	105.00	16.37	38.44	5.99	3.77	0.59
2	637.06	537.57	542.56	640.55	99.49	15.62	94.50	14.83	3.49	0.55
3	642.96	527.96	608.85	646.81	115.00	17.89	34.11	5.30	3.85	0.60
4	626.23	526.11	588.27	629.68	100.12	15.99	37.96	6.06	3.45	0.55
5	631.78	529.31	594.33	635.01	102.48	16.22	37.45	5.93	3.22	0.51
6	643.36	540.37	605.42	647.09	102.99	16.01	37.94	5.90	3.73	0.58
7	639.79	541.18	605.12	643.09	98.61	15.41	34.67	5.42	3.30	0.52
8	627.79	532.60	589.69	631.44	95.19	15.16	38.10	6.07	3.65	0.58
9	644.65	547.04	603.34	648.01	97.60	15.14	41.31	6.41	3.36	0.52
10	638.50	535.08	601.06	642.02	103.42	16.20	37.44	5.86	3.52	0.55
Avg.	637.36	535.37	594.17	640.90	101.99	16.00	43.19	6.78	3.54	0.55

Notes: (1) $\text{Gap}_1 = \text{Z}_{\text{multi}} - Z_{\text{deter}}$, $\text{Gap}_2 = \text{Z}_{\text{multi}} - Z_{\text{two}}$, and $\text{Gap}_3 = Z_{\text{perfect}} - \text{Z}_{\text{multi}}$; (2) the values in columns $\text{Gap}_1/\text{Z}_{\text{multi}}$ (%), $\text{Gap}_2/\text{Z}_{\text{multi}}$ (%), and $\text{Gap}_3/\text{Z}_{\text{multi}}$ (%) are calculated by $\text{Gap}_1/\text{Z}_{\text{multi}} \times 100$, $\text{Gap}_2/\text{Z}_{\text{multi}} \times 100$, and $\text{Gap}_3/\text{Z}_{\text{multi}} \times 100$, respectively; (3) M$ denotes million dollars.

We then examine to what extent due to different fleet deployment decisions and to what extent due to different demand fulfillment and allocation decisions that the multistage model outperforms the two-stage model. To this end, we design a multistage stochastic programming model using two-stage deployment decisions (i.e., fleet deployment decisions are first obtained by using the two-stage model [M_{two}], and demand fulfillment and allocation decisions are then obtained by using the multistage model). The expected profits of the two-stage method, multistage method, and

multistage stochastic programming model using two-stage deployment decisions are denoted by Z_{two}, Z_{multi}, and $Z_{\text{multi}}^{\text{two deploy}}$, respectively, and compared in the last two columns of Table 3-10. We can see that 10% ($= (Z_{\text{multi}} - Z_{\text{multi}}^{\text{two deploy}})/(Z_{\text{multi}} - Z_{\text{two}})$) of the benefit brought by the multistage model over the two-stage model is due to better fleet deployment decisions and 90% ($= (Z_{\text{multi}}^{\text{two deploy}} - Z_{\text{two}})/(Z_{\text{multi}} - Z_{\text{two}})$) of the benefit is due to better demand fulfillment and allocation decisions.

Table 3-10 Impact of uncertainty on the operations management of liner companies.

Case ID	Routing capacity			Two-stage stochastic programming (SP)			Multistage SP			Multistage SP using two-stage deployment decisions			Benefits (M$)	
	C_{deter} (TEU)	C_{two} (TEU)	C_{multi} (TEU)	Z_{two} (M$)	Total accept (TEU)	Total delay (TEU)	Z_{multi} (M$)	Total accept (TEU)	Total delay (TEU)	$Z_{\text{multi}}^{2\text{ dep}}$ (M$)	Total accept (TEU)	Total delay (TEU)	Z_1	Z_2
1	16,848	35,272	35,272	603.08	835,143	183,910	641.52	845,523	36,892	641.52	845,523	36,892	0.00	38.44
2	16,848	29,558	35,272	542.56	769,236	235,139	637.06	842,148	35,861	595.05	790,602	49,581	42.01	52.49
3	16,848	36,554	36,554	608.85	847,286	166,515	642.96	856,691	35,599	642.96	856,691	35,599	0.00	34.11
4	17,258	35,272	35,272	588.27	815,106	170,823	626.23	827,593	33,928	626.23	827,555	33,765	0.00	37.96
5	16,848	35,272	35,272	594.33	823,101	172,035	631.78	835,037	37,229	631.78	835,037	37,230	0.00	37.45
6	16,848	35,272	35,272	605.42	832,316	178,617	643.36	844,117	36,458	643.32	843,317	36,062	0.04	37.90
7	17,668	35,272	35,272	605.12	831,868	163,257	639.79	843,321	35,966	639.79	843,328	35,971	0.00	34.67
8	17,258	35,272	35,272	589.69	817,472	174,055	627.79	829,224	34,284	627.79	829,225	34,284	0.00	38.10
9	17,668	35,272	35,272	603.34	835,420	184,431	644.65	847,835	31,762	644.65	847,835	31,763	0.00	41.31
10	17,258	35,272	36,554	601.06	830,737	176,504	638.50	845,432	33,152	638.48	842,885	39,715	0.02	37.42
Avg.	17,135	34,829	35,528	594.17	823,769	180,529	637.36	841,693	35,114	633.16	836,200	37,087	4.21	38.99

Notes: (1) C_{deter}, C_{two}, and C_{multi} denote the total routing capacities on all ship routes using deterministic programming, two-stage stochastic programming, and multistage stochastic programming, respectively; (2) Z_{two}, Z_{multi}, and $Z_{\text{multi}}^{2\text{ depl}}$ denote the expected profits using two-stage stochastic programming, multistage stochastic programming, and multistage stochastic programming with two-stage deployment decisions, respectively; (3) the values in the "Total accept" and "Total delay" columns are the expected total number of accepted container and the expected total number of delayed containers, respectively; (4) values in "Z_1" and "Z_2" columns are calculated by $\text{Z}_{\text{multi}} - \text{Z}_{\text{multi}}^{2\text{ dep}}$ and $\text{Z}_{\text{multi}}^{2\text{ dep}} - \text{Z}_{\text{two}}$, respectively; (5) M$ denotes million dollars.

3.6.3 Managerial insights for liner shipping

This chapter then discusses three practical questions regarding the driver analysis of liner company profitability, the benefit analysis of adaptive fleet sizes, and the influence of pandemic diseases on liner shipping. Case ID "M8" in Table 3-6 is selected as the computational instance in this experiment.

We first report liner company profitability in Table 3-11 with various operational characteristics ($f_{h,r}$, $c_{k,r}$, g_k, $p_{o,d}$, and m_k) and the demand parameters ($l_{o,d}$, and $q_{o,d,t}^s$). Three random cases are conducted, and values of parameters listed in Table 3-

11 are changed based on the value setting introduced in Section 3.6.1. Values in the "Profit" columns are objective values of model [M3-1], and values in the "Gap" columns are calculated by the difference between the objective values of the original case and that of the changed value setting divided by the objective value of the original case and times 100.

Table 3-11 Driver analyses of liner company profitability.

Parameters	Value setting	Case 1		Case 2		Case 3	
		Profit (M$)	Gap (%)	Profit (M$)	Gap (%)	Profit (M$)	Gap (%)
Operational parameters	Increase $f_{h,r}$ by 25%	625.74	−1.78	631.25	−1.82	614.92	−1.81
	Increase $f_{h,r}$ by 50%	614.43	−3.55	619.66	−3.62	603.61	−3.61
	Increase $c_{k,r}$ by 25%	621.97	−2.37	627.35	−2.43	611.15	−2.41
	Increase $c_{k,r}$ by 50%	606.89	−4.74	612.12	−4.80	596.07	−4.82
	Increase g_k by 25%	630.18	−1.08	635.86	−1.10	619.36	−1.10
	Increase g_k by 50%	623.83	−2.08	628.76	−2.21	612.48	−2.20
	Increase $p_{o,d}$ by 25%	635.62	−0.23	641.26	−0.26	624.77	−0.23
	Increase $p_{o,d}$ by 50%	634.63	−0.38	640.04	−0.45	623.81	−0.39
	Decrease m_k by 25%	634.33	−0.43	640.23	−0.42	623.50	−0.44
	Decrease m_k by 50%	631.73	−0.84	637.50	−0.85	620.77	−0.87
Demand parameter	Decrease $l_{o,d}$ by 25%	456.92	−28.28	460.60	−28.36	448.90	−28.32
	Decrease $l_{o,d}$ by 50%	280.82	−55.92	282.39	−56.08	275.42	−56.02
	Decrease $q^s_{o,d,t}$ by 25%	486.51	−23.63	491.73	−23.52	478.18	−23.64
	Decrease $q^s_{o,d,t}$ by 50%	326.27	−48.79	329.20	−48.80	319.97	−48.91

Notes: (1) The values in the "Profit" columns are objective values of model [M1], and the values in the "Gap" columns are calculated by the difference between the objective values of the original case and that of the changed value setting divided by the objective value of the original case times 100; (2) M$ denotes million dollars.

As expected, liner company profitability depends on both operational characteristics and shipment demands. Among all operational characteristics, the operating cost of ships ($c_{k,r}$) has the greatest impact on liner company profitability. Other operational variations remain moderate. For example, even massive increases in the penalty cost for delayed containers ($p_{o,d}$) (by up to 50%) or massive decreases in the revenue of chartering out a ship (m_k) (by up to 50%) induce very moderate profit decreases (within 1%). Moreover, massive increases in the repositioning cost ($f_{h,r}$), and rental cost of chartering in a ship (g_k) (by up to 50%) result in moderate profit decreases (within 4%). However, the impact of demand parameters ($l_{o,d}$ and $q^s_{o,d,t}$) is much larger than that of operational characteristics. For example, a 25% decrease in the shipment demand ($q^s_{o,d,t}$) reduces profits by more than 20% in the three cases. Therefore, in addition to improving operational capabilities, liner companies must pay more attention to the demand market to manage customer expectations and attract more shipment demands by pricing strategies, public relations campaigns, and marketing campaigns. Similar conclusions are also drawn from Wang et al. (2022).

Since shipment demand is the main driver of liner company profitability and varies greatly in practice, this chapter then discusses the impact of the uncertain container shipment demand on the operation of ship fleets. As introduced in Section 3.6.1, the number of container shipment demand during each period is assumed to be uniformly distributed in [0, 5000] TEUs. However, container shipment demand always fluctuates instead of staying the same across different periods. For example, from January to April 2020, the container throughput at the Port of Shanghai fell by 8.4% from the previous year (CWTN, 2021). Hence, we vary the distribution of the container shipment demand during each period to investigate its influence. We assume that the demand follows a log-normal distribution with mean represented by μ and variance represented by σ^2 because it is easy for a log-normal distribution to adjust its mean and variance and the log-normal distribution is widely used in the literature (Wang et al., 2013). The variance of the demand can be considered as a measure of risk in an uncertain shipping market. We further assume that the coefficient of variation σ/μ, denoted by λ, is the same for all O-D pairs, time periods, and scenarios. Values of μ, and λ are set to 2,500, and between 0 and 0.4 in intervals of 0.05, respectively. Ten sets of computational instances for each value of λ are conducted, and the average of the 10 objective values (OBJ) is shown in Figure 3-7. Obviously, the expected total profit decreases as λ increases. This makes sense because the variance of demands normally means that the originally deployed ship is more likely not to be suitable for the current demand; that is, there is sometimes a large amount of spare capacity onboard the ship, and the ship is sometimes too small to carry the required cargo, resulting in a decrease in the total profit of the liner company. However, equipped with the multi-stage stochastic programming model, the loss in profit is marginal: when λ increases from 0 to 0.4, the average total profit only decreases by $(661{,}465{,}745 - 649{,}172{,}756)/661{,}465{,}745 \times 100\% \approx 1.86\%$.

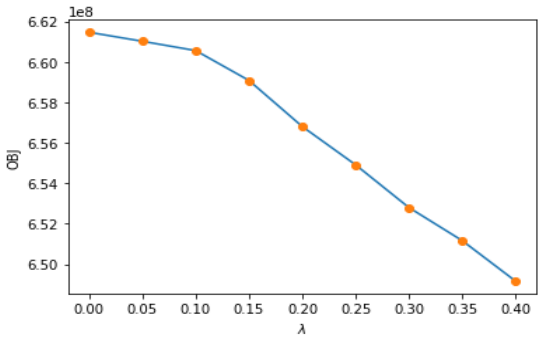

Figure 3-7 Impact of the uncertain container demand.

Finally, we investigate how the chartering in and out of the ships affect ship repositioning plans and profitability by changing the rental cost of chartering in ships and the revenue of chartering out ships. As shown in Table 3-12, five sets of scenarios are considered and three random computational experiments are conducted. The value setting in the base scenario is the value setting introduced in Section 3.6.1. N_1, N_2, and N_3 in Table 3-12 represent the total number of deployed own ships, the total number of deployed ships chartered (in) from other shipping liners, and the total number of ships chartered (out) to other shipping liners, respectively. And the five numbers in parentheses represent the numbers of deployed ships of type 1, type 2, type 3, type 4, and type 5, respectively. Recall that all ships owned by the liner company are of type 1. The rental cost of chartering in ships and the revenue of chartering out ships have little influence on the fleet decisions because the decisions of Case 2 and Case 3 in Table 3-12 are the same regardless of how g_k and m_k change, which is also reflected in Table 3-11. However, in Case 1 in Table 3-12, when the rental cost of chartering in ships increases or the revenue of chartering out ships decreases, the liner company tends to deploy its own ships and charter in less ships, which is reasonable because deploying own ships can help compensate for the decline in the company's profit.

Table 3-12 Influence of charter prices on fleet decisions.

Value setting	Case 1			Case 2			Case 3		
	N_1	N_2	N_3	N_1	N_2	N_3	N_1	N_2	N_3
Base	0	6 (0:1:1:2:2)	6	0	6 (0:0:2:2:2)	6	0	6 (0:1:1:2:2)	6
Increase g_k by 25%	0	6 (0:1:1:2:2)	6	0	6 (0:0:2:2:2)	6	0	6 (0:1:1:2:2)	6
Increase g_k by 50%	1 (1:0:0:0:0)	5 (0:0:1:2:2)	5	0	6 (0:0:2:2:2)	6	0	6 (0:1:1:2:2)	6
Decrease m_k by 25%	0	6 (0:1:1:2:2)	6	0	6 (0:0:2:2:2)	6	0	6 (0:1:1:2:2)	6
Decrease m_k by 50%	1 (1:0:0:0:0)	5 (0:0:1:2:2)	5	0	6 (0:0:2:2:2)	6	0	6 (0:1:1:2:2)	6

Notes: (1)N_1, N_2, and N_3 represent the total number of deployed own ships, the total number of deployed ships chartered in from other shipping liners, and the total number of ships chartered out to other shipping liners, respectively; (2) the values of N_1, N_2, and N_3 can be calculated by $\sum_{h\in H_1}\sum_{r\in R_{y_h}}\alpha_{h,r}$, $\sum_{h\in H_2}\sum_{r\in R_{y_h}}\alpha_{h,r}$, and $\sum_{h\in H_1}(u_h - \sum_{r\in R_{y_h}}\alpha_{h,r})$, respectively; (3) the five numbers in parentheses represent the numbers of deployed ships of type 1, type 2, type 3, type 4, and type 5, respectively.

When the planning horizon consists of multiple periods, the liner company can be more reactive to uncertain demand by adjusting fleet capacities in view of realized demand. We consider a set U consisting of OD pairs Singapore-Laem Chabang, Laem Chabang-Singapore, Singapore-Port Klang, Port Klang-Singapore, Singapore-Karachi, and Colombo-Singapore between which ships with capacities of 2,808 TEU (i.e., ships of type 1) can be deployed on an ad-hoc manner. An MILP model is developed in Appendix C to formulate the multistage stochastic program with adaptive

fleet size. Demand ($q^s_{o,d,t}$) is drawn from a log-normal distribution with mean 2,500 TEU and a large standard deviation of 5,000. Two scenarios, i.e., charter prices are independent of demands and charter prices are related to demands, are considered in this analysis. For the first scenario, the rental cost ($\hat{g}_{o,d,s}$) of chartering in such a ship to provide point-to-point shipping service from port o to port d, $(o,d) \in U$, under scenario s, $s \in S$, is assumed to be uniformly distributed in [(100,000 + the total sailing time periods (days) of a deployed ship × 19,800) times 0.5, (100,000 + the total sailing time periods (days) of a deployed ship ×19,800) ×3]. For the second scenario, the value of $x^{\text{cost}}_{o,d,s}$ is set to (100,000 + the total sailing time periods (days) of a deployed ship × 19,800)× $\frac{q^s_{o,d,t}}{2500} \times 1.75$.

Ten random sets of computational instances are conducted, and results of fixed fleet sizes, adaptive fleet sizes with charter prices independent of demands, and adaptive fleet sizes with charter prices related to demands are recorded in Table 3-13. Although adaptive fleet sizes can increase the profit of the liner company, the average relative gaps in the company profit of the above-mentioned two scenarios are only 1.09% and 1.76%, respectively. When adaptive fleet sizes are available (either the scenario of charter prices independent of demands or the scenario of charter prices related to demands), in the face of huge fluctuations in demand, the liner company prefer to deploy ships with smaller capacity in the first stage, and then charter in more point-to-point ships to respond to increased demand more flexibly. Besides, we reduce the standard deviation from 5,000 to 2,500, 1,250, and 625 and find that the relative gaps in the company profit are at most 0.63%, 0.20%, and 0.05%, respectively (detailed results are in Tables 3-14–3-16). Therefore, in practice, when demand fluctuation is moderate, liner companies, especially those without operational research decision-making support, can ignore adaptive fleet sizes because the benefits brought by this factor are too small but companies have to make a lot of decisions manually. Moreover, based on Tables 3-13–3-16, we find that there is no clear conclusion whether the liner company should charter in more point-to-point ships and whether it will earn more profits in the scenario of demand-related charter prices than in the scenario of demand-independent charter prices.

Table 3-13 Benefit analysis of adaptive fleet sizes for instances with standard deviation 5,000.

ID	Fixed fleet sizes		Adaptive fleet sizes											
			Charter prices independent of demand						Charter prices related to demand					
	P_1 (M$)	N_1 (TEU)	P_2 (M$)	G_1 (%)	N_1 (TEU)	d_1 (TEU)	d_2 (TEU)	N_2	P_3 (M$)	G_2 (%)	N_1 (TEU)	d_1 (TEU)	d_2 (TEU)	N_2
1	580.36	36,554	587.70	1.26	33,648	10,193	2,791	1.19	591.41	1.90	33,648	9,689	2,686	1.35
2	580.19	34,862	587.36	1.24	34,862	12,192	2,795	1.07	591.59	1.96	29,148	11,408	2,722	1.29
3	590.59	36,554	598.04	1.26	33,648	11,836	2,767	1.28	605.62	2.54	33,648	10,821	2,689	1.68
4	590.40	34,862	598.70	1.41	33,648	10,638	2,773	1.24	601.88	1.94	29,148	9,840	2,766	1.29
5	624.34	36,554	630.29	0.95	33,648	9,501	2,772	0.94	633.69	1.50	33,648	8,706	2,632	1.15
6	594.00	36,554	599.65	0.95	34,862	10,696	2,757	0.92	603.48	1.60	34,862	9,469	2,663	1.15
7	573.42	34,862	579.11	0.99	34,862	9,671	2,887	0.79	582.09	1.51	29,148	8,852	2,723	0.99
8	569.54	34,862	575.90	1.12	34,862	9,960	2,743	0.98	579.63	1.77	34,862	9,025	2,648	1.21
9	571.06	34,862	576.28	0.91	33,648	9,695	2,749	0.79	579.43	1.47	33,648	8,412	2,650	1.02
10	578.32	34,862	583.26	0.85	34,862	10,489	2,788	0.81	586.32	1.38	34,862	9,429	2,678	0.95
Avg.	585.22	35,539	591.63	1.09	34,255	10,488	2,783	1.00	595.51	1.76	32,662	9,566	2,686	1.21

Notes: (1) P_1, P_2, and P_3 represent the profit values of models considering fixed fleet sizes, adaptive fleet sizes with charter prices independent of demands, and adaptive fleet sizes with charter prices related to demands, respectively; (2) G_1, and G_2 represent the relative gaps (%) for the models considering fixed fleet sizes and adaptive fleet sizes with charter prices independent of demands, and the models considering fixed fleet sizes and adaptive fleet sizes with charter prices related to demands, respectively; the values of G_1, and G_2 can be calculated by $(P_2 - P_1) \div P_1 \times 100$ and $(P_3 - P_1) \div P_1 \times 100$, respectively; (3) N_1, and N_2 represent the total capacity of deployed ships in the first stage, and the average number of chartered point-to-point ships, respectively; (4) d_1, and d_2 represent the average demand per time period for each O-D pair in the scenario with the use of additional point-to-point ships, and the average shipping volume per point-to-point ship per O-D pair per time period in the scenario with the use of additional point-to-point ships, respectively; (5) M$ denotes million dollars.

Table 3-14 Benefit analysis of adaptive fleet sizes for instances with standard deviation 2,500.

ID	Fixed fleet sizes		Adaptive fleet sizes											
			Charter prices independent of demand						Charter prices related to demand					
	P_1 (M$)	N_1 (TEU)	P_2 (M$)	G_1 (%)	N_1 (TEU)	d_1 (TEU)	d_2 (TEU)	N_2	P_3 (M$)	G_2 (%)	N_1 (TEU)	d_1 (TEU)	d_2 (TEU)	N_2
1	623.08	36,554	626.96	0.62	34,862	7,610	2,753	0.66	627.33	0.68	34,862	7,375	2,696	0.65
2	616.20	34,862	620.72	0.73	34,862	8,506	2,692	0.71	621.04	0.79	34,862	8,021	2,662	0.71
3	627.75	34,862	630.35	0.41	34,862	6,753	2,595	0.45	630.64	0.46	34,862	6,401	2,554	0.47
4	614.41	34,862	618.32	0.64	34,862	7,173	2,716	0.68	618.99	0.75	34,862	6,974	2,681	0.66
5	647.63	34,862	651.44	0.59	34,862	6,985	2,706	0.60	651.75	0.64	34,862	6,634	2,604	0.63
6	615.37	34,862	618.55	0.52	34,862	6,896	2,662	0.52	618.85	0.57	34,862	6,600	2,586	0.54
7	631.62	34,862	635.11	0.55	34,862	7,386	2,651	0.58	635.38	0.60	34,862	7,009	2,576	0.58
8	612.73	34,862	615.46	0.45	22,299	7,050	2,744	0.46	615.72	0.49	34,862	7,008	2,675	0.44
9	642.73	34,862	647.02	0.67	34,862	7,801	2,734	0.67	647.21	0.70	24,648	7,898	2,724	0.60
10	631.43	36,554	634.34	0.46	34,862	7,137	2,717	0.59	635.31	0.61	34,862	6,972	2,704	0.61
Avg.	626.30	35,200	629.83	0.56	33,606	7,330	2,697	0.59	630.22	0.63	33,841	7,090	2,647	0.59

Notes: (1) P_1, P_2, and P_3 represent the profit values of models considering fixed fleet sizes, adaptive fleet sizes with charter prices independent of demands, and adaptive fleet sizes with charter prices related to demands, respectively; (2) G_1, and G_2 represent the relative gaps (%) for the models considering fixed fleet sizes and adaptive fleet sizes with charter prices independent of demands, and the models considering fixed fleet sizes and adaptive fleet sizes with charter prices related to demands, respectively; the values of G_1, and G_2 can be calculated by $(P_2 - P_1) \div P_1 \times 100$ and $(P_3 - P_1) \div P_1 \times 100$, respectively; (3) N_1, and N_2 represent the total capacity of deployed ships in the first stage, and the average number of chartered point-to-point ships, respectively; (4) d_1, and d_2 represent the average demand per time period for each O-D pair in the scenario with the use of additional point-to-point ships, and the average shipping volume per point-to-point ship per O-D pair per time period in the scenario with the use of additional point-to-point ships, respectively; (5) M$ denotes million dollars.

Table 3-15 Benefit analysis of adaptive fleet sizes for instances with standard deviation 1,250.

ID	Fixed fleet sizes		Adaptive fleet sizes												
			Charter prices independent of demand						Charter prices related to demand						
	P_1 (M$)	N_1 (TEU)	P_2 (M$)	G_1 (%)	N_1 (TEU)	d_1 (TEU)	d_2 (TEU)	N_2	P_3 (M$)	G_2 (%)	N_1 (TEU)	d_1 (TEU)	d_2 (TEU)	N_2
1	637.03	34,862	638.74	0.27	34,862	5,965	2,674	0.31	638.63	0.25	34,862	6,198	2,582	0.28
2	646.88	34,862	647.74	0.13	29,148	4,530	2,497	0.18	647.58	0.11	34,862	4,646	2,439	0.17
3	636.61	34,862	637.56	0.15	34,862	4,625	2,321	0.21	637.42	0.13	34,862	4,714	2,388	0.19
4	638.45	34,862	640.24	0.28	34,862	4,951	2,568	0.34	640.04	0.25	34,862	4,973	2,534	0.32
5	648.03	34,862	649.34	0.20	34,862	4,787	2,550	0.26	649.06	0.16	34,862	4,902	2,505	0.23
6	635.54	34,862	637.09	0.24	34,862	4,957	2,519	0.33	636.76	0.19	29,148	5,003	2,604	0.20
7	648.57	35,272	649.67	0.17	34,862	4,848	2,382	0.27	649.47	0.14	34,862	4,897	2,434	0.24
8	659.63	34,862	661.00	0.21	34,862	5,128	2,492	0.29	660.68	0.16	34,862	5,250	2,549	0.26
9	644.15	34,862	645.26	0.17	34,862	4,817	2,472	0.26	645.01	0.13	34,862	4,860	2,486	0.24
10	643.59	34,862	644.61	0.16	34,862	4,847	2,405	0.21	644.43	0.13	24,648	4,913	2,487	0.18
Avg.	643.85	34,903	645.13	0.20	34,291	4,946	2,488	0.27	644.91	0.16	33,269	5,036	2,501	0.23

Notes: (1) P_1, P_2, and P_3 represent the profit values of models considering fixed fleet sizes, adaptive fleet sizes with charter prices independent of demands, and adaptive fleet sizes with charter prices related to demands, respectively; (2) G_1, and G_2 represent the relative gaps (%) for the models considering fixed fleet sizes and adaptive fleet sizes with charter prices independent of demands, and the models considering fixed fleet sizes and adaptive fleet sizes with charter prices related to demands, respectively; the values of G_1, and G_2 can be calculated by $(P_2 - P_1) \div P_1 \times 100$ and $(P_3 - P_1) \div P_1 \times 100$, respectively; (3) N_1, and N_2 represent the total capacity of deployed ships in the first stage, and the average number of chartered point-to-point ships, respectively; (4) d_1, and d_2 represent the average demand per time period for each O-D pair in the scenario with the use of additional point-to-point ships, and the average shipping volume per point-to-point ship per O-D pair per time period in the scenario with the use of additional point-to-point ships, respectively; (5) M$ denotes million dollars.

Table 3-16 Benefit analysis of adaptive fleet sizes for instances with standard deviation 625.

ID	Fixed fleet sizes		Adaptive fleet sizes												
			Charter prices independent of demand						Charter prices related to demand						
	P_1 (M$)	N_1 (TEU)	P_2 (M$)	G_1 (%)	N_1 (TEU)	d_1 (TEU)	d_2 (TEU)	N_2	P_3 (M$)	G_2 (%)	N_1 (TEU)	d_1 (TEU)	d_2 (TEU)	N_2
1	653.18	34,862	653.45	0.04	34,862	3,801	1,751	0.10	653.36	0.03	34,862	3,978	2,147	0.06
2	660.50	34,862	660.85	0.05	34,862	4,031	2,112	0.10	660.72	0.03	34,862	4,207	2,271	0.07
3	654.26	34,862	654.53	0.04	34,862	3,846	1,922	0.08	654.45	0.03	24,648	4,173	2,317	0.04
4	661.31	34,862	661.51	0.03	34,862	3,610	1,720	0.10	661.44	0.02	34,862	3,589	1,907	0.07
5	653.10	34,862	653.31	0.03	34,862	3,582	1,793	0.08	653.22	0.02	34,862	3,571	1,857	0.06
6	654.02	34,862	654.19	0.03	29,148	3,560	2,177	0.05	654.12	0.02	34,862	3,559	2,613	0.04
7	656.78	34,862	657.44	0.10	34,862	4,279	2,199	0.13	657.35	0.09	34,862	4,401	2,282	0.12
8	645.73	34,862	646.05	0.05	24,648	3,850	2,012	0.08	645.96	0.04	34,862	4,178	1,956	0.09
9	650.60	34,862	650.85	0.04	34,862	3,758	2,015	0.09	650.77	0.03	24,648	3,916	1,973	0.06
10	655.41	34,862	655.90	0.07	30,362	3,903	2,006	0.13	655.80	0.06	24,648	3,804	2,083	0.11
Avg.	654.49	34,862	654.81	0.05	32,819	3,822	1,971	0.09	654.72	0.04	31,798	3,938	2,141	0.07

Notes: (1) P_1, P_2, and P_3 represent the profit values of models considering fixed fleet sizes, adaptive fleet sizes with charter prices independent of demands, and adaptive fleet sizes with charter prices related to demands, respectively; (2) G_1, and G_2 represent the relative gaps (%) for the models considering fixed fleet sizes and adaptive fleet sizes with charter prices independent of demands, and the models considering fixed fleet sizes and adaptive fleet sizes with charter prices related to demands, respectively; the values of G_1, and G_2 can be calculated by $(P_2 - P_1) \div P_1 \times 100$ and $(P_3 - P_1) \div P_1 \times 100$, respectively; (3) N_1, and N_2 represent the total capacity of deployed ships in the first stage, and the average number of chartered point-to-point ships, respectively; (4) d_1, and d_2 represent the average demand per time period for each O-D pair in the scenario with the use of additional point-to-point ships, and the average shipping volume per point-to-point ship per O-D pair per time period in the scenario with the use of additional point-to-point ships, respectively; (5) M$ denotes million dollars.

Finally, we investigate the influence of pandemic diseases on liner shipping. Many ports require foreign ships to undergo a compulsory quarantine for 14 days or even 28 days during the COVID-19 pandemic, which greatly increases the repositioning time. Hence, we set the preparation time, denoted by N, to 0, 2, 4, 6, 8, 10, 12, 14, 16, 18, 20, 22, 24, 26, and 28 days. Profit values, i.e., $\mathrm{OBJ}(N)$, related to the number of preparation days (N) are recorded in Table 3-17. From this table, we can see that the total profit decreases as the number of days for preparation increases. This is reasonable because a longer preparation time inevitably leads to an increase in the repositioning time, thereby increasing the repositioning cost and reducing the profit. To show the change of the objective function value more directly, the differences in objective values for adjacent computational instances in Table 3-17, i.e., $\mathrm{OBJ}(N) - \mathrm{OBJ}(N+2)$, are also recorded in Figure 3-8. It is obvious that when the number of preparation days is less than ten days, the objective value is very sensitive

to changes in the number of preparation days. Hence, governments need to think carefully about how to set the proper number of quarantine days for foreign ships to balance the trade-off between containing diseases and the profit for liner companies.

Table 3-17 Influence of the COVID-19 pandemic on liner shipping.

Preparation days (N)	OBJ (N) (M$)	Preparation days (N)	OBJ (N) (M$)	Preparation days (N)	OBJ (N) (M$)
0	689.79	10	545.54	20	460.21
2	658.57	12	526.29	22	444.92
4	627.35	14	508.11	24	429.95
6	597.03	16	491.35	26	414.98
8	569.03	18	475.70	28	400.01

Note: M$ denotes million dollars.

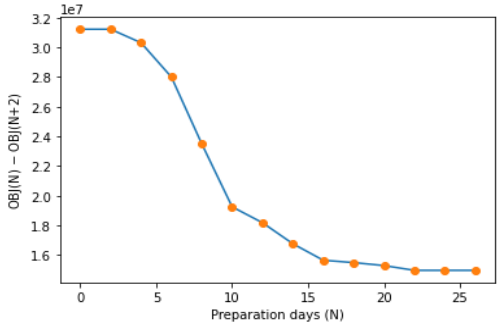

Figure 3-8 Influence of the COVID-19 pandemic on liner shipping.

3.6.4 Summary of the managerial insights

This section summarizes managerial insights from our computational experiments to help decision-makers of liner companies. First, using the proposed BBC algorithm to solve our problem is fast. Hence, with the help of our solution method, decision-makers of liner companies can obtain a quick plan with fleet deployment, fleet repositioning, ship chartering, demand fulfillment, and cargo allocation to deal with uncertainties in the shipping market. Besides, since the average gap value between the objective values of the multistage stochastic programming and the perfect information is less than 0.55%, and the multistage stochastic programming can provide much better solutions than the two-stage stochastic (6.78% higher profits) and the deterministic (16.00% higher profits) programming formulations (similar conclusions were drawn by Huang and Ahmed (2009)), multistage stochastic programming can help decision-makers to better operate and manage liner companies. Moreover, an intensive analysis of why multistage stochastic programming can lead to better solutions is also conducted. Benefits brought by multistage over two-stage stochastic programming are divided into two categories: one is the improved fleet deployment decisions, and the other is demand fulfillment and allocation decisions

with full utilization of demand information. The latter accounts for 90% of the total benefit.

Next, we studied three practical questions regarding the driver analysis of liner company profitability, the benefit analysis of adaptive fleet sizes, and the influence of pandemic diseases on liner shipping. First, we find that liner company profitability depends mainly on the revenue generated by each accepted container (i.e., freight rate) and shipment demand, and operational characteristics such as penalty cost for delayed containers and revenue of chartering out a ship have a much smaller impact on the profitability. Since the freight rate is mainly determined by the market, liner companies must pay more attention to the demand market to manage customer expectations and attract more shipment demands by pricing strategies, public relations campaigns, and marketing campaigns. Similar conclusions are also drawn from Wang et al. (2022). Since container shipment demand has such a huge impact on the operations of liner companies, the influence of uncertain demand is also investigated. The liner company's profit generally decreases as the coefficient of variation of uncertain demand increases. Wang et al. (2013) also observed that the average total cost generally increases with the value of the coefficient of variation when all shipment demand must be fulfilled. Hence, we believe that the variability of the uncertain demand has a significant effect on the planning solutions because fluctuations in the container shipment demand in the shipping market greatly affect the revenue of liner companies. Hence, the way liner companies respond to market fluctuations at the beginning is crucial. As shown in the numerical experiments, using the multi-stage programming model, the average total profit only decreases by 1.86% when the coefficient of variation increases from 0 to 0.4.

For the second question about the benefit of adaptive fleet sizes, although adaptive fleet sizes can increase the profit of the liner company, the relative gap in the company profit is at most 1.76% on average for the case with the coefficient of variation equal to 2, and the relative gaps are less than 0.63% for the with coefficient values of variation equal to 1, 0.5, and 0.25. Hence, in practice, when demand fluctuation is moderate, liner companies, especially those without operational research decision-making support, can ignore adaptive fleet sizes because the benefits brought by this factor are too small.

Finally, in terms of the influence of pandemic diseases on liner shipping, when the number of preparation days is less than ten days, the expected profit is very sensitive to changes in the number of preparation days. Therefore, governments need to think carefully about how to set the proper number of quarantine days for foreign ships so that liner companies can make money and remain in operation.

3.7 SUMMARY

This chapter shows how to operate ship fleets under uncertainty to deal with a liner's multi-period heterogeneous FDP in an uncertain shipping network considering fleet repositioning, ship chartering, demand fulfillment, and cargo allocation. While this issue is crucial for liner company operations, it has hardly been studied in the scientific literature. To fill this research gap, we first introduce this multistage optimization problem and developed a mixed-integer linear programming model for the problem. Since this problem is NP-hard, we design a Benders-based branch-and-cut approach to solve the model. Two types of acceleration strategies are applied to improve the performance of the proposed algorithm. Contributions of this paper are summarized from the following three aspects.

From the perspective of modeling, we formulate the problem as a multistage stochastic programming model. In the first stage, the model determines the number of deployed ships of different types on ship routes in the network of the liner company, the sailing sequence of these deployed ships, and the numbers of charter-in and charter-out ships when there is a deficit or a surplus in some ship types; in the following stages, when the container shipment demands become realized, the model determines the numbers of accepted, delayed and shipped containers for each O-D pair during each time period under each scenario. Moreover, we also formulate a multistage MILP model to allow for adaptive fleet sizes, i.e., liner companies may rent additional point-to-point ships for transportation in addition to deployed ships from the decisions in the first stage.

From the perspective of algorithm design, the NP-hardness of the problem does not stop us from looking for an exact and efficient algorithm to solve the problem of practical scale with realistic data. We design a BBC algorithm to solve the formulated model. To tackle the challenge of solving the multistage optimization problem, we derive two types of acceleration strategies, including approximate upper bound

tightening inequalities and Pareto-optimal cuts, to improve the performance of the proposed algorithm. The accuracy and efficiency of the proposed BBC algorithm for computational instances are verified.

From the perspective of managerial insights, we first investigate the impact of uncertainty on the operations management of liner companies and find using multistage stochastic programming can lead to higher profit than using two-stage stochastic programming or deterministic programming. We next conduct an intensive analysis of why multistage stochastic programming can lead to better solutions and find benefits brought by multistage are divided into two categories: one is the improved deployment decisions, and the other is demand fulfillment and allocation decisions with full utilization of demand information. The latter accounts for 90% of the total benefit. Finally, we discuss three practical questions regarding the driver analysis of liner company profitability, the benefit analysis of adaptive fleet sizes, and the influence of pandemic diseases on liner shipping. With the help of our solution method, decision-makers of liner companies can obtain a quick plan with fleet deployment, fleet repositioning, ship chartering, demand fulfillment, and cargo allocation scheduling to deal with uncertainties in the shipping market.

Chapter 4: Joint routing, scheduling, and speed optimization for government ships considering health impacts

4.1 INTRODUCTION

Hong Kong is a world maritime center, connecting almost 600 destinations worldwide, with about 270 international container ships departing weekly (GovHK, 2022). At the same time, the Port of Hong Kong, renowned as one of the busiest container ports in the world, handled almost 18 million 20-foot equivalent units in 2021, of which more than 60% were transshipment cargo (GovHK, 2022). As a result, the large volume of vessel traffic is one of the most significant sources of air emissions. To reduce air emissions from ships, the Hong Kong government has implemented a number of marine control measures, such as the Clean Air Plan for Hong Kong released in 2013 (Environment Bureau, 2013) and the Air Pollution Control (Fuel for Vessels) Regulation came into effect in 2019 (Environmental Protection Department, 2018). Hence, faced with the current stringent regulations on air emissions from ships, the government should lead by example by strictly scheduling government ships.

Government ships carry out a number of routine trips for routine tasks, such as patrol of territorial water areas, maintenance works, and training. For example, Hong Kong has more than 900 government ships to serve 14 government departments in 2021 (Hong Kong Police Force, 2022). These trips are planned based on solely on the requirement of the tasks (e.g., two trips each week) without considering the health effects of the air emissions from ships. However, with the large volume of vessel traffic and the current stringent regulations on air emissions from ships, it can be challenging to further reduce the absolute amounts of air pollutants from government ships. Fortunately, environmental science demonstrates that the damage to the health of the population caused by unit amount of air pollutant varies significantly with the weather conditions. This creates an opportunity for multi-disciplinary research on the management of the location and time of air pollutant emissions from ships to minimize the total health effect on the population.

To control emissions from government ships, all government ships of Hong Kong are powered with Euro V diesel (sulphur content not exceeding 0.001%) (Environmental Protection Department, 2022). In addition to cleaner marine fuel, several operation decisions, such as task completion sequence and sailing speeds which further influence the environmental effect of air pollutant emissions from ships, can be jointly optimized to reduce the environmental effect. Hence, investigating how to schedule government ships considering environmental effects and weather conditions is critical to reducing the health effects of the air emissions from ships.

This chapter draws inspiration from the aforementioned real-world issue in environmentally sustainable shipping. It aims to enhance the operations management of government ships by proposing mathematical optimization models for a joint routing, scheduling, and speed optimization of government ships that account for the environmental impact of air pollutant emissions in different weather conditions. Based on the weather forecast for the planning cycle, this chapter first uses environmental science models to predict the environmental damage of one kilogram of each pollutant (e.g., SO_X, NO_X, and particulate matter) emitted at each space and time grid. This chapter then formulates several mathematical optimization models for the integrated routing, scheduling, and speed optimization of government ships. The objective is to minimize a sum of the ship's fuel cost and the health damage of the air pollutants from the trips, considering the varied effects in space and time. The decision variables are the timing of the ship activities, the routing of the ships, and the sailing speed of the speeds. A branch-and-price-and-cut (BPC) algorithm is designed to seek the optimal decision, which leads to the lowest cost to the society. This chapter aims to develop mathematical optimization models for the integrated routing, scheduling, and speed optimization of government ships that account for the environment impact of air pollutant emissions in different weather conditions, and conducts case studies using shipping data. A total of 32 sets of numerical experiments are conducted to validate the performance of the proposed model and method.

The remainder of this chapter is organized as follows. Section 4.2 offers a review of relevant literature. In Section 4.3, the background of the problem is introduced, and both a trip-based model and a set-covering model are proposed for the joint optimization problem. Section 4.4 designs a BPC algorithm to solve the problem. The efficiency of the proposed algorithm is assessed through computational experiments

and reported in Section 4.5. Finally, Section 4.6 presents a summary of the chapter's key points.

4.2 LITERATURE REVIEW

This chapter aims to address the environmental issue of air pollutant emissions released by government ships, which receives little attention in the existing literature. Of the very few papers that focus on air pollutant emissions from government ships, most only examine ship design (Keuning and Walree, 2006; Nabawi, 2021) or the feasibility of alternative energy sources (Searcy, 2017; Nguyen et al., 2021). Therefore, this chapter aims to address the environmental issue of government ships from the tactical and operational levels. The core part of this chapter is the joint routing and scheduling problem for government ships. This class of problem can be regarded as a two-stage problem with finding the optimal task execution schedule and the optimal path design among task points for daily execution plans. Moreover, the execution plan for the government ship affects its visiting path design, and different visiting paths affect the task execution plan in reverse. The majority of the literature on ship routing and scheduling, such as Ronen (1983, 1993), Christiansen et al. (2004, 2013), Kontovas (2014), and Ksciuk et al. (2023), primarily focuses on designing ports of call and subsequently determining departure and arrival times at each port of call within a predetermined shipping route. This approach, however, significantly differs from the scope of our problem. Therefore, this section reviews the relevant literature from two key aspects: (i) the vehicle routing problem (VRP), which closely aligns with the core aspect of our problem, and (ii) the algorithms employed in solving the problem.

This problem is a variation of the VRP, namely a multi-trip VRP with time windows (MTVRPTW) where a time window is associated with each task. Since vehicles normally have limited capacity, vehicles have to perform several trips per day, which introduces the multi-trip aspect. Research on MTVRPTW can be found in Hernandez et al. (2016), Paradiso et al. (2020), and Yang (2023). Unlike typical VRP studies, this chapter introduces a temporal dimension, allowing ships to complete all tasks within the planning period. In other words, trips assigned to the same vehicle may not necessarily be completed within a single day. This consideration arises from the fact that in real-life scenarios, emissions from ships released at different times and locations have varying environmental impacts. Therefore, when designing routing and

scheduling for government ships, we not only take into account the impact of the route's length but also consider the emission impact at different times and in different route segments. As far as we are aware, there is a lack of existing literature specifically addressing an MTVRPTW with the consideration of the emission impact at different times and in different route segments. Moreover, speed optimization is integrated into our problem because the amount of air emissions is directly determined by fuel consumption, which is, in turn, directly influenced by the ship's speed. Wang and Meng (2012b) introduced the relationship between fuel consumption and sailing speed for ships and provided an efficient outer-approximation method. However, classical VRP studies assume a fixed speed for vehicles and treat fuel cost as input data, overlooking the fact that fuel consumption is heavily influenced by travel speed. Only few papers, such as Fukasawa et al. (2018), and Ma et al. (2021), consider speed optimization. Fukasawa et al. (2018) formulated an integrated speed and routing optimization problem as a set-partitioning model for vehicles to minimize operating costs. Ma et al. (2021) proposed an MIP model for a VRP with speed optimization to minimize a weighted objective containing the travel distance, the travel time, and energy consumption. To our understanding, there is no literature devoted to a combined routing, scheduling, and speed optimization problem for government ships, particularly one that incorporates the impact of emissions at different times and in different route segments.

There is a rich literature developing exact algorithms to solve the VRP because these algorithms can ensure optimal solutions for this combinatorial optimization problem. To this end, many papers treat the problem as a tree exploration problem, employing branch-and-bound (B&B) algorithms for solving. However, the problem's NP-hardness limits the use of exact algorithms primarily to small-scale instances. In particular, in the case of MTVRPTW, Hernandez et al. (2016) developed two branch-and-price frameworks. These frameworks are based on two set-covering formulations, one featuring columns representing routes (a sequence of consecutive trips), and the other with columns representing individual trips. Computational results on instances with 25 customers show that some instances that cannot solved by the first framework can be solved by the second one. Paradiso et al. (2020) proposed an exact solution method based on column enumeration, column generation, and cutting plane to solve four variants of the capacitated MTVRPTW; their results shown that almost all cases

involving 40 customers and some cases involving 50 customers can be solved to optimality by the proposed solution framework within three hours. Drawing inspiration from Paradiso et al. (2020), Yang (2023) proposed an exact price-cut-and-enumerate algorithm to solve the capacitated MTVRPTW and indicated that the proposed algorithm can solve all instances with 70 customers to optimality.

In summary, few works related to the MTVRPTW consider speed optimization. However, this factor is particularly crucial for the joint routing and scheduling of government ships that take environmental effects into consideration, as the speed of a ship significantly influences its fuel consumption, thereby affecting air emissions from the ship. Specifically, we allow for the consideration of the environmental emissions of ships at different times and locations. This characteristic further distinguishes this study from existing literature. To the best of our knowledge, this chapter is the first to jointly optimize routing, scheduling, and speed optimization for government ships with the consideration of the environmental impact at different times and locations. More importantly, government ships should undertake more green shipping responsibilities than commercial ships, as the government should not solely prioritize cost considerations. However, existing papers on government ships scarcely explored how to schedule government ships considering environmental effects. To fill this research gap, this chapter develops a linear MIP model to minimize the sum of the fuel cost and the health damage of the air pollutants from the trips for routing and scheduling of government ships that account for the health effects of air pollutant emissions. Additionally, some ignored operating limits, e.g., the dispersion of air pollutant emissions, different weather conditions, new trip setup time, and ship endurance, are considered in this paper.

4.3 PROBLEM DESCRIPTION AND MODEL FORMULATION

This chapter focuses on government ships considering the environmental effects of air pollutant emissions in different weather conditions. This study aims to address a routing, scheduling, and speed optimization problem of government ships that account for the environmental effects of air pollutant emissions at different times and locations. This section begins by outlining the problem's detailed background in Section 4.3.1, introduces the dispersion of air pollutant emissions in Section 4.3.2, elaborates on the problem's objective function in Section 4.3.3, presents the mathematical model as a trip-based formulation in Section 4.3.4, linearizes the nonlinear part of the trip-based

model in Section 4.3.5, and finally proposes a set-covering formulation for the problem in Section 4.3.6.

4.3.1 Problem background

A significant proportion of the global population lives near coastlines, with New York State serving as a prominent example. The total population of the state is approximately 19.7 million, and 81% of this population lives in coastal areas (NOAA, 2023). Consequently, emissions (e.g., SO_X, NO_X, and PM_{10}) generated by government ships during their routine operations pose a significant threat to the air quality of the coastal regions and the health of nearby residents (Yau et al., 2012). Although the IMO has promulgated several regulations, such as a sulphur cap of 0.50% as stipulated in MARPOL Annex VI (IMO, 2019), to reduce air pollutant emissions, government ships often do not consider the environmental effects when carrying out their tasks because these government ships basically operate in inland waters, and they are not bound by international regulations. However, the environmental effects of air emissions tend to be more severe because the ships are closer to the coast where the population lives. Hence, the environmental effects of air emissions should be integrated into the joint routing, scheduling, and speed optimization of government ships.

Routine voyages of government ships are dedicated to tasks such as patrols of territorial water areas, maintenance works, and training. For example, Hong Kong contains more than 900 government ships to serve 14 government departments in 2021 (MD, 2021). However, in contrast to weekly scheduled liner shipping services, the routine trips of government ships are flexibly planned according to task requirements, such as two trips per week. As shown in Figure 4-1, which consists of 16 task nodes and one depot, a government ship plans to perform routine tasks along the coastline. To complete the routine task of all nodes, the government ship needs to visit all task nodes exactly once. In general, the government seeks the optimal sequence of the task nodes to visit such that the total distance traveled by the government ship is minimized. However, in reality, a severe problem for these government ships is that they usually do not consider the environmental effects of air emissions from ships when performing their routing trips.

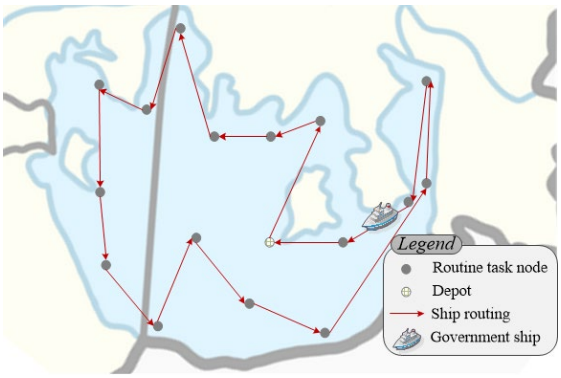

Figure 4-1 Example of a government ship performing routine tasks.

This chapter aims to determine a set of government ship task execution schedules, including the timing of ship activities (i.e., performing routine tasks) and the routing of the ship, to ensure the completion of all routine tasks in a maritime area. Specifically, we have a single government ship performing several routine tasks over a set T of days indexed by t. Due to the government's typical practice of pre-recording all routine tasks to be completed within a planning cycle and allowing for parallel execution of all tasks, we utilize a predefined set I to record all routine task nodes, indexed by i. Since the government ship consumes fuels during task execution and cannot sustain continuous sailing operations indefinitely, it necessitates regular returns to the depot for refueling. Furthermore, let s represent the setup time for preparing a new trip. For the example illustrated in Figure 4-1, it is nearly impossible for a ship to visit all task nodes in a single trip. To better reflect reality, multiple trips are permitted. We call a closed circle a trip and record all trips as the set R. As depicted in Figure 4-2, all task nodes are visited by the government ship in three trips. In each trip, the ship departs from a depot (indexed by 0 or $n+1$ depending on whether it is the initial or terminal node of a trip), then visits all nodes in this trip one by one, and finally returns to the depot. To simplify, let I^-, and I^+ denote the set of $I \cup \{0\}$, and set of $I \cup \{n+1\}$, respectively.

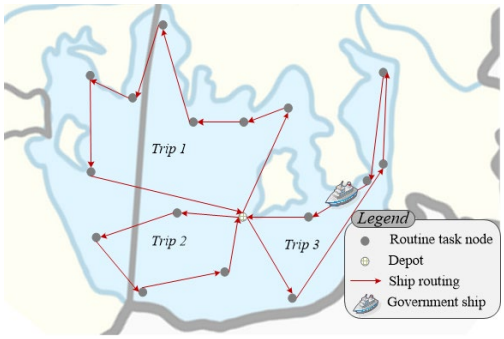

Figure 4-2 Example of a government ship performing routine tasks in three trips.

The joint routing, scheduling, and speed optimization problem in this chapter is subject to several operational and geographical constraints. Specifically, due to the necessity of crew members for the operation and execution of routine tasks on the government ship, the operational hours of the ship must align with the working hours of the crew. This implies that the government ship's operating time must fall within the time window $[a, b]$, where a and b represent the time constraints for performing routine tasks. Each routine task node, e.g., i, is characterized by its corresponding task execution time q_i ($q_0 = q_{n+1} = 0$). The total time spent on task execution and in transit along different trips should not exceed the endurance, denoted by e, of the government ship (that is, the maximum time that can be spent on task execution and in transit before being refueled at the depot). The distance between two nodes (e.g., i and j) is denoted by d_{ij}. Besides, the government ship travels at a constant speed from node i to j, which is denoted by ω_{ij}. In summary, (i) the *routing problem* to be solved is finding the optimal routes for the government ship starting from the depot, visiting each of a specified group of routine task nodes exactly once, and then returning to the depot. (ii) the *scheduling problem* must be feasible to the geographical network (consisting of the routine task nodes and the depot), the endurance of the government ship, the duration of the mandatory replenishment break (layover time) which occurs when the government ship returns to the depot, the time constraints for performing routine tasks, and the weather conditions. Regarding the timing problem of the ship activities, because the damage to the health of the population caused by a unit amount of air pollutant varies significantly with the weather conditions, we consider different weather conditions over the planning horizon to determine the optimal performing day of task node i, $i \in I$. (iii) the *speed optimization problem* determines the sailing speed of the government ship in each sailing segment. Sailing speed is a crucial factor in maritime transportation, directly influencing the ship's arrival time, energy consumption, and exhaust emissions in each segment. By optimizing the sailing speed of the ship, significant benefits can be realized, including reducing fuel costs, decreasing air emissions, and better meeting the time requirements of tasks. The speed optimization problem is closely intertwined with the first two problems, meaning that addressing these three problems requires consideration of the interdependencies among them. For instance, speed optimization is not only influenced by the ship's task execution schedule but also be constrained by the refueling and time window

limitations. This tight intertwinement necessitates a comprehensive consideration of multiple factors to find an overall optimal solution, posing greater challenges in modeling and solving.

4.3.2 Dispersion of air emissions

When considering the environmental effects of air emissions, weather conditions are essential because various weather conditions such as sunny, rainy, cloudy, and windy (the wind blowing inland or blowing ocean), directly affect the diffusion of air emissions and ultimately affect the environmental effects. Hence, this chapter studies a joint routing, scheduling, and speed optimization problem of government ships that account for the environmental effects of air pollutant emissions in different weather conditions.

This section begins by introducing the Gaussian plume model, an important part of the model being formulated. The Gaussian plume model is based on the general transport-diffusion equation, assuming steady-state conditions with no temporal changes, a homogeneous and flat spatial area, wind moving solely along the x-axis, and negligible dispersion without chemical reactions. Commonly used in atmospheric dispersion modelling, especially for regulatory purposes (Holmes and Morawska, 2006), the Gaussian plume model calculates pollution levels at specific receptor nodes, i.e., coastal areas, in this chapter. It incorporates factors such as wind velocity, horizontal and vertical dispersion, weather conditions, and effective emission height. Figure 4-3 illustrates this with a three-dimensional coordinate axis (x, y, z). The base of the chimney of the government ship is exactly at point (0,0,0), and a coastal area locates at the back of the ship and is affected by the ship's exhaust. The actual stack height is denoted by H_s. When the pollutants are emitted, they have initial momentum, and the pollutants are affected by air buoyancy. Because of the above two reasons, pollutants will be elevated, resulting in a plume rise, represented by Δh. Hence, the pollutant release height, also known as the effective stack height and denoted by H, is the sum of H_s and Δh. The wind is blowing continuously in a direction of the x-axis with a speed u_0 (m/s).

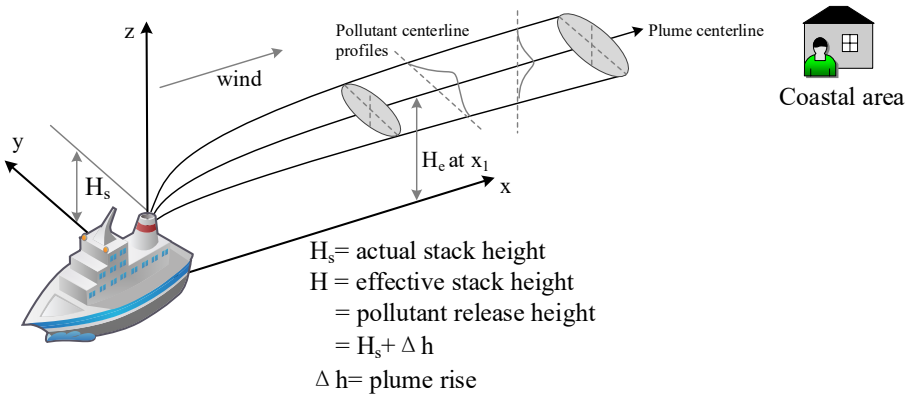

Figure 4-3 An example of the Gaussian plume model.

For the example of the chimney in Figure 4-3, most plumes are emitted close to the ground instead of spreading in free air. Hence, as the plume spreads downwards and upwards, it eventually hits the ground as it moves downwind from the source. Clearly, the plume cannot continue to spread into the ground, which means $z < 0$ is not considered. Instead, it is reflected into the air above the ground. The effect of the ground boundary is included in the downwind concentration equation mathematically by using a fictitious "mirror-image" source, and the downwind concentration (kg/m^3) at point (x, y, z) is represented by $C(x, y, z)$. Because this chapter focuses on the health effects of the population in a coastal area, i.e., assessing the exposure of humans to the pollutant, only downwind concentrations at ground level are required, which means $z = 0$. Hence, we can calculate the downwind concentrations at ground level by Equation (4-1) which is given by Pasquill (1961).

$$C(x, y, 0) = \frac{Q}{\pi \sigma_y(x) \sigma_z(x) u_0} \exp\left(-\frac{1}{2}\left(\frac{y}{\sigma_y(x)}\right)^2\right) \exp\left(-\frac{1}{2}\left(\frac{H}{\sigma_z(x)}\right)^2\right), \tag{4-1}$$

where Q is the emission rate (kg/s), $\sigma_y(x)$ and $\sigma_z(x)$ (m) are the dispersion coefficients along the crosswind and vertical axes, respectively, u_0 is the wind speed (m/s), and H is the effective stack height, illustrating that the concentration of pollutants downwind is proportional to the emission rate Q and inversely proportional to the wind speed u_0.

The government ship sails stably at a certain speed v during the voyage, but the previous Gaussian plume model does not take into account the influence of the sailing speed of the ship on the diffusion direction of pollution emissions. Because both the sailing speed v of the ship and the wind speed u_0 are vectors, we use the resultant of the two vectors as the improved wind speed to overcome the above issue. As shown in

Figure 4-4(a), the ship sails along the negative direction of the x-axis at speed v, which means that the positive direction of the x-axis is the diffusion direction of the ship's exhaust when there is no wind. The apparent wind, illustrated in Figure 4-4(b), is the wind u_0 which blows in the positive direction of the y-axis. The resultant wind direction is u. Let a_1, and a_2 be the angle between the apparent wind direction and resultant wind direction, and the angle between the resultant wind direction and the positive direction of the x-axis, respectively. After the above transformation, we can take the base of the chimney of the ship as the origin of the two-dimensional coordinate axis (x, y), and treat the ship as immobile. The exhaust emissions diffuse in the direction of the newly resultant wind speed, which can be calculated by Equation (4-2). The direction of plume diffusion is a_2, which can be calculated by Equation (4-3), radians counterclockwise from the reverse direction of the ship's heading direction. In this case, the base of the chimney of the ship, and the newly resultant wind direction are regarded as the origin of the two-dimensional coordinate axis (x, y), and the positive direction of the x-axis, respectively. The horizontal and vertical coordinates of the coastal area in the above coordinate system can be obtained, and thus the downwind concentration of the coastal area can also be calculated by Equation (4-1).

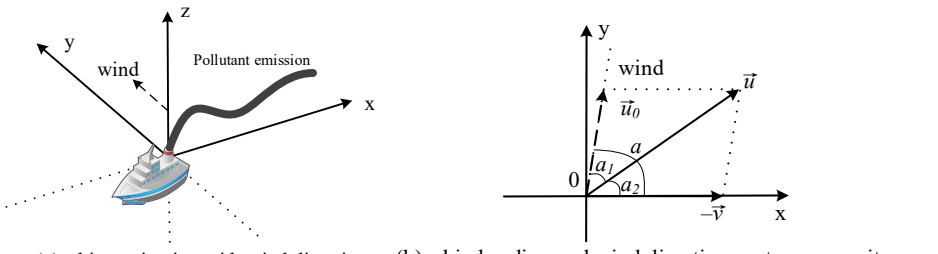

(a): ship navigation with wind direction (b): ship heading and wind direction vector composite map

Figure 4-4 Air emission diffusion of the government ship.

$$||u|| = \sqrt{(v + ||u_0 \cos a||)^2 + (u_0 \sin a)^2} \tag{4-2}$$

$$a_2 = \arccos(u^2 + v^2 - u_0^2/2u \times v). \tag{4-3}$$

4.3.3 Objective function

The problem aims to minimize the sum of the fuel cost and the health damage of the air pollutants from the trips. The first part, i.e., the fuel cost, depends on the sailing speed and the node visiting sequence for all trips. Let A represent the set of all arcs in a complete directed graph of all nodes $((i, j) \in A, i \in I^-, j \in I^+)$. Noted that the arc

$(0, n+1)$ is dummy and the distance from node 0 to $n+1$ is zero. Let d_{ij} denote the distance traveling from node i to j (n mile). As a common practice in maritime transportation (Wang and Meng, 2012b; Brouer et al., 2014; Aydin et al., 2017), the fuel cost for the sailing segment from node i to j is $d_{ij}\dot{c}(\omega_{ij})^{\ddot{c}}$, where $\dot{c}$ and $\ddot{c}$ are coefficients to calculate the unit fuel cost for travelling per nautical mile. The variable θ_{rij}, binary variable, represents whether a ship travels directly from node i to j ($i \in I^-, j \in I^+$), during trip r. Hence, the total fuel cost is $\sum_{r\in R}\sum_{(i,j)\in A}\theta_{rij}d_{ij}\dot{c}(\omega_{ij})^{\ddot{c}}$.

The second part of the objective function involves the health damage caused by the air pollutants from the trips, whose vivid calculation description is illustrated in Figure 4-5. Suppose several patrol nodes (white dot) are scattered in a maritime area, a depot is represented by a red dot, and a government ship is performing a trip $0 \rightarrow 1 \rightarrow 2 \rightarrow 3 \rightarrow 4 \rightarrow 5$. We first discretize each leg, e.g., $1 \rightarrow 2$, with unit distance (e.g., 1 n mile) and label these as solid red nodes in Figure 4-5. As introduced in Section 4.3.2, the government ship sails stably at a certain speed v during the voyage. Both the sailing speed v and the apparent wind u_0 influence the resultant wind direction u. After the transformation introduced in Section 4.3.2, we can take the base of the chimney of the government ship as the origin of the coordinates, and treat the ship as immobile. The exhaust emissions diffuse in the direction of the newly resultant wind speed, which can be calculated by Equation (4-2). The direction of plume diffusion can be calculated by Equation (4-3). Let w_t and $u_{0,t}$ denote the weather condition and apparent wind condition on day t, respectively. Hence, we can calculate the downwind concentration at the coastal area under weather condition w_t and apparent wind $u_{0,t}$ on day t caused by the ship during the voyage from i to j, and let $m_{i,j,w_t,u_{0,t}}$ represent that value. Besides, let h, and π_{rt} denote the health cost of the air pollutants from the trips per unit of concentration (USD per kg/m^3), and a binary variable which is set to 1 exclusively when the government ship undertakes trip r on day t, and 0 otherwise, respectively. Recall that θ_{rij} denote a binary variable which is set to 1 only when the ship immediately travels from nodes i to j, $(i,j) \in A$, in trip r, and 0 otherwise. Consequently, the total health cost is calculated by $\sum_{r\in R}\sum_{t\in T}\sum_{(i,j)\in A} h\pi_{rt}\theta_{rij}m_{i,j,w_t,u_{0,t}}$.

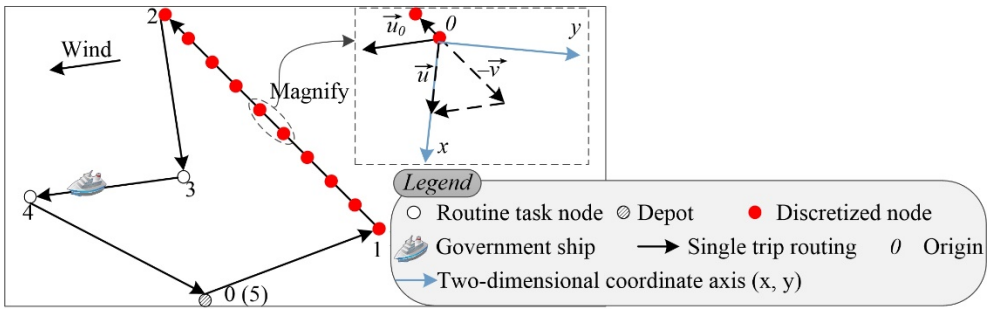

Figure 4-5 Illustration of calculating the downwind concentration.

In summary, this problem aims to minimize the sum of the fuel cost and the health damage of the air pollutants from the trips, i.e., $\text{Min} \sum_{r\in R} \sum_{(i,j)\in A} \theta_{rij} d_{ij} \dot{c} (\omega_{ij})^{\ddot{c}} + \sum_{r\in R} \sum_{t\in T} \sum_{(i,j)\in A} h\pi_{rt} \theta_{rij} m_{i,j,w_t,u_{0,t}}$.

4.3.4 Trip-based formulation

In light of the previously discussed objective function, this chapter formulates an MIP model. An underlying assumption in this chapter is that the government ship can begin to perform its routine tasks whenever it arrives at the task node. Prior to delving into the mathematical model for this chapter, the notation utilized in this model is summarized below.

Indices and sets:

I: set of all routine task nodes, i (or j) $\in I$.

I^-, I^+: set of $I \cup \{0\}$, and set of $I \cup \{n+1\}$, respectively, where nodes 0 and $n+1$ denote the depot depending on whether it is the initial or terminal node of a trip.

A: set of all arcs in a complete directed graph, $(i,j) \in A, i \in I^-, j \in I^+$, where arc $(0, n+1)$ is dummy and the distance from node 0 to $n+1$ is zero.

T: set of days in a planning cycle, $t \in T$.

R: set of all trips, where each trip starts and ends at the depot, $r \in R$.

Z^+: set of non-negative integers.

Parameters

a, b: time window for executing routine tasks, aligning with the working hours of the crews.

$\dot{c}, \ddot{c}$: coefficients for determining the unit fuel cost per nautical mile.

d_{ij}: distance traveling from node i to j (n mile).

e: endurance of the government ship (that is, the maximum time that can be spent on task execution and in transit before being replenished at the depot) (sec).

q_i: task execution time at node i (sec).

s: setup time for preparing a new trip (sec).

$\underline{v}$, $\overline{v}$: minimum and maximum speed of the government ship (n mile/hour), respectively.

h: health cost of the air pollutants from the trips per unit of concentration (USD per kg/m^3).

$u_{0,t}$: apparent wind condition on day t, including the wind direction and speed.

w_t: atmospheric condition on day t, $w_t \in \{0, 1,2,3,4\}$; 0, 1, 2, 3, and 4 represent conditions of extremely unstable, moderately unstable, near neutral, moderately stable, and extremely stable, respectively.

$m_{i,j,w_t,u_{0,t},v}$: downwind concentration at the coastal area under the atmospheric condition w and apparent wind condition u_0 on day t caused by the ship sailing at speed v during the voyage from i to j.

M_1, M_2: two sufficiently large positive numbers.

Variables

α_{ri}: binary, equals 1 if and only if node i is in trip r; 0 otherwise.

θ_{rij}: binary, equals 1 if and only if the ship travels immediately from node i to j, $(i,j) \in A$, in trip r; 0 otherwise.

ρ_{rst}: binary, equals 1 if and only if trip s is performed immediately after trip r, $r < s$, on day t, by the government ship; 0 otherwise.

ε_{ri}: integer, task execution start time at node i in trip r (ε_{r0} and $\varepsilon_{r(n+1)}$ denote the start time and end time of trip r, respectively).

π_{rt}: binary, equals 1 if and only if trip r is fulfilled by the government ship on day t; 0 otherwise.

ω_{ij}: integer, sailing speed of the government ship from node i to j, $(i,j) \in A$, (n mile/hour).

$\delta_{i,j,w_t,u_{0,t}}(\omega_{ij})$: downwind concentration at the coastal area under the atmospheric condition w and apparent wind condition u_0 on day t caused by the ship sailing at speed ω_{ij} during the voyage from i to j.

Mathematical model

Building upon these parameter and variable definitions, a nonlinear MIP model is formulated.

[**M4-1**] $\text{Min} \sum_{r\in R} \sum_{(i,j)\in A} \theta_{rij} d_{ij} \dot{c}(\omega_{ij})^{\ddot{c}} +$

$$\sum_{r\in R} \sum_{t\in T} \sum_{(i,j)\in A} h\pi_{rt} \theta_{rij} \delta_{i,j,w_t,u_{0,t}}(\omega_{ij}) \quad (4\text{-}4)$$

subject to

$$\sum_{t\in T} \pi_{rt} = 1 - \theta_{r0(n+1)} \qquad \forall r \in R \quad (4\text{-}5)$$

$$\sum_{r\in R} \alpha_{ri} = 1 \qquad \forall i \in I \quad (4\text{-}6)$$

$$\sum_{j\in I^+} \theta_{rij} = \alpha_{ri} \qquad \forall r \in R, i \in I \quad (4\text{-}7)$$

$$\sum_{j\in I^-} \theta_{rji} - \sum_{j\in I^+} \theta_{rij} = 0 \qquad \forall r \in R, i \in I \quad (4\text{-}8)$$

$$\sum_{j\in I^+} \theta_{r0j} = 1 \qquad \forall r \in R \quad (4\text{-}9)$$

$$\sum_{i\in I^-} \theta_{ri(n+1)} = 1 \qquad \forall r \in R \quad (4\text{-}10)$$

$$\varepsilon_{r0} \geq (a+s)(1 - \theta_{r0(n+1)}) \qquad \forall r \in R \quad (4\text{-}11)$$

$$\varepsilon_{r,(n+1)} - \varepsilon_{r0} \leq e(1 - \theta_{r0(n+1)}) \qquad \forall r \in R \quad (4\text{-}12)$$

$$a\alpha_{ri} \leq \varepsilon_{ri} \leq b\alpha_{ri} \qquad \forall r \in R, i \in I \quad (4\text{-}13)$$

$$\varepsilon_{ri} + q_i + \left\lceil 3600(d_{ij}/\omega_{ij}) \right\rceil - (1 - \theta_{rij})M_1 \leq \varepsilon_{rj} \quad \forall r \in R, (i,j) \in A \quad (4\text{-}14)$$

$$\varepsilon_{s,0} + (1 - \rho_{rst})M_2 \geq \varepsilon_{r(n+1)} + s \qquad \forall r,s \in R(r<s), t \in T \quad (4\text{-}15)$$

$$0 \leq \sum_{r\in R} \pi_{rt} - \sum_{r\in R} \sum_{s\in R\ (s>r)} \rho_{rst} \leq 1 \qquad \forall t \in T \quad (4\text{-}16)$$

$$\sum_{r\in R}\theta_{rij}\underline{v} \le \omega_{ij} \le \sum_{r\in R}\theta_{rij}\overline{v} \qquad \forall (i,j)\in A \qquad (4\text{-}17)$$

$$\delta_{i,j,w_t,u_{0,t}}(\omega_{ij}) = m_{i,j,w_t,u_{0,t},\omega_{ij}} \qquad \forall (i,j)\in A, t\in T \qquad (4\text{-}18)$$

$$\alpha_{ri} \in \{0,1\} \qquad \forall r\in R, i\in I \qquad (4\text{-}19)$$

$$\theta_{rij} \in \{0,1\} \qquad \forall r\in R, (i,j)\in A \qquad (4\text{-}20)$$

$$\pi_{rt} \in \{0,1\} \qquad \forall r\in R, t\in T \qquad (4\text{-}21)$$

$$\rho_{rst} \in \{0,1\} \qquad \forall r,s\in R, t\in T \qquad (4\text{-}22)$$

$$\varepsilon_{ri} \ge 0 \qquad \forall r\in R, i\in I\cup\{0, n+1\} \qquad (4\text{-}23)$$

$$\omega_{ij} \in Z^{+} \qquad \forall (i,j)\in A \qquad (4\text{-}24)$$

$$\delta_{i,j,w_t,u_{0,t}}(\cdot) \ge 0 \qquad \forall (i,j)\in A, t\in T. \qquad (4\text{-}25)$$

Objective (4-4) minimizes the sum of the fuel cost of the government ship as well as the health damage of the air pollutants from the ship. Constraints (4-5) guarantee that the government ship must fulfill each non-dummy trip at a specific day within the planning cycle. Constraints (4-6) guarantee that each routine task node should be visited exactly once. Constraints (4-7) define the relationship between variables α_{ri} and θ_{rij}. Constraints (4-8)–(4-10) are flow conservation constraints that describe the government ship trip. Constraints (4-11)–(4-15) ensure the time feasibility of the schedule, i.e., time window of executing tasks, endurance of the ship, and setup time for preparation. Constraints (4-16) guarantee the proper trip sequence of the government ship on a certain day. Constraints (4-17) ensure that the traveling speed of the ship satisfies its minimum and maximum speed requirements. Constraints (4-18) calculate the downwind concentration of pollutants from the ship at the coastal area. Constraints (4-19)–(4-25) state the ranges of the decision variables. Obviously, the trip-based formulation belongs to a variant of the MTVRPTW.

4.3.5 Linearization of the model

The formulation outlined above contains several nonlinear parts, specifically the objective function (4-4) as well as constraints (4-14) and (4-18). This section linearizes these nonlinear parts in turn.

The first step in linearization addresses the objective function (4-4) by introducing a new decision variable, τ_{ijv}, which equals one if and only if the speed value of the ship traveling from node i to j is v, and zero otherwise. Nonlinear parts in the objective are $\sum_{r\in R}\sum_{(i,j)\in A}\theta_{rij}d_{ij}\dot{c}(\omega_{ij})^{\ddot{c}}$ and $\sum_{r\in R}\sum_{t\in T}\sum_{(i,j)\in A}h\pi_{rt}\theta_{rij}\delta_{i,j,w_t,u_{0,t}}(\omega_{ij})$, which is rewritten as $\sum_{r\in R}\sum_{(i,j)\in A}\sum_{v\in V}\theta_{rij}\tau_{ijv}d_{ij}\dot{c}v^{\ddot{c}}$ and $\sum_{r\in R}\sum_{t\in T}\sum_{(i,j)\in A}\sum_{v\in V}h\pi_{rt}\theta_{rij}\,\tau_{ijv}m_{i,j,w_t,u_{0,t},v}$, respectively. To facilitate this linearization, several new notations and constraints are introduced below:

Newly defined index and set

V: set of feasible sailing speeds, $v \in V = \{\underline{v}, \underline{v}+1, \cdots, \overline{v}-1, \overline{v}\}$.

Newly defined variables

τ_{ijv}: binary, equals 1 if and only if the speed value of the ship sailing from node i to j, $(i,j) \in A$, is v; 0 otherwise.

Newly defined constraints

$$\sum_{v\in V\cup\{0\}}\tau_{ijv}v = \omega_{ij} \qquad \forall(i,j)\in A \qquad (4\text{-}26)$$

$$\sum_{v\in V\cup\{0\}}\tau_{ijv} = 1 \qquad \forall(i,j)\in A \qquad (4\text{-}27)$$

$$\tau_{ijv} \in \{0,1\} \qquad \forall(i,j)\in A, v\in V\cup\{0\}. \qquad (4\text{-}28)$$

Additional variables, namely β_{rijv} and σ_{rijvt}, are introduced to enable the linearization of objective (4-4). The following are the needed decision variables and constraints:

Newly defined variables

β_{rijv}: binary, equals 1 if and only if both variables θ_{rij} and τ_{ijv} are equal to one; 0 otherwise.

σ_{rijvt}: binary, equals 1 if and only if both variables π_{rt} and β_{rijv} are equal to one; 0 otherwise.

Newly defined constraints

$$\beta_{rijv} \geq \theta_{rij} + \tau_{ijv} - 1 \qquad \forall r \in R, (i,j) \in A, v \in V \cup \{0\} \quad (4\text{-}29)$$

$$\beta_{rijv} \leq \theta_{rij} \qquad \forall r \in R, (i,j) \in A, v \in V \cup \{0\} \quad (4\text{-}30)$$

$$\beta_{rijv} \leq \tau_{ijv} \qquad \forall r \in R, (i,j) \in A, v \in V \cup \{0\} \quad (4\text{-}31)$$

$$\sigma_{rijvt} \geq \pi_{rt} + \beta_{rijv} - 1 \qquad \forall r \in R, (i,j) \in A, v \in V \cup \{0\}, t \in T \quad (4\text{-}32)$$

$$\sigma_{rijvt} \leq \pi_{rt} \qquad \forall r \in R, (i,j) \in A, v \in V \cup \{0\}, t \in T \quad (4\text{-}33)$$

$$\sigma_{rijvt} \leq \beta_{rijv} \qquad \forall r \in R, (i,j) \in A, v \in V \cup \{0\}, t \in T \quad (4\text{-}34)$$

$$\beta_{rijv} \in \{0,1\} \qquad \forall r \in R, (i,j) \in A, v \in V \cup \{0\} \quad (4\text{-}35)$$

$$\sigma_{rijvt} \in \{0,1\} \qquad \forall r \in R, (i,j) \in A, v \in V \cup \{0\}, t \in T. \quad (4\text{-}36)$$

Then, the objective function of model [M4-1] is transformed as follow.

$$\text{Min} \sum_{r \in R} \sum_{(i,j) \in A} \sum_{v \in V} \beta_{rijv} d_{ij} \dot{c} v^{\ddot{c}} + \sum_{r \in R} \sum_{t \in T} \sum_{(i,j) \in A} \sum_{v \in V} \sigma_{rijvt} m_{i,j,w_t,u_{0,t},v} h. \quad (4\text{-}37)$$

Next is the linearization process of constraints (4-14). Constrains (4-14) can be revised to the following constrains (4-38). Specifically, when the value of v is zero, the value of θ_{rij} is also zero, leading to the left-hand side of constraints (4-38) becoming a sufficiently small negative number.

$$\varepsilon_{ri} + q_i + \left[\sum_{v \in V} 3600 \tau_{ijv} (d_{ij}/v)\right] - (1 - \theta_{rij}) M_1 \leq \varepsilon_{rj} \quad \forall r \in R, (i,j) \in A. \quad (4\text{-}38)$$

The final version of the linear trip-based formulation becomes to [M4-2].

[**M4-2**] objective (4-37)

subject to constraints (4-5)–(4-13), (4-15)–(4-17), (4-19)–(4-24), (4-26)–(4-36), (4-38).

4.3.6 Set-covering formulation

Typically, the instance size of model [M4-2] that Gurobi can optimally solve is quite limited, which suggests that the trip-based formulation developed in Section 4.3.5 may not be practical for reasonably sized real-world instances. In practice, for solving classical VRPs, the most efficacious exact algorithms typically leverage the

branch-and-price algorithm (Pecin et al., 2017; Mhamedi et al., 2022). This approach involves solving a set-covering (or -partitioning) model using a B&B algorithm. Within this framework, the linear programming relaxation at every node in the B&B tree is solved by column generation, and the problem of obtaining a column with a negative reduced cost in the linear programming is known as the pricing problem. Therefore, this chapter proposes a set-covering formulation. Each column in the MP of our set-covering formulation represents a feasible ship route (i.e., a sequence of consecutive trips) for a certain day. To develop this set-covering model, new index, set, parameters, and variables are summarized below.

Newly defined index and set:

P_t: set of all feasible routes on day t, $t \in T$; a route contains a sequence of trips where every trip starts and ends at the depot, $p \in P_t$, $P = \bigcup_{t \in T} P_t$.

Newly defined parameters

f_p: total cost of route p, which combines the fuel cost of the ship and the health damage cost, and can be calculated by constraint (4-60).

g_{ip}: binary coefficient, equals 1 if and only if node i is included in route p; 0 otherwise.

Newly defined variable

γ_p: binary, equals 1 if and only if route p, $p \in P_t$, is chosen in a solution; 0 otherwise.

Utilizing the previously defined notation, the MP is developed as follows.

[**MP**] $\quad \text{Min} \sum_{t \in T} \sum_{p \in P_t} f_p \gamma_p$ (4-39)

subject to $\sum_{t \in T} \sum_{p \in P_t} g_{ip} \gamma_p = 1 \qquad \forall i \in I$ (4-40)

$\sum_{p \in P_t} \gamma_p \leq 1 \qquad \forall t \in T$ (4-41)

$\gamma_p \in \{0,1\} \qquad \forall t \in T, p \in P_t.$ (4-42)

Objective function (4-39) minimizes the total cost of the selected routes in the solution. Constraints (4-40) guarantee that every routine task node is visited exactly once. Constraints (4-41) ensure that no more than one route can be executed per day.

Constraints (4-42) are binary integrality constraints. Consequently, a solution is a subset of routes $P' \subseteq P$ that visits each routine task node exactly once.

4.4 BRANCH-AND-PRICE-AND-CUT ALGORITHM

This section aims to address the challenge of solving reasonably sized instances of this problem by designing a BPC algorithm. Specifically, this section first outlines the framework of BPC algorithm, followed by detailed descriptions of its key components. These include the column generation, branching and node selection strategies, generation of initial solutions, and the implementation of cutting planes, all of which are further elaborated in the subsequent sections.

4.4.1 Framework of BPC

The BPC algorithm, a branch-and-bound algorithm, utilizes column generation for computing lower bounds by solving linear relaxations (for minimization problems), hereafter called MPs, and may include additional cuts for strengthening these MPs. The framework used in this study is introduced in Algorithm 4-1. Specifically, column generation iterates between solving a restricted master problem (RMP) and one or more pricing subproblems. For our specific problem, the RMP is the linear relaxation of model [MP] proposed in Section 4.3.6. Solving the RMP yields both primal and dual solutions. Utilizing the dual solution, pricing subproblems are framed similar to the elementary shortest path problems with resource constraints (ESPPRC), focusing on identifying feasible route variables (i.e., columns) with the most negative reduced cost. These columns are incorporated into the RMP in each iteration. Column generation stops when no further columns can be found, indicating an optimal solution to the linear relaxation of the MP and also a valid lower bound for the original problem. Additionally, to enhance efficiency and reduce iterations, valid inequalities are introduced to strengthen the lower bound prior to implementing branching process.

4.4.2 Column generation

Column generation (CG) is used in solving the linear relaxation of the master problem (LMP), which provides a lower bound for the corresponding B&B node. Given the typically vast number of feasible options, the linear relaxation of the set-covering formulation often has a huge number of variables, making it impossible to explicitly enumerate all possible columns. Consequently, CG is an iterative method

Algorithm 4-1. BPC Framework introduction

```
1  Initialize the search tree T: T ← {õ} // õ is the root node representing the initial
   RLMP model without branching constraints
2  LB ← −∞ // LB records the global lower bound of RLMP
3  UB ← ∞ // UB records the global upper bound of RLMP
4  When T is nonempty do
5     Select a node o ∈ T according to the node selection rule
6     Remove o from T
7     If o = õ (i.e., o is the root node) then
8        Generate initial solutions (columns) and the corresponding cost by the
         initial solution generation approach
9        LB ← the cost obtained by line 8
10       Add the initial columns to the RLMP and record this node as ō
11       T := T ∪ {ō}
12    Else (i.e., o is not the root node)
13       Solve the RLMP model and obtain its corresponding cost OBJ
14       If OBJ > UB then
15          Prune the node
16       Else
17          Search columns (routes) with negative reduced costs by solving the
            pricing problem
18          If columns with negative reduced cost exist then
19             Add the column with the most negative cost to the RLMP
20             Go to line 13
21          Else
22                Generate valid cuts
23                If new valid cuts exist and non-duplicating then
24                   Add the valid cuts to the RLMP model
25                   Go to line 13
26                Else
27                   If γ contains fractional parts then
28                      Branch according to the branching rule, leading to nodes
                        o_1 and o_2, L := L ∪ {o_1, o_2}.
29                   Else if all elements in γ are integral
30                      UB ← OBJ
31                      Prune the node
32                   End if
33                End if
34             End if
35          End if
36       End if
37    End if
38 End while
```

that cannot solve the LMP directly due to limitations in enumerating columns. Instead, it alternates between solving a linear relaxation of the restricted MP (RLMP) and solving a pricing subproblem. The RLMP is a version of the LMP constrained to a subset $P' \subseteq P$ of columns, which can be efficiently solved using the simplex method. The primary objective in the pricing subproblem is to identify columns in $P \backslash P'$ that have negative reduced costs relative to the dual optimal solution to the current RLMP.

If no such columns are found, the CG process will terminate, yielding the optimal solution to the LMP is equivalent to the optimal solution to the current RLMP. However, if columns with negative reduced cost is found, columns with the most negative reduced cost are incorporated into the current RLMP, and the CG cycle restarts.

CG is extensively studied by academic scholars. Therefore, this chapter briefly introduces the definitions of the MP and the pricing subproblem; more details on the branch-and-price algorithm and CG are available in Barnhart et al. (1998) and Desaulniers et al. (2006).

Section 4.3.6 presents the set-covering formulation of the MP, where each column represents a feasible ship route composed of one or several consecutive trips on a given day. This section sequentially develops then LMP, RLMP, and the dual of the RLMP as defined within the CG framework. The linear relaxation of the MP is first formulated below.

[**LMP**] objective (4-39)

subject to constraints (4-40)–(4-41),

$$\gamma_p \geq 0 \qquad \forall t \in T, p \in P_t. \tag{4-43}$$

However, model [LMP] includes numerous variables, as it records all potential routes for each day within the planning horizon in its formulation. Moreover, enumerating all possible routes is highly time-consuming, especially for large-scale instances. Thus, establishing an RLMP with selected routes is an efficient way for solving model [LMP] in the CG procedure. In constructing the RLMP within the CG framework, a subset of feasible routes, denoted by $P_t' \subseteq P_t$, is chosen. Given the potentially large number of columns, these columns are incrementally introduced into the LMP, leading to a sequence of RLMPs, which are formulated as follows.

[**RLMP**] $\text{Min} \sum_{t\in T} \sum_{p\in P_t'} f_p \gamma_p$ (4-44)

subject to $\sum_{t\in T} \sum_{p\in P_t'} g_{ip} \gamma_p \geq 1 \qquad \forall i \in I$ (4-45)

$$\sum_{p\in P_t'} \gamma_p \leq 1 \qquad \forall t \in T \tag{4-46}$$

$$\gamma_p \geq 0 \qquad \forall t \in T, p \in P'_t. \tag{4-47}$$

Following the Dantzing rule, the CG procedure iteratively adds new columns, representing new feasible routes, to the RLMP. This addition continues until it is no longer possible to include new columns. In each CG iteration, the RLMP is solved, and the dual variables are got by solving the following dual linear model.

$$[\textbf{RLMP-D}] \quad \text{Max} \sum_{i\in I} \mu_i + \sum_{t\in T} \varphi_t \tag{4-48}$$

$$\text{subject to } \sum_{i\in I} g_{ip}\mu_i + \varphi_t \leq f_p \qquad \forall t \in T, p \in P'_t \tag{4-49}$$

$$\mu_i \geq 0 \qquad \forall i \in I \tag{4-50}$$

$$\varphi_t \leq 0 \qquad \forall t \in T, \tag{4-51}$$

where μ_i and φ_t are the dual variables of constraints (4-45) and (4-46), respectively. These dual variables related to the RLMP's optimal solution are used to define a pricing subproblem. This subproblem aims to identify ship routes with negative reduced costs. Once identified, these routes (columns) are added to the current RLMP, forming the basis for the next RLMP. This process repeats until no more routes with negative reduced costs are found, leading to the optimal solution to the LMP.

The purpose of solving the pricing subproblem is to identify columns with the most negative reduced costs and incorporate them into the RLMP. Each CG iteration requires solving $|T|$ pricing subproblems, each corresponding to a specific day (e.g., day t). For each day, an optimal route p^* is generated. Among all the $|T|$ optimal route plans derived from the pricing problems, only those with negative reduced costs can be passed into the RLMP. This means that in each CG iteration, up to $|T|$ columns can be incorporated into the RLMP. Next, we define the pricing subproblem for day t as PP_t. For sake of the exposition, the parameters and variables used in the following model PP_t omit the subscript t. The mathematical model PP_t corresponding to day t is formulated as follows.

$$[\textbf{PP}_\textbf{t}] \quad \text{Min } PP_t = f_p - \sum_{i\in I} g_{ip}\mu_i - \varphi_t \tag{4-52}$$

subject to constraints (4-7)–(4-13), (4-17), (4-19), (4-20), (4-23), (4-24), (4-26)–(4-31), (4-35), (4-38),

$$\pi_r = 1 - \theta_{r0(n+1)} \qquad \forall r \in R \qquad (4\text{-}53)$$

$$\sum_{r\in R} \alpha_{ri} \leq 1 \qquad \forall i \in I \qquad (4\text{-}54)$$

$$\varepsilon_{s,0} + (1 - \rho_{rs})M_2 \geq \varepsilon_{r(n+1)} + s \qquad \forall r, s \in R(r < s) \qquad (4\text{-}55)$$

$$0 \leq \sum_{r\in R} \pi_r - \sum_{r\in R} \sum_{s\in R\ (s>r)} \rho_{rs} \leq 1 \qquad (4\text{-}56)$$

$$\sigma_{rijv} \geq \pi_r + \beta_{rijv} - 1 \qquad \forall r \in R, (i,j) \in A, v \in V \cup \{0\} \qquad (4\text{-}57)$$

$$\sigma_{rijv} \leq \pi_r \qquad \forall r \in R, (i,j) \in A, v \in V \cup \{0\} \qquad (4\text{-}58)$$

$$\sigma_{rijv} \leq \beta_{rijv} \qquad \forall r \in R, (i,j) \in A, v \in V \cup \{0\} \qquad (4\text{-}59)$$

$$f_p \geq \sum_{r\in R} \sum_{(i,j)\in A} \sum_{v\in V} \beta_{rijv} d_{ij} \dot{c} v^{\ddot{c}} + \sum_{r\in R} \sum_{(i,j)\in A} \sum_{v\in V} \sigma_{rijv} m_{i,j,w,u_0,v} h \qquad (4\text{-}60)$$

$$\pi_r \in \{0,1\} \qquad \forall r \in R \qquad (4\text{-}61)$$

$$\rho_{rs} \in \{0,1\} \qquad \forall r, s \in R \qquad (4\text{-}62)$$

$$\sigma_{rijv} \in \{0,1\} \qquad \forall r \in R, (i,j) \in A, v \in V \cup \{0\} \qquad (4\text{-}63)$$

$$f_p \geq 0. \qquad (4\text{-}64)$$

The objective (4-52) minimized the reduced cost. Constraints (4-53)–(4-54), (4-55)–(4-56), (4-57)–(4-59), (4-61)–(4-62), and (4-63) corresponds to constraints (4-5)–(4-6), (4-15)–(4-16), (4-32)–(4-34), (4-21)–(4-22), and (4-36), respectively. Constraint (4-60) calculates the cost of the government ship's route, i.e., the element used in the objective function. Constraint (4-64) states the range of the variables f_p. Here, notice that f_p is a decision variable for the pricing problem. Once a particular route plan, p, is selected as a newly added column in the RLMP, the corresponding cost (f_p) becomes a cost constant for the newly added route plan p. The cost is then incorporated into the objective function of the RLMP, i.e., objective (4-44).

Given that these pricing subproblems are variants of the two-dimensional knapsack problem, the Gurobi solver can be employed for solving them. However, each pricing subproblem is actually an ESPPRC, classified as NP-hard in the strong sense, and requires substantial computing time (Dror, 1994).

4.4.3 Branching and node selection strategies

CG is implemented at each node of the search tree in the B&B algorithm. Completion of the CG procedure yields optimal LP solutions, which often turn out to be fractional and hence infeasible for the MP. To obtain optimal integral solutions, specific branching rules are applied to eliminate fractional solutions in the nodes of the B&B tree.

The branching strategy outlined in this chapter adopts a straightforward yet effective method, known as maximum fractional branching. This method involves selecting the variable with the greatest degree of integer violation for branching purposes. Regarding the node selection strategy, the strategy employed is a best-first policy. In this approach, the exploration of the search tree is conducted by sorting subproblems in ascending order based on the values of their lower bounds.

4.4.4 Initial solution generation

To initialize the CG procedure, it is essential to generate a set of initial feasible route plans for the RLMP. To obtain these initial solutions, we design a straightforward yet effective method, which comprises the following steps. The fundamental principle of the initial solution generation algorithm is to minimize the number of execution days while maximizing the utilization of all selected execution days. We start by generating $|I|$ number of trips for individual routine task node visits. Subsequently, these trips are sorted in decreasing order of their travel times.

Algorithm 4-2. Initial solution generation	
Step 1	*Trip Generation and Sorting*: Generate a total of $\|I\|$ trips for all routine task nodes, each including the journey from the depot to the task node and then returning to the depot. Sort these trips in descending order based on their travel time, under the assumption that the ship travels at its maximum speed.
Step 2	*Route Initialization*: Establish an initial empty ship route.
Step 3	*Trip Allocation and Route Formation*: Sequentially consider trips based on their sorted travel time. Allocate a trip to the initial route if it satisfies time feasibility constraints. In cases where an additional task node cannot be incorporated into the current route, initiate a new empty route and revert to this step, continuing until all task nodes are allocated to one route.
Step 4	*Route Allocation*: Routes are sequentially allocated within the planning cycle, adhering to the predefined sequence for each route.

4.4.5 Cutting planes

In the area of set-covering formulations for VRPs, a variety of valid inequalities can be applied. A key concern with these inequalities is that they may necessitate

modifications which could potentially impair the efficiency of the algorithms solving the pricing subproblems. However, this potential decrease in performance is often justified when the improvement in the quality of the lower bound is significant enough to outweigh the extra computation time.

A particularly effective type of valid inequality for set-covering (-partitioning) formulations is the subset row cuts, as introduced by Jepsen et al. (2008) for the VRP with time windows and subsequently widely adopted in the field (e.g., Zhen et al., 2022). In this study, the subset row cuts are adapted for the set-covering formulation to include variables related to different modes. Commonly, these cuts are based on subsets of three task nodes. For a set $S = \{i_1, i_2, i_3\} \subset I$, the corresponding inequality ensures that the number of routes/columns covering at least two nodes in S does not exceed one. We incorporate ship trips performed from day 1 to $|T|$. As a result, the subset row cut for our problem is stated as follows.

$$\sum_{t\in T}\sum_{p\in P'_t}\left\lfloor \frac{1}{\kappa}\sum_{i\in S} g_{ip}\right\rfloor \gamma_p \le \left\lfloor \frac{|S|}{\kappa}\right\rfloor \qquad \forall S \subset I, \tag{4-65}$$

where $1 \le \kappa \le |S|$, and $\lfloor x \rfloor$ represents the largest integer not great than x. In our algorithm, $|S|$ and κ are fixed at 3 and 2, respectively, aligning with the corresponding setting in Yang et al. (2021). The subset row cuts can be separated by enumerating all possible set S, and these valid cuts can be added to the RLMP in a cutting plane method. After adding these cuts to the RLMP, the objective function of the pricing problem is revised as the following equality.

$$\text{Min } PP_t = f_p - \sum_{i\in I} g_{ip}\mu_i - \varphi_t - \sum_{S\subset I}\left\lfloor \frac{1}{\kappa}\sum_{i\in S} g_{ip}\right\rfloor \eta_S. \tag{4-66}$$

4.5 NUMERICAL EXPERIMENTS

To evaluate the effectiveness of the proposed model and the efficiency of the BPC algorithm, a total of 32 numerical experiments are conducted using a laptop (Intel Core i7; 2.6 GHz; Memory 16 GB). The mathematical models and algorithms proposed in this chapter are implemented using Gurobi 11.0 (PyCharm, Python).

4.5.1 Experimental setup

The experimental setup begins with a summary of the parameter values. A simulation environment measuring 50 by 10 (n mile), depicted in Figure 4-6, is created

to represent a maritime region. Routine task nodes are uniformly distributed over the maritime area, and the coastal area which is also the depot is located in the lower left corner of the maritime area because this coastal city is a very high-density cape city. Sailing distance (d_{ij}) between any two nodes is the Euclidean distance. This chapter assumes that the minimum and maximum sailing speeds is 10 and 40 knots, respectively. The earliest working time (a) and the latest working time (b) are set to 6 am and 9 pm, respectively. Value of $\dot{c}$ and $\ddot{c}$ are fixed at 0.25 and 2.6, respectively, aligning with the parameters used in previous studies (Wang and Meng, 2012b). The value of h is set to 2.0858×10^{12} USD per kg/m^3, which is in line with Garbatov and Georgiev (2022). Atmospheric condition for each day of the week is randomly assigned from a set $\{0, 1, 2, 3, 4\}$. And apparent wind condition on each day is related to the corresponding atmospheric condition. Specifically, apparent wind direction for each day of the week is uniformly distributed over [north, south, east, and west], and apparent wind speed (knot) for each day is uniformly distributed over [39, 49] for extremely unstable atmospheric condition, [29, 38] for moderately unstable atmospheric condition, [12, 28] for near neutral atmospheric condition, [6, 11] for moderately stable atmospheric condition, and [0, 5] for extremely stable atmospheric condition. Setup time (s) for preparing a new trip is set to 30 min. Task execution time (q_i) at each routine task node is uniformly distributed over [5, 30] min. Endurance (e) of the government ship is assumed to be 6 hours.

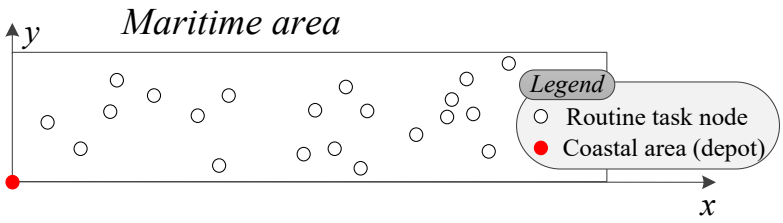

Figure 4-6 Illustration of a 50 by 10 (n mile) simulation environment.

4.5.2 Experiment results

A total of 32 sets of computational instances containing small-, medium-, and large-scale instances are conducted in this section. The number of routine task nodes ($|I|$) varies from three to ten in our experiment. Two solving methods are used to solve all numerical instances. Specifically, the first method involves employing the Gurobi to directly solve model [M4-2] and record the corresponding results in columns three to five; the second method utilizes the proposed BPC algorithm to solve the RLMP

model and record the corresponding results in columns six to eight in Table 4-1. Here, notice that the maximum solution time is set at six hours. When the method reaches the six-hour time limit without identifying the optimal solution, the incumbent best objective (i.e., upper bound of the problem) and its associated gap value are respectively recorded in the third and fifth columns for the first method (sixth and eighth columns for the second method).

Table 4-1 Comparison of the two methods for different scale instances.

ID	$\|I\|$	CPLEX			BPC	
		OBJ_1	T_1 (s)	Gap_1 (%)	OBJ_2	T_2 (s)
1	3	11770.12	2		11770.12	17
2	3	520961625.44	3		520961625.44	15
3	3	28040.52	2		28040.52	33
4	3	41983.04	3		41983.04	17
5	4	53412.55	12		53412.56	84
6	4	23724.43	10		23724.43	116
7	4	27166.89	12		27166.89	84
8	4	6126.98	5		6126.98	74
9	5	13667.25	57		14662.90	295
10	5	58721.28	25		58721.28	103
11	5	32310.83	224		32310.83	599
12	5	54507.94	96		54507.94	243
13	6	53656.85	502		53656.85	971
14	6	40001.25	21600	65.8%	40001.25	21600
15	6	35238.77	21600	40.4%	33832.01	21600
16	6	16802.83	21600	4.0%	16399.77	21600
17	7	64699.12	21600	92.6%	63672.86	21600
18	7	35079.22	21600	88.9%	24050.59	21600
19	7	55262.09	21600	91.3%	54597.85	21600
20	7	57192.18	21600	93.0%	57192.18	21600
21	8	138456.67	21600	98.9%	138456.67	21600
22	8	68934.86	21600	99.1%	108258.342	21600
23	8	56013.78	21600	98.6%	119939.73	21600
24	8	19329.90	21600	95.3%	19329.90	21600
25	9	70161.64	21600	100.0%	69803.41	21600
26	9	512380.14	21600	95.0%	512380.14	21600
27	9	59755.79	21600	100.0%	55534.01	21600
28	9	58051.87	21600	100.0%	58051.87	21600
29	10	78794.66	21600	100.0%	69802.41	21600
30	10	66364.99	21600	100.0%	60267.15	21600
31	10	57658.35	21600	100.0%	58809.82	21600
32	10	39795.09	21600	100.0%	39795.10	21600

As evident from Table 4-1, for scenarios where the total number of routine task nodes does not exceed six, the first method not only obtains the optimal solution within six hours but also surpasses the second method in terms of solution speed. Conversely,

when the total number of routine task nodes exceeds seven, the first method is unable to identify the optimal solution within six hours, yielding the best solution with a gap exceeding 90%. In most of these cases, although the second method also fails to obtain the optimal solution within six hours, the quality of its best solution significantly outperforms that of the first method.

4.6 SUMMARY

The existing literature lacks research on the joint routing, scheduling, and speed optimization problem of government ships that account for the health impact of air pollutant emissions at different times and locations. To address this research gap, this chapter introduces a nonlinear MIP model that encompasses various operational aspects. This chapter then designs a tailored exact algorithm for the model. The contributions of this chapter are twofold: (1) A nonlinear MIP model is formulated for the integrated routing, scheduling, and speed optimization problem of government ships that account for the environmental impact of air pollutant emissions under different weather conditions, which is then linearized to a linear model. The model also considers some overlooked operational constraints, such as the dispersion of air pollutant emissions, different weather conditions, new trip setup time, and ship endurance, are considered in this chapter. (2) In response to the complexities of solving the developed trip-based formulations, a BPC algorithm is proposed by considering specific characteristics of the problem. Efficiency of this algorithm is verified.

Chapter 5: Summary and Future Research

5.1 SUMMARY

This thesis investigates large-scale optimization for shipping operations management by considering three important issues, and correspondingly it comprises three main problems. The first problem focuses on a maritime decarbonization problem by investigating the EEOI value; the second problem aims to address the fleet repositioning issue to help liner company to respond to uncertain container shipment demand; the third problem studies the health impact of air pollutant emissions under different weather conditions. My thesis introduces three novel conceptual frameworks for understanding the shipping operations management, which makes this thesis significantly different from the existing literature.

In the first problem, the EEOI value, an important carbon intensity indicator, is investigated within the domain of green shipping. The current literature often overlooks an integrated approach to optimizing speed, voyage planning, and fleet deployment, particularly considering how voyage options, displacement, and sailing speed influence fuel consumption. To bridge this research gap, this chapter introduces a nonlinear MIP model that encapsulates all these aspects and designs a specific exact algorithm for it. This research is instrumental in guiding shipping operations management with a keen focus on maritime decarbonization.

In the second problem, fleet repositioning is integrated into the integrated fleet deployment, ship chartering, demand fulfillment, and cargo allocation problem. This integration is crucial for liner companies to effectively respond to uncertain container shipment demands. To address this, this chapter develops an MILP model to capture all these elements. Additionally, for this NP-hard problem, a BBC algorithm is designed. The efficacy of this algorithm is further enhanced by employing two acceleration strategies (approximate UBT inequalities and Pareto optimal cuts).

In the third problem, the focus of optimization is on government ships, as governments should set an example in strict compliance with current stringent maritime emission regulations by meticulously scheduling their official vessels. When scheduling government ships, the aim should be minimizing the sum of the direct trip

cost and the health damage of the air pollutants released by these government ships instead of only minimizing the direct trip cost. To this end, an integrated routing, scheduling, and speed optimization problem of government ships that account for the health effects of air pollutant emissions under different weather conditions is investigated. Two mathematical models are formulated for this problem and a BPC algorithm is designed to solve the model.

5.2 FUTURE RESEARCH

Large-scale optimization for shipping operations management is an intertwined and complicated problem. To study this problem, more realistic issues should be considered. My future research direction is to bring our research much closer to the reality.

First, incorporating uncertain port weather conditions into the existing framework that currently accounts for uncertain shipping demand is a future direction of expansion. Weather plays an important role in determining the availability of ships at ports, with adverse conditions potentially causing significant disruptions. To adequately capture this additional layer of complexity, the mathematical model requires an expansion to include new variables and constraints. This expansion, in turn, underscores the need for the development of more effective algorithms capable of handling the increased intricacy brought about by considering weather disturbances alongside shipping demand uncertainties. Second, beyond the implementation of green shipping practices, the uncertainty of the ever-changing shipping market, and the health impact of shipping activities, several maritime elements, such as the repositioning of empty containers and ship refuelling, can also be incorporated into the shipping operations management.

Appendix: Supplement for Chapter 3

Appendix A

Callback functions

Magnanti and Wong (1981) indicated that one major computational bottleneck when using the BD algorithm is repeatedly solving master problems (IP models). In the classical implementation of BD, the master problem is solved to optimality, which means a search tree is constructed from the beginning at every iteration (Bayram and Yaman, 2018). Alternatively, the BD algorithm can be implemented with a "single search tree" master problem via user cut callbacks and lazy constraint callbacks (IBM, 2017). Both of them belong to the advanced programming techniques of the CPLEX solver. When solving an MILP model, the researcher may can find a set of constraints which are unlikely to be violated (i.e., lazy constraints) or already know a group of helpful cutting planes (i.e., user cuts). In order to avoid adding all of these constraints to the model at the beginning, which may result in a very slow solving process, these constraints can be added via lazy constraint callbacks or user cut callbacks. Lazy constraints are only verified when an integer feasible solution is obtained while user cuts for violation may be checked at any stage of the optimization (IBM, 2017).

Appendix B

The deterministic programming model, two-stage stochastic programming model, and perfect information model

A deterministic programming model, a two-stage stochastic programming model, and a perfect information model are formulated in this appendix.

The deterministic programming model assumes that the newly generated container shipment demand in each period $t \in T$ for an O-D pair $(o, d) \in D$ is equal to the average value of demand in the multistage programming model over $s \in S$ for a fair comparison. Before we formulate the deterministic programming model, we define the following parameters and decision variables:

Newly defined parameters:

$\dot{q}_{o,d,t}$: newly generated container shipment demand (number of containers) in period t at port o to be transported to port d in the deterministic problem, $\dot{q}_{o,d,t} = \mathbb{E}_s[q^s_{o,d,t}]$.

Newly defined decision variables:

$\dot{\theta}_{o,d,t}$: continuous, number of accepted containers for the demand of O-D pair $(o,d) \in D$ accumulated in period $t \in T$ in the deterministic problem, $\dot{\theta}_{o,d,t} \leq \dot{q}_{o,d,t}$.

$\dot{\varphi}_{o,d,t}$: continuous, number of delayed containers for the demand of O-D pair $(o,d) \in D$ up to period $t \in T \cup \{0\}$ in the deterministic problem, where by convention, $\dot{\varphi}_{o,d,0} := 0$.

$\dot{\varepsilon}_{o,d,t}$: continuous, number of shipped containers for the demand of O-D pair $(o,d) \in D$ in period t (including both those accepted in period t and the delayed containers in previous periods) in the deterministic problem.

According to the notation introduced, the deterministic programming model is formulated as follows:

$$[\mathrm{M}_{\mathrm{deter}}] \quad \mathrm{Max} \sum_{(o,d)\in D} \sum_{t\in T} (l_{o,d}\dot{\theta}_{o,d,t} - p_{o,d}\dot{\varphi}_{o,d,t}) - \sum_{h\in H} \sum_{r\in R_{y_h}} f_{h,r}\alpha_{h,r} -$$

$$\sum_{k\in K} \sum_{r\in R_k} c_{k,r}\beta_{k,r} - \sum_{h\in H_2} \sum_{r\in R_{y_h}} g_{y_h}\alpha_{h,r} + \sum_{h\in H_1} m_{y_h}(u_h - \sum_{r\in R_{y_h}} \alpha_{h,r}) \quad \text{(A1)}$$

subject to constraints (3-2)–(3-5), (3-14)–(3-16),

$$\dot{\theta}_{o,d,t} + \dot{\varphi}_{o,d,t-1} = \dot{\varepsilon}_{o,d,t} + \dot{\varphi}_{o,d,t} \qquad \forall (o,d) \in D, t \in T \qquad \text{(A2)}$$

$$\sum_{(o,d)\in D} \sum_{t\in T} a_{r,e,i,o,d,t}\, \dot{\varepsilon}_{o,d,t} \leq \sum_{k\in K_r} v_k\, \pi_{k,r,j_{re}} \quad \forall\, r \in R, e \in E_r, i \in I_r \qquad \text{(A3)}$$

$$\dot{\theta}_{o,d,t} \leq \dot{q}_{o,d,t} \qquad \forall\, (o,d) \in D, t \in T \qquad \text{(A4)}$$

$$\dot{\varphi}_{o,d,0} = 0 \qquad \forall (o,d) \in D \qquad \text{(A5)}$$

$$\dot{\varphi}_{o,d,|T|} = 0 \qquad \forall (o,d) \in D \qquad \text{(A6)}$$

$$\dot{\theta}_{o,d,t} \geq 0, \dot{\varepsilon}_{o,d,t} \geq 0 \qquad \forall (o,d) \in D, t \in T \qquad \text{(A7)}$$

$$\dot{\varphi}_{o,d,t} \geq 0 \qquad \forall (o,d) \in D, t \in T \cup \{0\}. \qquad \text{(A8)}$$

Objective function (A1) maximizes the operational revenue earned by the liner company during the planning horizon in the deterministic problem. Constraints (A2)–(A8) update the related constraints for the deterministic problem.

The optimal fleet deployment decision (including ship repositioning decision) is implemented according to the deterministic programming model [$\mathrm{M}_{\mathrm{deter}}$], denoted by $\alpha_{h,r}^{\mathrm{deter}}$, $\beta_{k,r}^{\mathrm{deter}}$, and $\pi_{k,r,j}^{\mathrm{deter}}$. The demand fulfillment and allocation decisions cannot be implemented because in reality, the actual demand is likely to be different from $\dot{q}_{o,d,t}$ used in [$\mathrm{M}_{\mathrm{deter}}$]. This chapter assumes that once the optimal fleet deployment decision (including ship repositioning decision) is implemented, the scheduling of the actual numbers of accepted, delayed, and shipped containers (i.e., demand fulfillment and allocation decisions) after observing the actual demand of all O-D pairs in each period is carried out in a greedy manner. Specifically, for each scenario $s \in S$, at the beginning of each period $t \in T$, we have already made decisions on the actual numbers of accepted, delayed, and shipped containers in the previous time periods 1,…, $t-1$, denoted by $\theta_{o,d,1}^{s,\mathrm{deter}}$,…, $\theta_{o,d,t-1}^{s,\mathrm{deter}}$, $\varphi_{o,d,1}^{s,\mathrm{deter}}$,…, $\varphi_{o,d,t-1}^{s,\mathrm{deter}}$, and $\varepsilon_{o,d,1}^{s,\mathrm{deter}}$,…, $\varepsilon_{o,d,t-1}^{s,\mathrm{deter}}$, respectively. Then, we observe the actual demand $q_{o,d,t}^{s}$ for the current period, assume that future demands are zero, and solve the following model [$\mathrm{M}_{\mathrm{deter}}(s,t)$] to obtain the value of $Z_{\mathrm{deter}}(s,t)$ in period t under scenario s.

[$\mathrm{M}_{\mathrm{deter}}(s,t)$]

$$Z_{\mathrm{deter}}(s,t) = \mathrm{Max} \sum_{(o,d)\in D} \sum_{t\in T} (l_{o,d}\dot{\theta}_{o,d,t} - p_{o,d}\dot{\varphi}_{o,d,t}) - \sum_{h\in H} \sum_{r\in R_{y_h}} f_{h,r}\alpha_{h,r} -$$

$$\sum_{k\in K} \sum_{r\in R_k} c_{k,r}\beta_{k,r} - \sum_{h\in H_2} \sum_{r\in R_{y_h}} g_{y_h}\alpha_{h,r} + \sum_{h\in H_1} m_{y_h}(u_h - \sum_{r\in R_{y_h}} \alpha_{h,r}) \quad \text{(A9)}$$

subject to constraints (A2)–(A3), (A5)–(A8), and

$$\dot{\varphi}_{o,d,t'} = \varphi_{o,d,t'}^{s,\mathrm{deter}}, \dot{\theta}_{o,d,t'} = \theta_{o,d,t'}^{s,\mathrm{deter}}, \dot{\varepsilon}_{o,d,t'} = \varepsilon_{o,d,t'}^{s,\mathrm{deter}} \quad \forall (o,d) \in D, t' = 1,\dots,t-1 \quad \text{(A10)}$$

$$\dot{\theta}_{o,d,t} \le q_{o,d,t}^{s} \qquad \forall (o,d) \in D \qquad \text{(A11)}$$

$$\dot{\theta}_{o,d,t'} \le 0 \qquad \forall (o,d) \in D, t' = t+1,\dots,|T| \qquad \text{(A12)}$$

$$\alpha_{h,r} = \alpha_{h,r}^{\mathrm{deter}} \qquad \forall h \in H, r \in R_{y_h} \qquad \text{(A13)}$$

$$\beta_{k,r} = \beta_{k,r}^{\text{deter}} \qquad \forall k \in K, r \in R_k \qquad \text{(A14)}$$

$$\pi_{k,r,j} = \pi_{k,r,j}^{\text{deter}} \qquad \forall k \in K, r \in R_k, j \in \{1, \dots, n_r\}. \qquad \text{(A15)}$$

Then, the value of Z_{deter} can be calculated by

$$Z_{\text{deter}} = \frac{1}{|S|} \sum_{s \in S} Z_{\text{deter}}(s, |T|). \qquad \text{(A16)}$$

The difference between Z_{multi} and Z_{deter} is the actual advantage of using multistage stochastic programming over deterministic programming.

The two-stage stochastic programming model assumes, under a specific scenario, that the values of demand of an O-D pair in each period are the same as the demand of the O-D pair in multistage stochastic programming. However, in period 1, the decision maker already knows what scenario occurs and thus knows demand in all future periods. The two-stage stochastic programming model is formulated as follows:

$[\text{M}_{\text{two}}]$ objective (3-1)

subject to constraints (3-2)–(3-10), (3-14)–(3-16), and

$$\theta_{o,d,t}^{s} \geq 0, \varepsilon_{o,d,t}^{s} \geq 0 \qquad \forall (o,d) \in D, t \in T, s \in S \qquad \text{(A17)}$$

$$\varphi_{o,d,t}^{s} \geq 0 \qquad \forall (o,d) \in D, t \in T \cup \{0\}, s \in S. \qquad \text{(A18)}$$

This chapter also designs a new method for calculating the actual objective value of the two-stage stochastic programming model. The optimal fleet deployment decision (including ship repositioning decision) to the two-stage stochastic programming model $[\text{M}_{\text{two}}]$, denoted by $\alpha_{h,r}^{\text{two}}$, $\beta_{k,r}^{\text{two}}$, and $\pi_{k,r,j}^{\text{two}}$, will be implemented. The demand fulfillment and allocation decisions cannot be implemented because in reality, the decision maker cannot know which scenario actually occurs in periods 1, 2,…, $|T| - 1$. Similar to $[\text{M}_{\text{deter}}]$, this chapter assumes that once the optimal fleet deployment decision is implemented, the demand fulfillment and allocation decisions after observing the actual demand in each period are carried out in a greedy manner. Specifically, for each scenario $s \in S$, at the beginning of each period $t \in T$, we have already made decisions on the actual numbers of accepted, delayed, and shipped containers in the first previous time periods 1,…, $t - 1$, denoted by $\theta_{o,d,1}^{s,\text{two}}$,…, $\theta_{o,d,t-1}^{s,\text{two}}$, $\varphi_{o,d,1}^{s,\text{two}}$,…, $\varphi_{o,d,t-1}^{s,\text{two}}$, and $\varepsilon_{o,d,1}^{s,\text{two}}$,…, $\varepsilon_{o,d,t-1}^{s,\text{two}}$, respectively. Then, we observe the actual

demand $q^s_{o,d,t}$ for the current period, assume that future demand is zero, and solve the following model $[\mathrm{M}_{\mathrm{two}}(s,t)]$ to obtain the value of $Z_{\mathrm{two}}(s,t)$ in period t under scenario s.

$[\mathrm{M}_{\mathrm{two}}(s,t)]$

$$Z_{\mathrm{two}}(s,t) = \mathrm{Max} \sum_{(o,d)\in D} \sum_{t\in T} (l_{o,d}\dot{\theta}_{o,d,t} - p_{o,d}\dot{\varphi}_{o,d,t}) - \sum_{h\in H} \sum_{r\in R_{y_h}} f_{h,r}\alpha_{h,r} -$$

$$\sum_{k\in K} \sum_{r\in R_k} c_{k,r}\beta_{k,r} - \sum_{h\in H_2} \sum_{r\in R_{y_h}} g_{y_h}\alpha_{h,r} + \sum_{h\in H_1} m_{y_h}(u_h - \sum_{r\in R_{y_h}} \alpha_{h,r}) \quad \text{(A19)}$$

subject to constraints (3-2)–(3-5), (3-14)–(3-16), (A2)–(A3), (A5)–(A8), and

$$\dot{\varphi}_{o,d,t'} = \varphi^{s,\mathrm{two}}_{o,d,t'}, \dot{\theta}_{o,d,t'} = \theta^{s,\mathrm{two}}_{o,d,t'}, \dot{\varepsilon}_{o,d,t'} = \varepsilon^{s,\mathrm{two}}_{o,d,t'} \quad \forall (o,d)\in D, t' = 1,\dots,t-1 \quad \text{(A20)}$$

$$\dot{\theta}_{o,d,t} \le q^s_{o,d,t} \qquad \forall (o,d)\in D \quad \text{(A21)}$$

$$\dot{\theta}_{o,d,t'} \le 0 \qquad \forall (o,d)\in D, t' = t+1,\dots,|T| \quad \text{(A22)}$$

$$\alpha_{h,r} = \alpha^{\mathrm{two}}_{h,r} \qquad \forall h\in H, r\in R_{y_h} \quad \text{(A23)}$$

$$\beta_{k,r} = \beta^{\mathrm{two}}_{k,r} \qquad \forall k\in K, r\in R_k \quad \text{(A24)}$$

$$\pi_{k,r,j} = \pi^{\mathrm{two}}_{k,r,j} \qquad \forall k\in K, r\in R_k, j\in\{1,\dots,n_r\}. \quad \text{(A25)}$$

Then, the value of Z_{two} can be calculated by

$$Z_{\mathrm{two}} = \frac{1}{|S|}\sum_{s\in S} Z_{\mathrm{two}}(s,|T|). \quad \text{(A26)}$$

The difference between Z_{multi} and Z_{two} is a measure of the actual advantage of using multistage stochastic programming over two-stage stochastic programming.

The last model is the perfect information model. This method solves a set of deterministic models, each of which is related to a particular scenario. Before formulating the perfect information model, some parameters and decision variables are defined as follows:

Newly defined parameters:

$\ddot{q}^s_{o,d,t}$: actual newly generated container shipment demand (number of containers) in period t at port o to be transported to port d under scenario s in the perfect information problem, $\ddot{q}^s_{o,d,t} = q^s_{o,d,t}$.

Newly defined decision variables:

$\ddot{\alpha}_{h,r}^{s}$: integer, number of ships from group $h \in H$ deployed on route $r \in R$ under scenario s in the perfect information problem.

$\ddot{\beta}_{k,r}^{s}$: integer, number of ships of type $k \in K_r$ deployed on route $r \in R$ under scenario s in the perfect information problem.

$\ddot{\pi}_{k,r,j}^{s}$: binary, if a ship of type $k \in K_r$ is deployed on the j^{th} ($j \in \{1, \dots, n_r\}$) sequence position of route $r \in R$ (i.e., the j^{th} ship on route r belongs to type k) under scenario s in the perfect information problem, it equals 1; otherwise it equals 0.

$\ddot{\theta}_{o,d,t}^{s}$: continuous, number of actual accepted containers for the demand of O-D pair $(o,d) \in D$ accumulated in period $t \in T$ under scenario s in the perfect information problem, $\ddot{\theta}_{o,d,t}^{s} \leq \ddot{q}_{o,d,t}^{s}$.

$\ddot{\varphi}_{o,d,t}^{s}$: continuous, number of actual delayed containers for the demand of O-D pair $(o,d) \in D$ up to period $t \in T \cup \{0\}$ under scenario s in the perfect information problem, where by convention, $\ddot{\varphi}_{o,d,0}^{s} := 0$.

$\ddot{\varepsilon}_{o,d,t}^{s}$: continuous, number of actual shipped containers for the demand of O-D pair $(o,d) \in D$ in period t (including both those accepted in period t and the delayed containers in previous periods) under scenario s in the perfect information problem.

According to the notation introduced, the perfect information model is formulated as follows:

$[\mathrm{M}_{\mathrm{perfect}}]$

$$\text{Max} \sum_{s\in S} w^s \Big[\sum_{(o,d)\in D} \sum_{t\in T} \big(l_{o,d} \ddot{\theta}_{o,d,t}^{s} - p_{o,d} \ddot{\varphi}_{o,d,t}^{s} \big) - \sum_{h\in H} \sum_{r\in R_{y_h}} f_{h,r} \ddot{\alpha}_{h,r}^{s} - \sum_{k\in K} \sum_{r\in R_k} c_{k,r} \ddot{\beta}_{k,r}^{s} - \sum_{h\in H_2} \sum_{r\in R_{y_h}} g_{y_h} \ddot{\alpha}_{h,r}^{s} + \sum_{h\in H_1} m_{y_h} \big(u_h - \sum_{r\in R_{y_h}} \ddot{\alpha}_{h,r}^{s} \big) \Big] \quad \text{(A27)}$$

subject to

$$\ddot{\beta}_{k,r}^{s} = \sum_{j\in\{1,\dots,n_r\}} \ddot{\pi}_{k,r,j}^{s} \qquad \forall k \in K, r \in R_k, s \in S \quad \text{(A28)}$$

$$\sum_{k\in K_r} \ddot{\pi}_{k,r,j}^{s} = 1 \qquad \forall\, r \in R, j \in \{1, \dots, n_r\}, s \in S \quad \text{(A29)}$$

$$\sum_{r\in R_{y_h}} \ddot{\alpha}_{h,r}^{s} \leq u_h \qquad \forall\, h \in H, s \in S \quad \text{(A30)}$$

$$\sum_{h\in H, y_h=k} \ddot{\alpha}^s_{h,r} = \ddot{\beta}^s_{k,r} \qquad \forall k \in K, r \in R_k, s \in S \qquad \text{(A31)}$$

$$\ddot{\theta}^s_{o,d,t} + \ddot{\varphi}^s_{o,d,t-1} = \ddot{\varepsilon}^s_{o,d,t} + \ddot{\varphi}^s_{o,d,t} \qquad \forall (o,d) \in D, t \in T, s \in S \qquad \text{(A32)}$$

$$\sum_{(o,d)\in D} \sum_{t\in T} a_{r,e,i,o,d,t}\, \ddot{\varepsilon}^s_{o,d,t} \le \sum_{k\in K_r} v_k\, \pi_{k,r,j_{re}} \quad \forall r \in R, e \in E_r, i \in I_r, s \in S \qquad \text{(A33)}$$

$$\ddot{\theta}^s_{o,d,t} \le \ddot{q}^s_{o,d,t} \qquad \forall (o,d) \in D, t \in T, s \in S \qquad \text{(A34)}$$

$$\ddot{\varphi}^s_{o,d,0} = 0 \qquad \forall (o,d) \in D, s \in S \qquad \text{(A35)}$$

$$\ddot{\varphi}^s_{o,d,|T|} = 0 \qquad \forall (o,d) \in D, s \in S \qquad \text{(A36)}$$

$$\ddot{\alpha}^s_{h,r} \in Z_+ \qquad \forall\, h \in H, r \in R_{y_h}, s \in S \qquad \text{(A37)}$$

$$\ddot{\beta}^s_{k,r} \in Z_+ \qquad \forall k \in K, r \in R_k, s \in S \qquad \text{(A38)}$$

$$\ddot{\pi}^s_{k,r,j} \in \{0,1\} \qquad \forall k \in K, r \in R_k, j \in \{1, \dots, n_r\}, s \in S \qquad \text{(A39)}$$

$$\ddot{\theta}^s_{o,d,t} \ge 0,\ \ddot{\varepsilon}^s_{o,d,t} \ge 0 \qquad \forall (o,d) \in D, t \in T, s \in S \qquad \text{(A40)}$$

$$\ddot{\varphi}^s_{o,d,t} \ge 0 \qquad \forall (o,d) \in D, t \in T \cup \{0\}, s \in S. \qquad \text{(A41)}$$

Objective function (A27) maximizes the average operational revenue earned by the liner company during the planning horizon in the perfect information problem. Constraints (A28)–(A41) update the related constraints for the deterministic problem. The optimal objective value of model $\mathrm{M}_{\mathrm{perfect}}$ is recorded as Z_{perfect}, which is theoretically meaningful and represents how much money the liner company would earn on average if the future demand were known. The difference between Z_{perfect} and Z_{multi} is the value of perfect information.

Appendix C

Model considering adaptive fleet sizes

This chapter also formulates an MILP model to allow for adaptive fleet sizes. This model assumes that if an O-D pair is in particularly high demand, liner companies may charter in additional ships for point-to-point transportation in addition to ships deployed in the first stage. Specifically, let U represent a subset of O-D pairs of ports

that can provide additional point-to-point ships in the shipping network, $(o, d) \in U$, and assume that each origin in U has an infinite number of point-to-point ships ready to be chartered in by the liner company. These additional point-to-point ships are of a fixed size, such as 4,500 TEUs. Suppose that the transportation demand for an O-D pair suddenly increases in a certain period. For example, if additional 3,000 TEUs of cargo needs to be transported for a specific O-D pair, the ships initially deployed by the liner company cannot satisfy the surge in transportation volume. In this case, the liner company may charter in an additional 4,500-TEU ship to complete the point-to-point transportation of the 3,000 TEUs of cargo; if additional 6,000 TEUs of cargo needs to be transported for a specific O-D pair, two additional point-to-point ships may be deployed for the O-D pair. Therefore, by frequently adjusting point-to-point ships, liner companies can better respond to uncertain demands.

Newly defined set:

U: subset of O-D pairs of ports that can provide additional point-to-point ships in the shipping network, $(o, d) \in U$, $U \subset D$.

Newly defined parameters:

$\hat{g}_{o,d,s}$: rental cost of chartering in a point-to-point ship completing a specific leg from port o to port d, $(o, d) \in U$, under scenario s, $s \in S$.

$\hat{v}$: number of containers that can be carried by point-to-point ships, which is the capacity of the ships.

Newly defined decision variables:

$\gamma^s_{o,d,t}$: integer, number of point-to-point ships completing a specific voyage leg from port o to port d, $(o, d) \in U$, departing from period t, $t \in T$, under scenario s, $s \in S$.

$\delta^s_{o,d,t}$: continuous, total number of shipped containers transported by point-to-point ships for the demand of O-D pair (o, d), $(o, d) \in U$, in period t (including both those accepted in period t and the delayed containers in previous periods), $t \in T$, under scenario s, $s \in S$.

According to the notation introduced, a multistage stochastic programming model considering adaptive fleet sizes is formulated as follows:

$[\mathrm{M}_{\mathrm{Multi-Adaptive}}]$

$$Z_{\text{Adaptive}} = \text{Max} \sum_{s\in S} w^s \sum_{t\in T} [\sum_{(o,d)\in D}(l_{o,d}\theta^s_{o,d,t} - p_{o,d}\varphi^s_{o,d,t}) + \sum_{(o,d)\in U}(l_{o,d}\delta^s_{o,d,t} - \hat{g}_{o,d,s}\gamma^s_{o,d,t})] - \sum_{h\in H}\sum_{r\in R_{y_h}} f_{h,r}\alpha_{h,r} - \sum_{k\in K}\sum_{r\in R_k} c_{k,r}\beta_{k,r} - \sum_{h\in H_2}\sum_{r\in R_{y_h}} g_{y_h}\alpha_{h,r} + \sum_{h\in H_1} m_{y_h}(u_h - \sum_{r\in R_{y_h}} \alpha_{h,r}) \quad \text{(A42)}$$

subject to constraints (3-2)–(3-5), (3-7), (3-8)–(3-18),

$$\delta^s_{o,d,t} \le \hat{v}\gamma^s_{o,d,t} \qquad \forall\,(o,d)\in U, t\in T, s\in S \qquad \text{(A43)}$$

$$\theta^s_{o,d,t} + \varphi^s_{o,d,t-1} = \varepsilon^s_{o,d,t} + \varphi^s_{o,d,t} \qquad \forall (o,d)\in D\backslash U, t\in T, s\in S \qquad \text{(A44)}$$

$$\theta^s_{o,d,t} + \varphi^s_{o,d,t-1} = \varepsilon^s_{o,d,t} + \delta^s_{o,d,t} + \varphi^s_{o,d,t} \qquad \forall (o,d)\in U, t\in T, s\in S \qquad \text{(A45)}$$

$$\gamma^s_{o,d,t} \in Z_+ \qquad \forall\,(o,d)\in U, t\in T, s\in S \qquad \text{(A46)}$$

$$\delta^s_{o,d,t} \ge 0 \qquad \forall (o,d)\in U, t\in T, s\in S. \qquad \text{(A47)}$$

Objective function (A42) maximizes the expected profit earned by the liner company during the planning horizon, which involves costs and revenues of regular ships and point-to-point ships. Constraints (A43) guarantee that the total number of shipped containers transported by point-to-point ships for O-D pair (o,d), $(o,d)\in U$ in period t under scenario s cannot exceed the total capacity of all deployed point-to-point ships completing the voyage leg from port o to port d departing from period t. Constraints (A44)–(A45) are the balance equations for the numbers of accepted, delayed, and shipped containers under the case of adaptive fleet sizes, between each O-D pair (o,d) in each time period $t\in T$ under each scenario s. Constraints (A46)–(A47) define the domains of the decision variables.

References

Acomi, N., Acomi, O. C., 2014. Improving the voyage energy efficiency by using EEOI. *Procedia-Social and Behavioral Sciences* 138, 531–536.

Adulyasak, Y., Cordeau, J. F., Jans, R., 2015. Benders decomposition for production routing under demand uncertainty. *Operations Research* 63(4), 851–867.

Akyüz, M. H., Lee, C. Y., 2016. Service type assignment and container routing with transit time constraints and empty container repositioning for liner shipping service networks. *Transportation Research Part B: Methodological* 88, 46–71.

Alharbi, A., Wang, S., Davy, P., 2015. Schedule design for sustainable container supply chain networks with port time windows. *Advanced Engineering Informatics* 29(3), 322–331.

Aydin, N., Lee, H., Mansouri, S. A., 2017. Speed optimization and bunkering in liner shipping in the presence of uncertain service times and time windows at ports. *European Journal of Operational Research* 259(1), 143–154.

Barnhart, C., Johnson, E. L., Nemhauser, G. L., Savelsbergh, M. W., Vance, P. H., 1998. Branch-and-price: Column generation for solving huge integer programs. *Operations Research* 46(3), 316–329.

Bayram, V., Yaman, H., 2018. Shelter location and evacuation route assignment under uncertainty: a Benders decomposition approach. *Transportation Science* 52(2), 416–436.

Birge, J. R. and Louveaux, F. (2011) Introduction to Stochastic Programming. Springer, New York.

Brouer, B. D., Alvarez, J. F., Plum, C. E., Pisinger, D., Sigurd, M. M., 2014. A base integer programming model and benchmark suite for liner-shipping network design. *Transportation Science* 48(2), 281–312.

Chen, J., Jia, S., Wang, S., Liu, Z., 2018. Subloop-based reversal of port rotation directions for container liner shipping network alteration. *Transportation Research Part B: Methodological* 118, 336–361.

Chen, J., Ye, J., Liu, A., Fei, Y., Wan, Z., Huang, X., 2022. Robust optimization of liner shipping alliance fleet scheduling with consideration of sulfur emission restrictions and slot exchange. *Annals of Operations Research* 1–31.

China Water Transport Network (CWTN), 2021. Hot focus: the “economic code” behind the container hot. <http://www.zgsyb.com/news.html?aid=582387> (accessed on 19.07.2021).

Christiansen, M., Fagerholt, K., Nygreen, B., and Ronen, D., 2013. Ship routing and scheduling in the new millennium. *European Journal of Operational Research* 228(3), 467–483.

Christiansen, M., Fagerholt, K., Ronen, D., 2004. Ship routing and scheduling: status and perspectives. *Transportation Science* 38(1), 1–18.

Christiansen, M., Hellsten, E., Pisinger, D., Sacramento, D., Vilhelmsen, C., 2020. Liner shipping network design. *European Journal of Operational Research* 286(1), 1–20.

Cordeau, J.-F., Pasin, F., Solomon, M. M., 2006. An integrated model for logistics network design. *Annals of Operations Research* 144(1), 59–82.

Desaulniers, G., Desrosiers, J. and Solomon, M. M. (Eds.) (2006) Column Generation. Springer Science & Business Media, US.

Dong, J. X., Lee, C. Y., Song, D. P., 2015. Joint service capacity planning and dynamic container routing in shipping network with uncertain demands. *Transportation Research Part B: Methodological* 78, 404–421.

Dror, M., 1994. Note on the complexity of the shortest path models for column generation in VRPTW. *Operations Research* 42(5), 977–978.

Engineer, F. G., Furman, K. C., Nemhauser, G. L., Savelsbergh, M. W. P., Song, J. H., 2012. A branch-price-and-cut algorithm for single-product maritime inventory routing. *Operations Research* 60(1), 106–122.

Environment Bureau, 2013. A clean air plan for Hong Kong. <https://www.eeb.gov.hk/en/files/New_Air_Plan_en.pdf> (accessed 29.01.2022).

Environmental Protection Department, 2018. A guide to the air pollution control (fuel for vessels) regulation. <https://www.epd.gov.hk/epd/english/environmentinhk/air/prob_solutions/guide-air-pollution-control-fuel-for-vessels-regulation.html#prohibition> (accessed 29.01.2022).

Environmental Protection Department, 2022. Air pollution control strategies. <https://www.epd.gov.hk/epd/english/environmentinhk/air/prob_solutions/strategies_apc.html#C> (accessed 29.01.2022).

Fransoo, J. C., Lee, C. Y., 2013. The critical role of ocean container transport in global supply chain performance. *Production and Operations Management* 22, 253–268.

Fukasawa, R., He, Q., Santos, F., Song, Y., 2018. A joint vehicle routing and speed optimization problem. *INFORMS Journal on Computing* 30(4), 694–709.

Garbatov, Y., Georgiev, P., 2022. Stochastic air quality dispersion model for defining queuing ships seaport location. *Journal of Marine Science and Engineering* 10(2), 140.

GovHK, 2022. LCQ8: enhancing Hong Kong's status as an international maritime centre. <https://www.info.gov.hk/gia/general/202202/23/P2022022300422.htm> (accessed 29.01.2022).

Geoffrion, A. M., Graves, G. W., 1974. Multicommodity distribution system design by Benders decomposition. *Management Science* 20(5), 822–844.

Hernandez, F., Feillet, D., Giroudeau, R., Naud, O., 2016. Branch-and-price algorithms for the solution of the multi-trip vehicle routing problem with time windows. *European Journal of Operational Research* 249(2), 551–559.

HKTDC, 2020. Egypt: Suez Canal temporarily slashes fees for Asia-bound shipping. <https://research.hktdc.com/en/article/NDI2MDE2NTg2> (accessed 05.07.2022).

Holmes, N. S., Morawska, L., 2006. A review of dispersion modelling and its application to the dispersion of particles: an overview of different dispersion models available. *Atmospheric Environment* 40(30), 5902–5928.

Hong Kong Police Force, 2022. The fleet. <https://www.police.gov.hk/ppp_en/14_marine/fleet.html> (accessed 26.08.2022).

Hou, Y. H., Kang, K., Liang, X., 2019. Vessel speed optimization for minimum EEOI in ice zone considering uncertainty. *Ocean Engineering* 188, 106240.

Hou, Y. H., Xiong, Y., Zhang, Y., Liang, X., Su, L., 2021. Vessel energy efficiency uncertainty optimization analysis in ice zone considering interval parameters. *Ocean Engineering* 232, 109114.

Huang, K., Ahmed, S., 2009. The value of multistage stochastic programming in capacity planning under uncertainty. *Operations Research* 57(4), 893–904.

IBM, 2017. IBM ILOG CPLEX optimization studio CPLEX user's manual. <https://www.ibm.com/docs/en/SSSA5P_12.8.0/ilog.odms.studio.help/pdf/usrcplex.pdf> (accessed 18.07.2021).

Ichsan, M., Pradana, M. F., Noche, B., 2019. Estimation and optimization of the voyage energy efficiency operational indicator (EEOI) on Indonesian sea tollway corridors. In Proceedings of the IOP Conference Series: Materials Science and Engineering 673(1), 012024.

International Maritime Organization (IMO), 2009. Guidelines for voluntary use of the ship energy efficiency operational indicator (EEOI). <https://gmn.imo.org/wp-content/uploads/2017/05/Circ-684-EEOI-Guidelines.pdf> (accessed 05.07.2022).

Intergovernmental Panel on Climate Change (IPCC), 2018. Summary for policymakers of IPCC special report on global warming of 1.5°C approved by governments. <https://www.ipcc.ch/2018/10/08/summary-for-policymakers-of-ipcc-special-report-on-global-warming-of-1-5c-approved-by-governments/> (accessed 10.11.2022).

IMO, 2011. Report of the marine environment protection committee on its sixty-second session. <https://euroshore.com/sites/euroshore.com/files/downloads/mepc%2062-24.pdf> (accessed 05.07.2022).

IMO, 2014. Third IMO greenhouse gas study. <https://gmn.imo.org/wp-content/uploads/2017/05/GHG3-Executive-Summary-and-Report_web.pdf> (accessed 05.07.2022).

IMO, 2018. Initial IMO GHG strategy. <https://www.imo.org/en/MediaCentre/HotTopics/Pages/Reducing-greenhouse-gas-emissions-from-ships.aspx> (accessed 03.07.2022).

IMO, 2019. 2019 Guidelines for consistent implementation of the 0.50% sulphur limit under MARPOL ANNEX VI. <https://wwwcdn.imo.org/localresources/en/OurWork/Environment/Documents/Resolution%20MEPC.320%2874%29.pdf> (accessed 03.05.2022).

Jepsen, M., Petersen, B., Spoorendonk, S., Pisinger, D., 2008. Subset-row inequalities applied to the vehicle-routing problem with time windows. *Operations Research* 56(2), 497–511.

Karsten, C. V., Ropke, S., Pisinger, D., 2018. Simultaneous optimization of container ship sailing speed and container routing with transit time restrictions. *Transportation Science* 52(4), 769–787.

Kepaptsoglou, K., Fountas, G., Karlaftis, M. G., 2015. Weather impact on containership routing in closed seas: a chance-constraint optimization approach. *Transportation Research Part C: Emerging Technologies* 55, 139–155.

Keuning, J. A., van Walree, F., (2006, November). The comparison of the hydrodynamic behaviour of three fast patrol boats with special hull geometries. In Proceedings of the 5th International Conference on High Performance Marine Vehicles: 137–152, Australia

Kontovas, C. A., 2014. The green ship routing and scheduling problem (GSRSP): a conceptual approach. *Transportation Research Part D: Transport and Environment* 31, 61–69.

Ksciuk, J., Kuhlemann, S., Tierney, K., Koberstein, A., 2023. Uncertainty in maritime ship routing and scheduling: A Literature review. *European Journal of Operational Research* 308(2), 499–524.

Lai, X., Wu, L., Wang, K., Wang, F., 2022. Robust ship fleet deployment with shipping revenue management. *Transportation Research Part B: Methodological* 161, 169–196.

Lee, C. Y., Shu, S., Xu, Z., 2021. Optimal global liner service procurement by utilizing liner service schedules. *Production and Operations Management* 30(3), 703–714.

Lee, C. Y., Song, D. P., 2017. Ocean container transport in global supply chains: overview and research opportunities. *Transportation Research Part B: Methodological* 95, 442–474.
Lloyd's List (Lloyd's), 2021. Shipowners focus on 2030 carbon cut target. <https://lloydslist.maritimeintelligence.informa.com/LL1136881/Shipowners-focus-on-2030-carbon-cut-target> (accessed 10.07.2022).
Lloyd's List (Lloyd's), 2022. Shipping emissions rise 4.9% in 2021. <https://lloydslist.maritimeintelligence.informa.com/LL1139627/Shipping-emissions-rise-49-in-2021> (accessed 26.07.2022).
Ma, B., Hu, D., Chen, X., Wang, Y., Wu, X., 2021. The vehicle routing problem with speed optimization for shared autonomous electric vehicles service. *Computers & Industrial Engineering* 161, 107614.
Maersk, 2022. New transpacific east coast service–TP28. <https://www.maersk.com/news/articles/2022/02/09/new-transpacific-east-coast-service-tp28> (accessed on 04.08.2022).
Magnanti, T. L., Wong, R. T., 1981. Accelerating Benders decomposition: Algorithmic enhancement and model selection criteria. *Operations Research* 29(3), 464–484.
Marine Department (MD), 2021. Hong Kong fact sheet. <https://www.mardep.gov.hk/en/fact/hkfactsheet.html> (accessed 01.05.2022).
Mhamedi, T., Andersson, H., Cherkesly, M., Desaulniers, G., 2022. A branch-price-and-cut algorithm for the two-echelon vehicle routing problem with time windows. *Transportation Science* 56(1), 245–264.
Meng, Q., Du, Y., Wang, Y., 2016. Shipping log data based container ship fuel efficiency modeling. *Transportation Research Part B: Methodological* 83, 207–229.
Meng, Q., Wang, S., Andersson, H., Thun, K., 2014. Containership routing and scheduling in liner shipping: overview and future research directions. *Transportation Science* 48(2), 265–280.
Nabawi, R. A., 2021. Study reduction of resistance on the flat hull ship of the semi-trimaran model: Hull vane vs stern foil. *CFD Letters* 13(12), 32–44.
NatureNews, 2022. Record-breaking carbon emissions, and more—this week's best science graphics. <https://www.nature.com/articles/d41586-022-03721-5> (accessed 23.11.2022).
Ng, M. W., 2014. Distribution-free vessel deployment for liner shipping. *European Journal of Operational Research* 238(3), 858–862.
Ng, M. W., 2017. Revisiting a class of liner fleet deployment models. *European Journal of Operational Research* 257(3), 773–776.
Ng, M. W., Lin, D. Y., 2018. Fleet deployment in liner shipping with incomplete demand information. *Transportation Research Part E: Logistics and Transportation Review* 116, 184–189.
Nguyen, H. P., Hoang, A. T., Nizetic, S., Nguyen, X. P., Le, A. T., Luong, C. N., Chu, V. D., Pham, V. V., 2021. The electric propulsion system as a green solution for management strategy of CO_2 emission in ocean shipping: a comprehensive review. *International Transactions on Electrical Energy Systems* 31(11), e12580.
NOAA Office for Coastal Management (NOAA), 2023. New York. <https://coast.noaa.gov/states/new-york.html> (accessed 05.12.2023).
Papadakos, N., 2008. Practical enhancements to the Magnanti–Wong method. *Operations Research Letters* 36(4), 444–449.
Paradiso, R., Roberti, R., Laganá, D., Dullaert, W., 2020. An exact solution framework for multitrip vehicle-routing problems with time windows. *Operations Research*

68(1), 180–198.
Pasha, J., Dulebenets, M. A., Fathollahi-Fard, A. M., Tian, G., Lau, Y. Y., Singh, P., Liang, B., 2021. An integrated optimization method for tactical-level planning in liner shipping with heterogeneous ship fleet and environmental considerations. *Advanced Engineering Informatics* 48, 101299.
Pasquill, F., 1961. The estimation of the dispersion of windborne material. *Meteorology Magazine* 90, 33–49.
Pearce, R. H., Forbes, M., 2018. Disaggregated Benders decomposition and branch-and-cut for solving the budget-constrained dynamic uncapacitated facility location and network design problem. *European Journal of Operational Research* 270(1), 78–88.
Pecin, D., Pessoa, A., Poggi, M., Uchoa, E., 2017. Improved branch-cut-and-price for capacitated vehicle routing. *Mathematical Programming Computation* 9(1), 61–100.
Prill, K., Behrendt, C., Szczepanek, M., Michalska-Pożoga, I., 2020. A new method of determining energy efficiency operational indicator for specialized ships. *Energies* 13(5), 1082.
Rei, W., Cordeau, J. F., Gendreau, M., Soriano, P., 2009. Accelerating Benders decomposition by local branching. *INFORMS Journal on Computing* 21(2), 333–345.
Ronen, D., 1983. Cargo ships routing and scheduling: survey of models and problems. *European Journal of Operational Research* 12(2), 119–126.
Ronen, D., 1993. Ship scheduling: the last decade. *European Journal of Operational Research* 71(3), 325–333.
Roy, D., de Koster, R., Bekker, R., 2020. Modeling and design of container terminal operations. *Operations Research* 68(3), 686–715.
Sherali, H. D., Lunday, B. J., 2013. On generating maximal nondominated Benders cuts. *Annals of Operations Research* 210(1), 57–72.
Ship and Bunker (S&B), 2022. World bunker prices. <https://shipandbunker.com/prices/av/global/av-g20-global-20-ports-average> (accessed 10.07.2022).
Searcy, T., 2017. Harnessing the wind: A case study of applying Flettner rotor technology to achieve fuel and cost savings for Fiji's domestic shipping industry. *Marine Policy* 86, 164–172.
Sun, C., Wang, H., Liu, C., Zhao, Y., 2019. Dynamic prediction and optimization of energy efficiency operational index (EEOI) for an operating ship in varying environments. *Journal of Marine Science and Engineering* 7(11), 402.
Tierney, K., Áskelsdóttir, B., Jensen, R. M., Pisinger, D., 2015. Solving the liner shipping fleet repositioning problem with cargo flows. *Transportation Science* 49(3), 652–674.
Tollefson, J., 2022. Carbon emissions hit new high: warning from COP27. <https://www.nature.com/articles/d41586-022-03657-w#author-0> (accessed 23.11.2022).
UNCTAD, 2022. Review of maritime transport 2022. <https://unctad.org/system/files/official-document/rmt2022_en.pdf> (accessed 11.12.2022).
Vis, I. F. A., Roodbergen, K. J., 2009. Scheduling of container storage and retrieval. *Operations Research* 57(2), 456–467.
United Nations (UN), 2015. Paris agreement. <https://unfccc.int/sites/default/files/english_paris_agreement.pdf> (accessed

05.07.2022).
United States Environmental Protection Agency (USEPA), 2022. Sources of greenhouse gas emissions. <https://www.epa.gov/ghgemissions/sources-greenhouse-gas-emissions> (accessed 26.07.2022).
Wang, K. and Jacquillat, A. (2020) A stochastic integer programming approach to air traffic scheduling and operations. *Operations Research* 68(5): 1375–1402.
Wang, K., Jacquillat, A. and Vaze, V. (2022) Vertiport planning for urban aerial mobility: an adaptive discretization approach. *Manufacturing & Service Operations Management* 24(6): 3215–3235.
Wang, S., 2013. Essential elements in tactical planning models for container liner shipping. *Transportation Research Part B: Methodological* 54, 84–99.
Wang, S., 2015. Optimal sequence of container ships in a string. *European Journal of Operational Research* 246(3), 850–857.
Wang, S., Meng, Q., 2012a. Liner ship fleet deployment with container transshipment operations. *Transportation Research Part E: Logistics and Transportation Review* 48(2), 470–484.
Wang, S., Meng, Q., 2012b. Sailing speed optimization for container ships in a liner shipping network. *Transportation Research Part E: Logistics and Transportation Review* 48(3), 701–714.
Wang, S., Meng, Q., 2017. Container liner fleet deployment: A systematic overview. *Transportation Research Part C: Emerging Technologies* 77, 389–404.
Wang, S., Meng, Q., Lee, C. Y., 2016. Liner container assignment model with transit-time-sensitive container shipment demand and its applications. *Transportation Research Part B: Methodological* 90, 135–155.
Wang, S., Zhuge, D., Zhen, L., Lee, C. Y., 2021. Liner shipping service planning under sulfur emission regulations. *Transportation Science* 55(2), 491–509.
Wang, T., Meng, Q., Wang, S., Tan, Z., 2013. Risk management in liner ship fleet deployment: a joint chance constrained programming model. *Transportation Research Part E: Logistics and Transportation Review* 60, 1–12.
Wang, Y., Meng, Q., 2020. Semi-liner shipping service design. *Transportation Science* 54(5), 1288–1306.
Wang, Y., Meng, Q., Du, Y., 2015. Liner container seasonal shipping revenue management. *Transportation Research Part B: Methodological* 82, 141–161.
Wang, Y., Meng, Q., Kuang, H., 2019. Intercontinental liner shipping service design. *Transportation Science* 53(2), 344–364.
Wetzel, D., Tierney, K., 2020. Integrating fleet deployment into liner shipping vessel repositioning. *Transportation Research Part E: Logistics and Transportation Review* 143, 102101.
Xia, J., Li, K. X., Ma, H., Xu, Z., 2015. Joint planning of fleet deployment, speed optimization, and cargo allocation for liner shipping. *Transportation Science* 49(4), 922–938.
Xu, Z., Lee, C. Y., 2018. New lower bound and exact method for the continuous berth allocation problem. *Operations Research* 66(3), 778–798.
Yang, W., Ke, L., Wang, D. Z., Lam, J. S. L., 2021. A branch-price-and-cut algorithm for the vehicle routing problem with release and due dates. *Transportation Research Part E: Logistics and Transportation Review* 145, 102167.
Yang, Y., 2023. An exact price-cut-and-enumerate method for the capacitated multitrip vehicle routing problem with time windows. *Transportation Science* 57(1), 230–251.
Yau, P. S., Lee, S. C., Corbett, J. J., Wang, C., Cheng, Y., Ho, K. F., 2012. Estimation

of exhaust emission from ocean-going vessels in Hong Kong. *Science of the Total Environment* 431, 299–306.

Young, S. S., 2022. Smoke and mirrors: new decarbonisation regulations meet rising emissions. <https://www.ssyonline.com/our-blog/posts/2022/january-2022/smoke-and-mirrors-new-decarbonisation-regulations-meet-rising-emissions/> (accessed 14.12.20).

Zhao, Y., Fan, Y., Fagerholt, K., Zhou, J., 2021a. Reducing sulfur and nitrogen emissions in shipping economically. *Transportation Research Part D: Transport and Environment* 90, 102641.

Zhao, Y., Fan, Y., Zhou, J., Kuang, H., 2019. Bi-objective optimization of vessel speed and route for sustainable coastal shipping under the regulations of emission control areas. *Sustainability* 11(22), 6281.

Zhao, Y., Zhou, J., Fan, Y., Kuang, H., 2020. Sailing speed optimization model for slow steaming considering loss aversion mechanism. *Journal of Advanced Transportation* 2020, 1–11.

Zhao, Y., Ye, J., Zhou, J., 2021b. Container fleet renewal considering multiple sulfur reduction technologies and uncertain markets amidst COVID-19. *Journal of Cleaner Production* 317, 128361.

Zhen, L., Hu, Y., Wang, S., Laporte, G., Wu, Y., 2019a. Fleet deployment and demand fulfillment for container shipping liners. *Transportation Research Part B: Methodological* 120, 15–32.

Zhen, L., Gao, J., Tan, Z., Wang, S., Baldacci, R., 2022. Branch-price-and-cut for trucks and drones cooperative delivery. *IISE Transactions*: 1–17.

Zhen, L., Wang, S., Laporte, G., Hu, Y., 2019b. Integrated planning of ship deployment, service schedule and container routing. *Computers & Operations Research* 104, 304–318.

Zhen, L., Wu, Y., Wang, S., Laporte, G., 2020. Green technology adoption for fleet deployment in a shipping network. *Transportation Research Part B: Methodological* 139, 388–410.

Zhou, J., Zhao, Y., Liang, J., 2021. Multiobjective route selection based on LASSO regression: When will the Suez Canal lose its importance? *Mathematical Problems in Engineering* 2021, 1–18.

Zhu, M., Yuen, K. F., Ge, J. W., Li, K. X., 2018. Impact of maritime emissions trading system on fleet deployment and mitigation of CO_2 emission. *Transportation Research Part D: Transport and Environment* 62, 474–488.

Zisi, V., Psaraftis, H. N., Zis, T., 2021. The impact of the 2020 global sulfur cap on maritime CO_2 emissions. *Maritime Business Review* 6(4), 339–357.